OXYGEN DEFICIENT METABOLISM IN ORGANS: A LINK TO COMBUSTION SCIENCE

A Thesis

by

JASON MATHEW MILLER

Submitted to the Office of Graduate and Professional Studies of
Texas A&M University
in partial fulfillment of the requirements for the degree of

MASTER OF SCIENCE

Chair of Committee,	Kalyan Annamalai
Committee Members,	Hong (Helen) Liang
	Stephen Guetersloh
Head of Department,	Andreas Polycarpou

December 2014

Major Subject: Mechanical Engineering

ABSTRACT

In an attempt to better understand and model transport of oxygen, O_2, from capillaries to living cells in surrounding tissue, the group combustion (O_2 deficient) concept from the field of combustion science in engineering is applied to the biological field of microvascular O_2 transport from capillaries to cells immersed in interstitial fluid (IF). The conventional Krogh model represents typical biological models, considering tissue cylinder with uniform oxygen source/sink term (US) ($\dot{m}'''$, g/s/cm^3) and O_2 transport from capillary on axis (COA) towards the surface; engineering models consider cylinders with O_2 supplied from the surface of cylinder (COS); in addition, they present i) transport (diffusion) and ii) kinetics limited sink rates and profiles for O_2. Diffusion limitation causes $\dot{m}'''$ to be proportional to local O_2 concentration. Thus, the present work modifies COS engineering models for COA cases and considers only diffusion limited transport of O_2 to metabolic cells from IF. O_2 profiles and resulting specific metabolic rates, SMRs (W/g), are generated for four models: I) COA with oxygen dependent consumption source term (O2) (COA-O2), II) COA-US, III) COS-O2, and IV) COS-US.

In order to validate the current approach, the model results are verified with the following different types of experimental data: A) If SMRs ($\dot{q}_m$ W/g) are given by the allometric law, $\dot{q}_m = a_k \; m_k^{\;b_k}$ for organ k, then COS models under limiting conditions suggest $-1/3<b_k<0$ where $b_k=0$ for small organs following isometric law

and -1/3 for large organs while COA models suggest $-2/3<b_k<0$ under similar conditions. Most experimental data for vital organs yield $-0.27<bk<0$ which suggests better correlation with COS models. B) Measured capillary-IF interface pressure of O_2 ($pO_{2,cap\text{-}IF}$) for rat mesentery system as given by Tsai et. al. is about 38 mmHg while predicted $pO_{2,cap\text{-}IF}$ is 54.5, 38.1, 55.3 and 46.2 mmHg for COA-O2, COS-O2, COA-US and COS-US respectively. C) Further, SMR for the average human liver is about 0.01 W/g as given by Wang et. al. (2010) while the COA-O2, COS-O2, COA-US and COS-US models yield 0.006, 0.032, 0.003 and 0.022 W/g respectively. COS models are of the same order magnitude as the experimental value while COS-US model is closest.

ACKNOWLEDGEMENTS

I would like to thank my committee chair and advisor, Dr. Annamalai, for his support and guidance throughout this project. Additionally, I would like to show my gratitude towards my colleagues, Siva Sankar and Tiyawut Tiyawongsakul, for their assistance. Finally, I would like to show appreciation towards my brother and parents for their love and support.

NOMENCLATURE

a	Radius of Cell Within Tissue
a_k	Allometric Constant
ATP	Adenosine Triphosphate
aq	Aqueous
b_k	Allometric Exponent
BS	Biological System
°C	Degrees Celsius
C	Carbon
CAP	Capillary
CH	Carbohydrate
CO_2	Carbon Dioxide
COA	Capillary on Axis
COS	Capillary on Surface
CST	Chemical Standard Temperature
d_{cell}	Diameter of Cell
D_{O2}	Diffusion Coefficient of Oxygen
DOE	Department of Energy
ERR	Energy Release Rate
F	Fat
F_{COS}	Fraction of Surface Area Covered by Capillaries

G	Group Combustion Number
H_{O2}	Henry's Constant
H_2O	Water Molecule
Hb	Hemoglobin
HHV	Higher Heating Value
HV	Heating Value
IF	Interstitial Fluid
K'	Permeability Coefficient
K^0_n'	Equilibrium Constants for Hb or Mb Reactions
LVF	Lethal Volume Fraction
m	Mass
$\dot{m}_k$	Mass Flow Rate of Species k
$\dot{m}_k$''	Consumption Rate of Species k per Unit Area
$\dot{m}_k$'''	Volumetric Consumption Rate of Species k
Mb	Myoglobin
n	Number of Cells per Volume
O_2	Oxygen Molecule
O2	Oxygen Dependent Consumptions Source Term
P	Protein
pO_2	Partial Pressure of Oxygen
Q	Heat Energy
$\dot{q}_{iso}$	Energy Release Rate of Isolated Particle or Cell

$\dot{q}_{m,iso}$	Specific Energy Release Rate of Isolated Particle or Cell
r	Radius From Center of the Geometry
R	Outer Radius of the Geometry
r_{cap}	Capillary Radius
R_{cl}	Cloud Radius
$R_{chem,O2}$	Chemical Resistance
$R_{diff,O2}$	Diffusion Resistance
RBC	Red Blood Cell
s	Geometric Constant
S_{cap}	Capillary Surface Area
$S_{cap,m}$	Specific Capillary Surface Area
$S_{O2,Hb}$	Oxygen Saturation Percent of Hemoglobin
$S_{O2,Mb}$	Oxygen Saturation Percent of Myoglobin
SBR	Specific Burn Rate
SERR	Specific Energy Release Rate
SMR	Specific Metabolic Rate
tcap	Capillary Wall Thickness
TER	Total Energy Release Rate
US	Uniform Oxygen Consumption Source Term
V	Tissue Volume
V_{Lethal}	Lethal Volume
V_{Reac}	Reacting Volume

vf_{lethal}	Lethal Volume Fraction
Y_k	Mass Fraction of Species k
α	Switch Term to Account for Lethal Volume
δ	Aerobic Shell Thickness
η_{eff}	Effectiveness Factor
ρ_{O2}	Density of Oxygen at CST
ρ_{bl}	Density of Blood
$(\rho D)_{eff}$	Effective Density and Diffusion Coefficient
$(\rho D)_{bp}$	Bulk Gas to Particle Density and Diffusion Coefficient
ξ	Dimensionless Radius
ξ_{cap}	Dimensionless Capillary Radius

TABLE OF CONTENTS

Page

LIST OF FIGURES

Page

LIST OF TABLES

Page

CHAPTER I

INTRODUCTION

The engineering power systems convert chemical energy of fossil fuels into thermal energy using high temperature oxidation process called combustion and then use thermal energy for extraction of useful work (e.g. automobiles obtaining mechanical work and power plants obtaining electrical work). Most of the energy needs of the air breathing biological species including humans is met by the oxidation process and called as metabolism in biology. The biological systems (BS) consume food and convert them into three main nutrients: carbohydrate (CH, e.g. glucose), fat (F, e.g. palmitic acid) and protein (P, e.g. amino acids) and oxidize mostly CH and F using oxygen (O_2) from air breathed in.

The O_2 from air breathed in enters alveoli in lungs (figure 1 and figure 2), mixes in the alveoli with CO_2 transported from blood capillaries around alveoli, transported from alveoli into capillary blood, dissolves in blood and then undergoes chemical reaction with hemoglobin (Hb; Red blood cells, RBC, figure 3) to produce HbO_2, $Hb(O_2)_2$, $Hb(O_2)_3$, and $Hb(O_2)_4$ which is the most predominant oxygenated Hb.

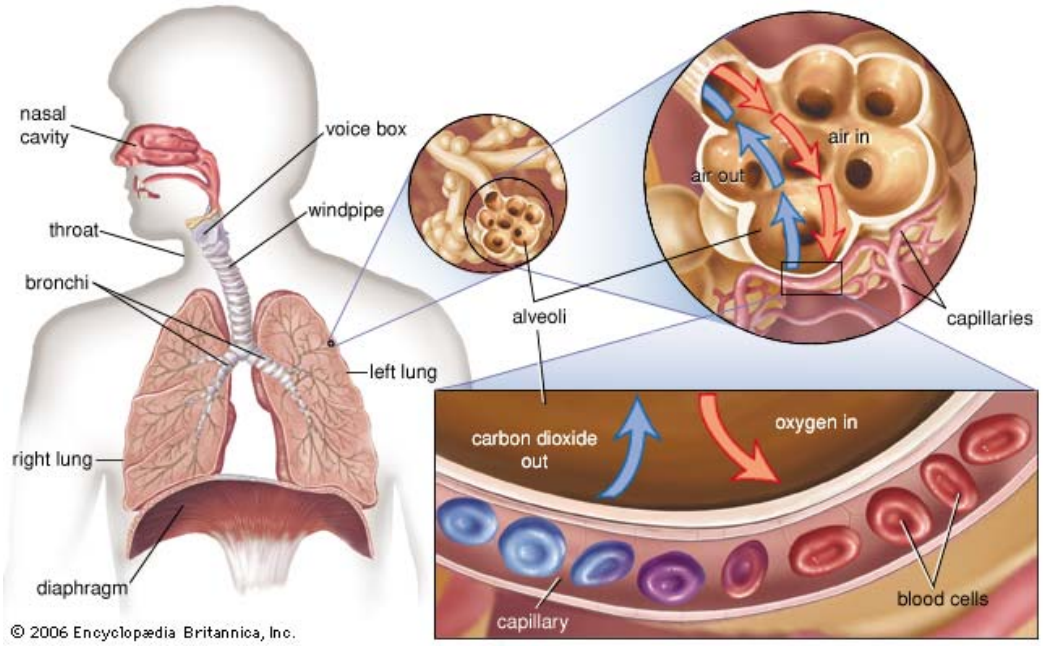

Figure 1. Diagram of respiratory system. Inhaled air flows into the alveoli of the lungs where oxygen and carbon dioxide are transferred to and from the cell respectively. Adopted from [1].

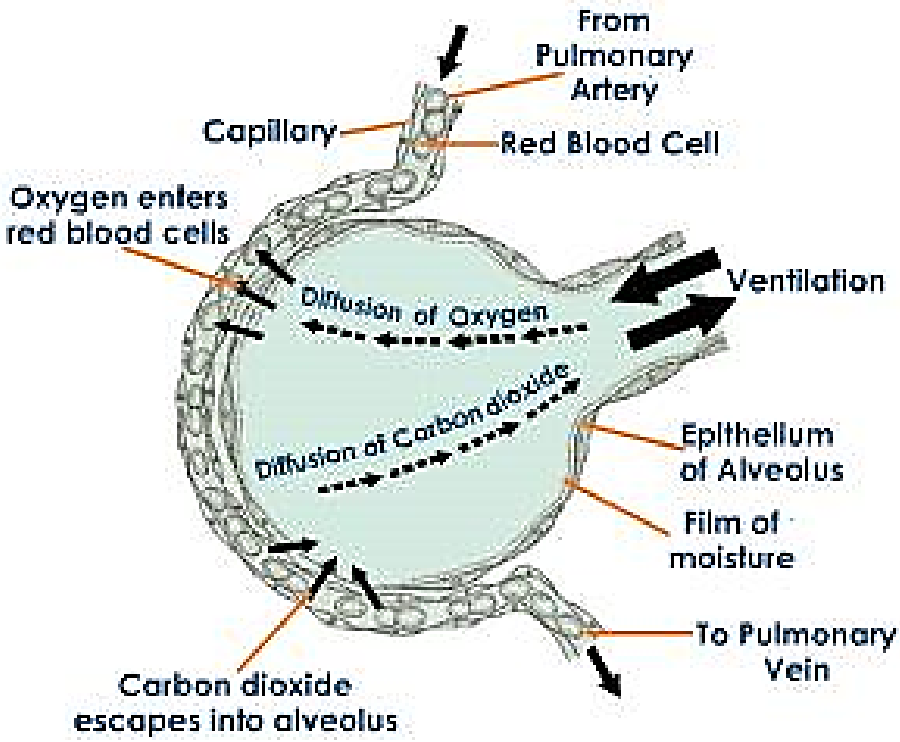

Figure 2. The O2 and CO2 transfer across alveoli membranes. O2 leaves at approximately 100 mmHg while pO2 in alveoli is about 104 mmHg due to the moisture in the lungs. Adopted from [2].

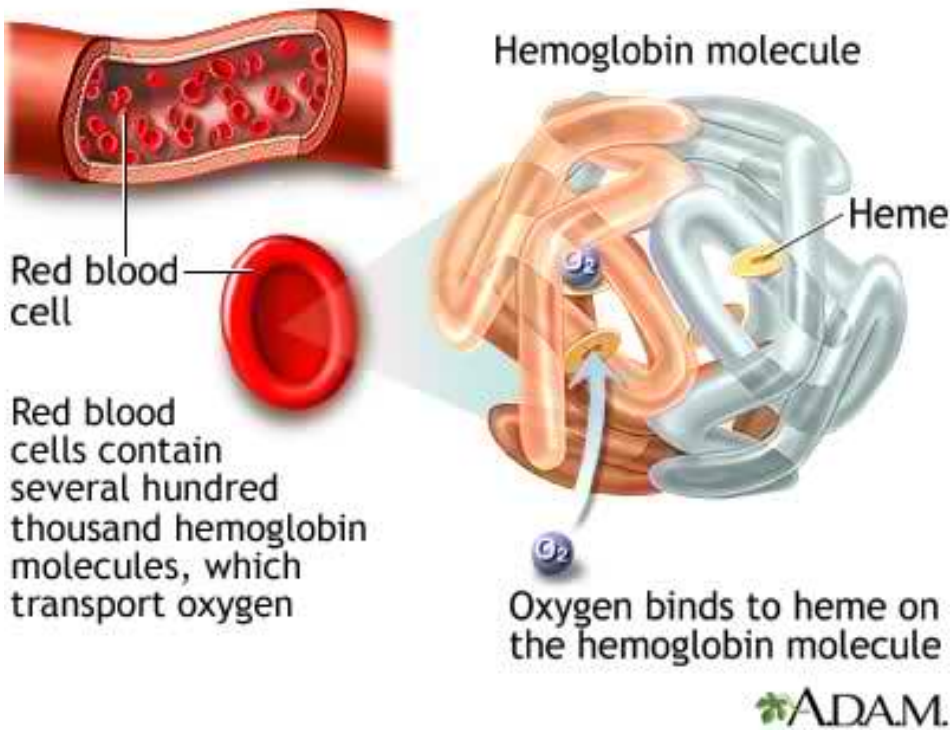

Figure 3. Red blood cells containing hemoglobin which binds O2 for transport throughout the circulatory system. Each hemoglobin molecule can bind with up to four O2 molecules. Adopted from [3].

The total oxygen in blood is a sum of oxygen chemically bound to Hb (almost 95-98%) and dissolved O_2 (only about 2-5%). The CH, F, P, dissolved O_2 and $Hb(O_2)_4$ (called premixed fuel and oxygen mixture in combustion science but don't undergo oxidation in absence of enzymes in blood) travel in blood stream and are delivered to various organs including skeletal muscles and finally delivered to metabolic cells within each organ (figure 4). The blood flow is depicted in figure 4 and figure 5.

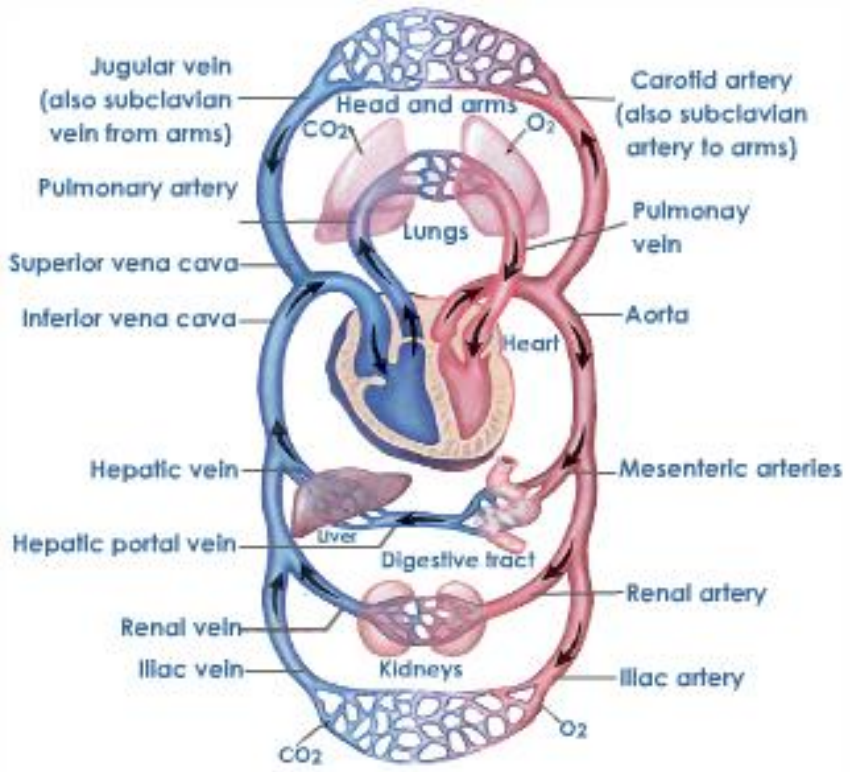

Figure 4. Diagram of the circulatory system giving a rough idea of the blood flow throughout the human body. Red vessels indicate a high concentration of O2 while blue vessels indicate a low concentration. Adopted from [4].

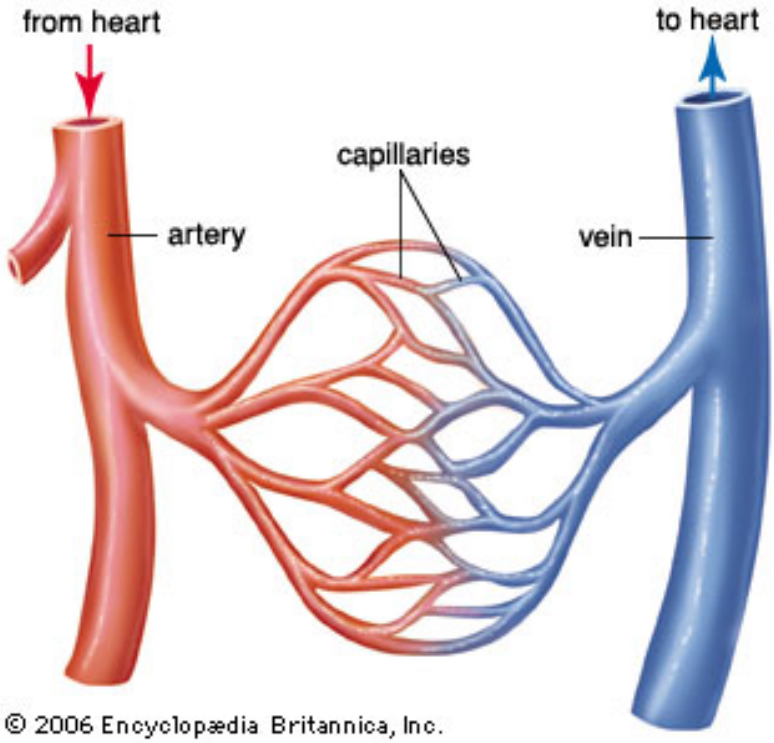

Figure 5. Diagram of capillaries demonstrating the blood flow between arteries and veins. One can imagine the tissue and living cells between the capillaries. Red vessels indicate a high concentration of O2 while blue vessels indicate a low concentration. The concentration of dissolved O2 at the arteriole end of the capillaries is about 95 mmHg. Adopted from [5].

The nutrients along with dissolved O_2 enter from the capillaries into interstitial fluid which bathes the metabolic cells (figure 6) where the CH and F are oxidized to CO_2 and H_2O. A part of energy is released as heat (Q) which is used to maintain body temperature at 37°C and part is converted into useful work in the form of Adenosine Triphosphate (ATP) called work currency of the body. For example, ATP delivers energy to skeletal muscles which enable the species to move. Thus it is seen that the transport processes govern the movement of O_2 for oxidation of nutrients, which is

called metabolism in biology (typically at low temperatures) and called combustion in engineering (typically at high temperatures). Low temperature metabolism occurs due to enzymes (or catalysts) present in cells.

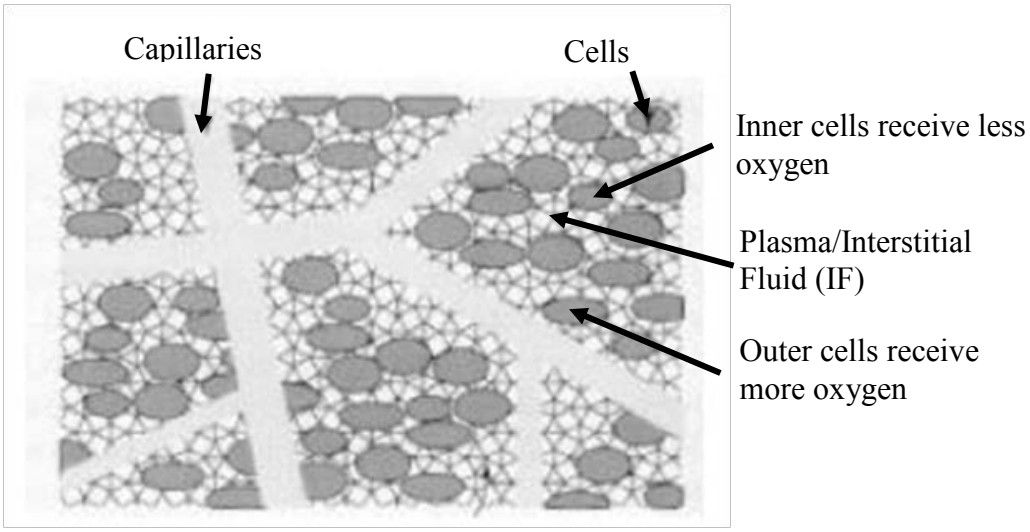

Figure 6. Illustration of O_2 rich and O_2 poor cells. As blood flows through capillaries, it transfers dissolved O_2 into IF and O_2 is transported form IF into cells through the cell membrane. Adopted from [6].

The group/O_2 deficient combustion can be illustrated as follows: if a single candle of mass m_{cd} is mounted on a balance and the mass of candle $m_{cd}(t)$ vs time is measured, one can determine mass burn rate as $\dot{m}_{cd}$ (kg/s); knowing the heating value of candle, the energy release rate of isolated candle, $\dot{q}_{iso}$ (J/s) and hence the specific energy release rate (SERR), $\dot{q}_{m,iso}$ (energy release rate of an isolated candle /candle mass, W/kg) can also be determined (figure 7). If N candles are spaced farther apart on the balance, then total energy release rate (TER) and hence specific energy release rate

(total energy release rate/total candle mass) of group of candles is found to be same as $\dot{q}_{m,iso}$ since TER increases in proportion to total mass to N m_{cd} when separation distance between candles is large. Hence the SERR of a group of candles remains invariant with number of candles within the candle cloud or size of the cloud. Such a law is called isometric law. If the same N candles are spaced at closer distance, the increase in TER is less than the increase in mass of candle cloud or SERR of candle cloud, $\dot{q}_{m,cl}$ decreases with increase in size of the cloud or number of candles within the group due to oxygen deficiency in the space between the closely spaced candles. If candles within candle cloud are replaced with liquid drop or solid carbon particles with each drop/particle burning inside the dense liquid sprays (or dense drop clouds) in gas turbines or solid carbon particles in coal fired plants, the SERR (W per kg cloud mass) decrease with increase in size of cloud. With past funding from DOE (1985-1994), the group/oxygen deficient combustion theory has been formulated to model and account for O_2 deficiency and simple expressions were developed to predict SERR of cylindrical, spherical and slab clouds as a function of characteristic size of cloud, R_{cl}. The model assumes complete combustion of Carbon and Hydrogen elements in fuel to CO_2 and H_2O with burn rate locally controlled by local oxygen concentration. The theory results show that i) the SERR is almost constant for dilute clouds following isometric law, ii) SERR decreases with increasing size (mass m_{cl} and radius R_{cl} for cylinder and sphere and half thickness for slab) thus following non-isometric law, iii) higher CO_2 concentration in the core of the cloud with increase in characteristic size of cloud and iv) there exists aerobic shell near cloud periphery with high energy release rate and oxygen deficient inner core

(anaerobic core) resulting in almost zero energy release rate particularly for larger or dense clouds. Several articles have been published in various engineering journals [7-11].

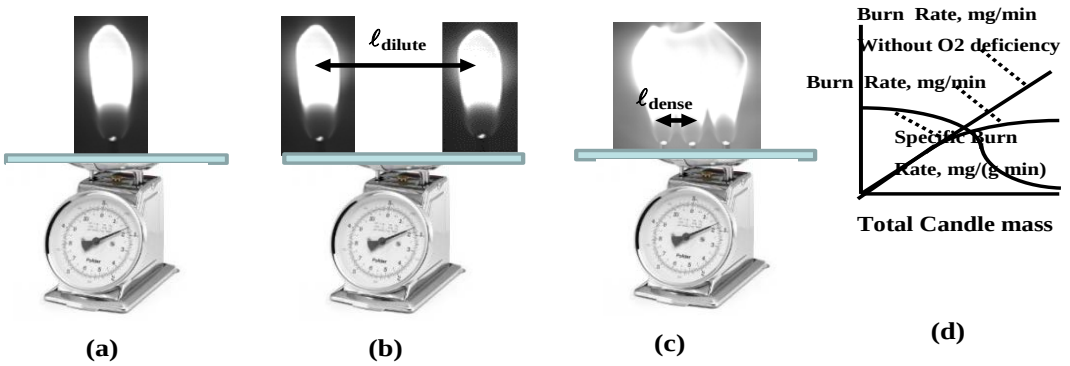

Figure 7. An example of Isolated and Candle Cloud. (a): Isolated Candle Burn rate: 80 mg/min; Energy release rate=61.6 W; Candle mass: 1.1 g, Specific burn rate= Burn rate/mass= 0.077 per min specific energy release rate = 56 W/g, (b) Two candles farther apart: total burn rate: 160 mg/min; energy release rate= 123.2 W. Mass of two Candles mass: 2.2 g, so burn rate ∝ mass of cloud called isometric law; burn rate per unit mass of candle cloud or specific rate= burn rate/mass= 0.077 per min or specific energy release rate = 56W/g. (c) Burn rate= 200 mg/min (i.e. < 240 mg/min due to O_2 deficiency), energy release rate = 154 W; mass of 3 candles: 3.3 g; specific burn rate= burn rate/mass= 0.061 per min; specific energy release rate =45.7 W per g. (d) Qualitative plots of burn rate without O2 deficiency, burn rate and specific burn rate vs total candle mass; correction factor, η = actual burn rate /total burn rate without O2 deficiency= 200/240=0.883 or 46.7/56=0.83. Adopted from [8].

Just as in group combustion where oxygen is transported into millions of carbon particles (which act oxygen sinks) for energy release, the CH, F and oxygen are transported from capillaries to millions of metabolic cells (which act as oxygen sinks in biology) within organ k of mass m_k and the relation between $SERR_k$ (W/kg organ k,

called as specific metabolic rate in biology, $\dot{q}_{m,k}$) and m_k is given by the following allometric law

$$\dot{q}_{m,k}\left(\frac{W}{kg\ of\ k}\right) = a_k\ m_k(kg)^{\ b_k} \qquad (1)$$

where a_k and b_k are allometric constants. The biology literature for 111 mammals suggest that $(-0.27) < b_k < 0$, thus, the larger the size of organ, the smaller the SERR.

Typical human of 70 Kg mass releases about 80 W and SERR of whole body is about 1.1 W/kg body mass. Almost 32 W out of 80 W is released by four vital organs (brain, kidney, liver, heart) whose combined mass is only about 2.5 kg i.e. the SERR of these vital organs is about 32 W/kg! Recent journal published articles in biology [12, 13] show that the SERR of organ vs size of organ consisting of metabolic cells (which act as oxygen sinks) is incredibly similar to that of combustion engineering literature. Qualitative plot of SERR of any organ vs organ size is given in figure 8b; the ordinate is proportional to SERR while the abscissa is proportional to ln (cloud radius). The curves are strikingly similar to figure 8a, except the oxygen deficient inner core of the organ undergoes anaerobic process (i.e. glycolysis) resulting in about 10 % of total energy release rate of organ. The model of Singer et al assumes that the aerobic shell thickness is fixed with uniform oxygen sinks as size of cloud is varied. In order to account for the effect of variation of oxygen concentration on the source strength of oxygen sinks, the oxygen profiles must be obtained around capillaries.

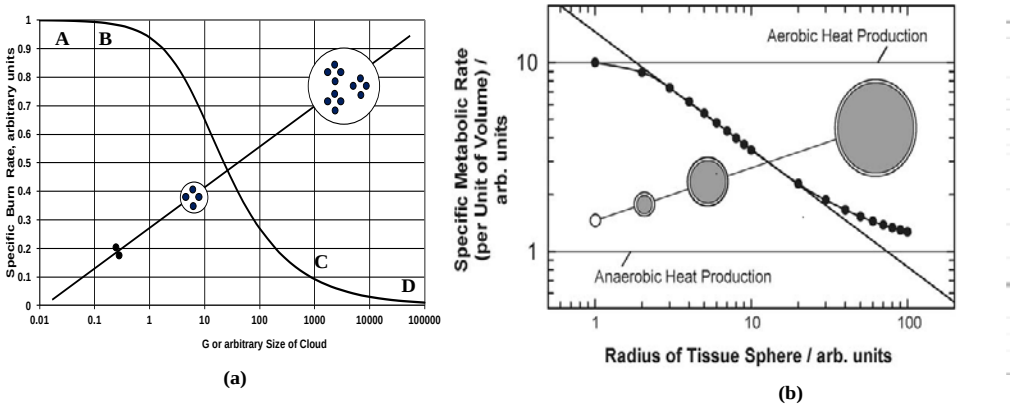

Figure 8. a) Variation of specific burn rate with cloud size. The ordinate is proportional to SERR while the abscissa is proportional to ln (cloud radius), CO_2 and bulk gas temperature increase at the inner core with increasing size (mass m_{cl} and radius R_{cl}). Adopted from [8]. b) Variation of Specific metabolic Rate with Organ size. Adopted from [12]. Influence of sample size on metabolic rate (crowding effect). An aerobic shell of constant thickness delta, surrounds an anaerobic sphere of increasing size. A small tissue slice or small cell cloud biopsy is aerobic; a large tissue with an aerobic shell and an anaerobic core. The heat output per unit of volume or mass decreases as size of slice is increased. Plots based on rough assumptions of critical depth of tissue aero-biosis (100 pm) and the ratio of aerobic to anaerobic metabolic rate of 10:1.

Can one transfer the literature in combustion science which deals with combustion of carbon particles and liquid droplets (which act as oxygen sinks) to metabolism within cells which act as oxygen sinks and improve the better understanding of energy release rate at the microvascular level? Secondly there exist extensive literature on oxygen deficient core group combustion in engineering and whether these results can also be used to explain the above allometric laws at organ level in biology. Can one predict the exponents in allometric laws of organs using oxygen deficient combustion theory? The present research attempts to apply the principles of combustion

science and more particularly the group combustion and thermodynamics to understand the metabolic processes in BS at the micro-level. Particularly, the engineering concept called group combustion (also known as oxygen deficient combustion) is used to estimate oxygen supply and energy release rate and explaining the allometric exponent.

CHAPTER II

LITERATURE REVIEW

All biological systems (BS) are comprised of a combination of cells which require a number of elements to survive. For the purpose of this paper, only animal cells will be considered and the human body will be used as reference. In order to survive, the cell needs to be provided oxygen and nutrients while carbon dioxide and wastes are removed. The nutrients provided include carbohydrates, proteins, fats, and various vitamins necessary to carry out the numerous activities of the cell. Oxygen is then used in the metabolic process of aerobic cellular respiration to convert some nutrients into the energy unit of the body, adenosine triphosphate (ATP). This ATP can then be used by other parts of the cell to undertake chemical reactions that would not otherwise be possible. Without oxygen, the cell resorts to more inefficient method of anaerobic cellular respiration [14]. Therefore, the transport of oxygen to the cells is an important process.

When air is inhaled, it travels through the respiratory system to small sacs in the lungs called alveoli. Here, oxygen, carbon dioxide, and nitrogen exist as gas. The oxygen concentration is high, while it is low with in the capillary beds that surround the alveoli. Capillaries are the smallest blood vessels and allow for diffusion of elements to and from the blood. The solution called blood consists of red blood cells (RBCs), plasma, and other blood cells such as platelets and white blood cells. RBCs contain the

protein hemoglobin, Hb, which is capable of carrying four oxygen molecules at a time and is the primary method for the transportation of oxygen (figure 9).

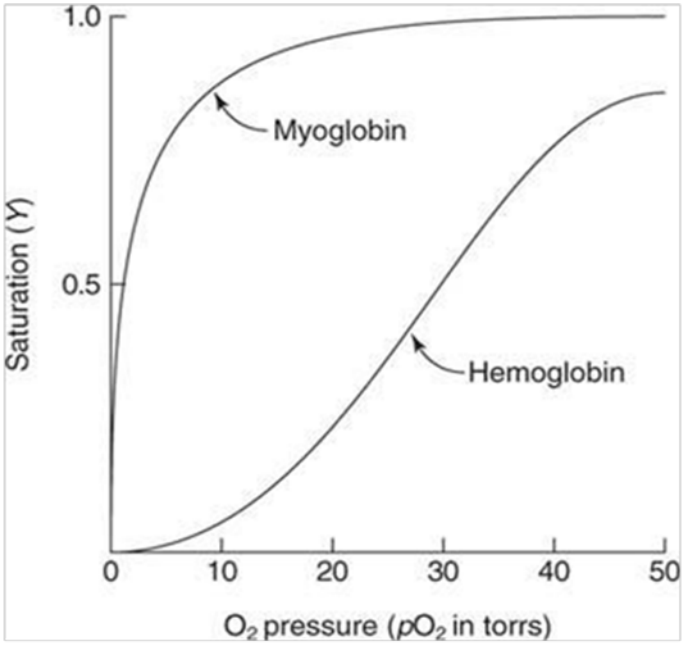

Figure 9. Dissolved O_2 reacts with Hb to produce HbO_2, $Hb(O_2)_2$, $Hb(O_2)_3$, and $Hb(O_2)_4$. Typically $Hb(O_2)_4$ dominates, thus for every one molecule of Hb, four molecules of O_2 are attached to Hb. Therefore the ratio of O_2 attached to Hb to the maximum amount that can be attached to all Hb molecules is called saturation fraction, which is the y axis. Similarly there are some organs in the body (heart and skeletal muscles) which contain myoglobin, Mb, and produce MbO_2. The ratio of O_2 attached to Mb to the maximum amount that can be attached if all Mb is oxidized is called saturation fraction for Mb. Particularly, Mb serves as O_2 carrier within interstitial fluid located between capillaries and cells while Hb serves as carrier for O_2 with blood flow. Adopted from [15].

Blood arriving at the lungs is high in carbon dioxide and low in oxygen concentrations. Since the air within the alveoli is rich in oxygen and the blood in the capillaries is poor, the oxygen will defuse from the alveoli into the blood stream and

dissolve becoming aqueous. Aqueous oxygen exists when water molecules surround the oxygen, dissolving it into the blood stream. This aqueous oxygen is then picked up by the Hb of the RBC. The oxygenated Hb, or saturated Hb, percentage is determined by the partial pressure of the oxygen within the alveoli and this plot is called the oxygen dissociation curve (figure 9). The curve can shift to the right or left depending on body conditions including carbon dioxide concentration, pH level, and temperature levels [16]. While most of the oxygen is taken up by the hemoglobin proteins, a very small amount remains dissolved in the plasma as aqueous oxygen.

From the lungs, the blood is pumped back to the heart and then throughout the body to deliver the oxygen to the cells of the body (figure 10). Figure 10 shows the circulation path of blood from heart to tissue cells. Once again the blood travels to the smallest of blood vessels, the capillaries. This time, the capillaries are surrounded by the tissue of the body. The tissue will be considered as a group of living cells suspended in interstitial fluid surrounding the capillaries. In contrast to the lungs, the surrounding tissue is low in oxygen concentration and high in carbon dioxide concentration; a product of the cellular respiration. Thus, the oxygen now diffuses from the blood stream into the tissue while the carbon dioxide is taken up by the blood and delivered back to the lungs. This paper will focus on the diffusion of oxygen from the capillary to the surrounding living cells of the tissue (figure 11). Everything in this process is treated as non-living except the actual cells.

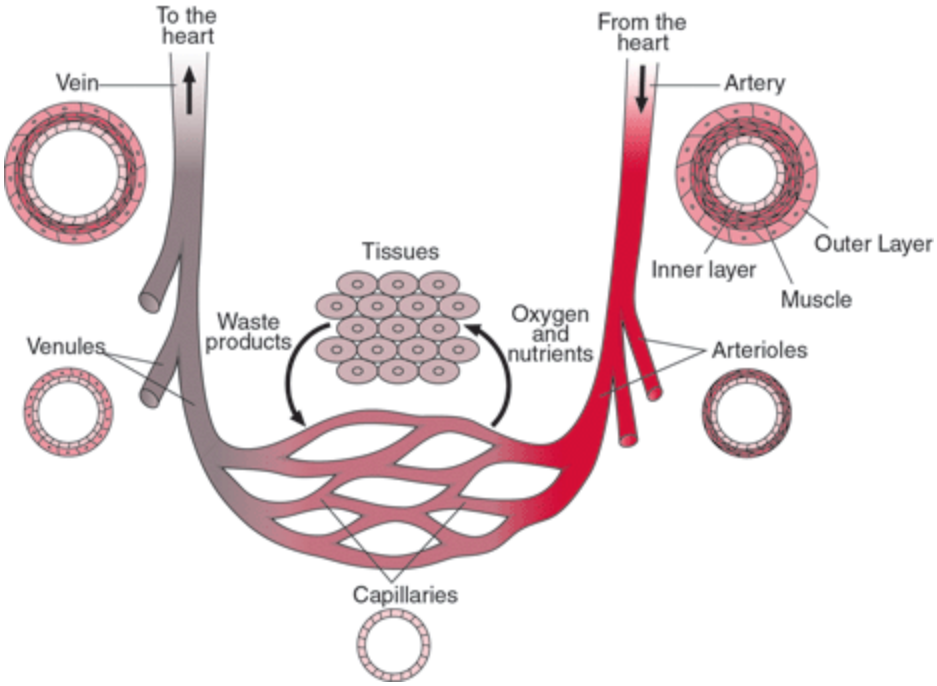

Figure 10. Blood flows from the heart through arteries which branch into arterioles which branch into capillaries, the smallest unit of blood vessel. Capillaries deliver oxygen and nutrients to the tissue cells in between the capillaries. Cross sections of each blood vessel are also shown, with capillaries having the thinnest walls. Adopted from [17].

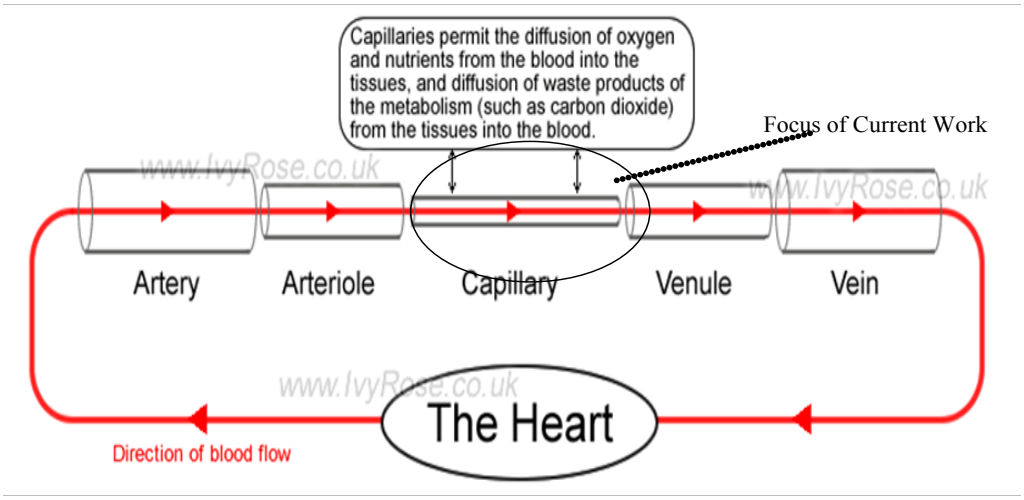

Figure 11. Circulation of blood indicating the flow through artery, arteriole, capillary, venule, and vein. The focus of the current work will be on the transport of O_2 from capillaries to the surrounding tissue. Adopted from [18].

Glucose is the fuel source of cellular respiration and is absorbed into the body from digested food. It is then stored as glycogen with the help of insulin in the liver. As needed, the glycogen becomes glucose again and is used by the cells [19]. For this study, it is assumed there is an adequate supply of glucose such that oxygen is the limiting factor of the cellular respiration process. The food energy digested is converted into work, thermal energy, or stored as fat (figure 12). Typically, most of the energy goes to thermal, used to maintain the body at 37 °C, but depends based on the amount of work, or physical activity, done. If more food energy is ingested than can be expended by the individual, then excess energy is stored, fat stores expand, and body weight is gained (figure 13).

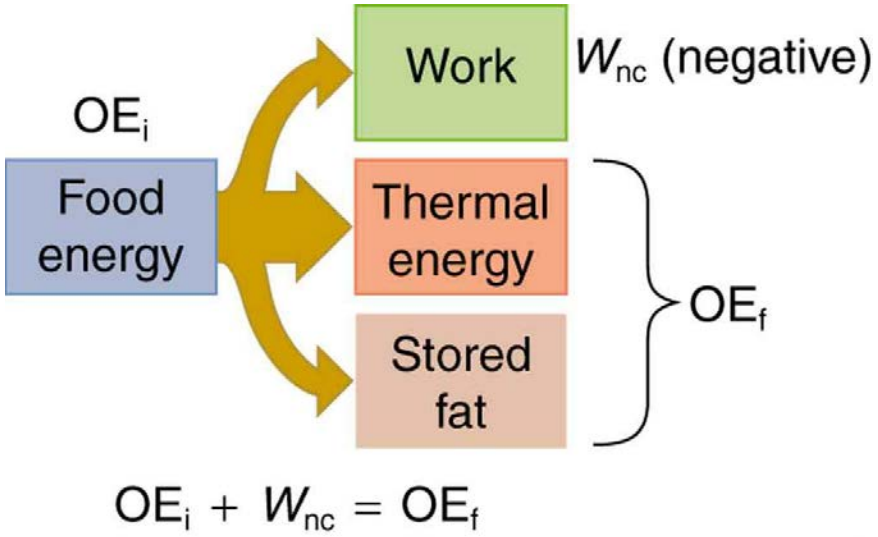

Figure 12. Energy released by oxidation of nutrients (about 80 W for a 70 kg person) is used to overcome heat loss (thermal energy), to supply work (e.g. climbing stairs), and part is stored as fat. The majority of energy goes to thermal energy, used to maintain the body's core temperature at 37 °C, but this may vary depending on physical activity. Adopted from [20].

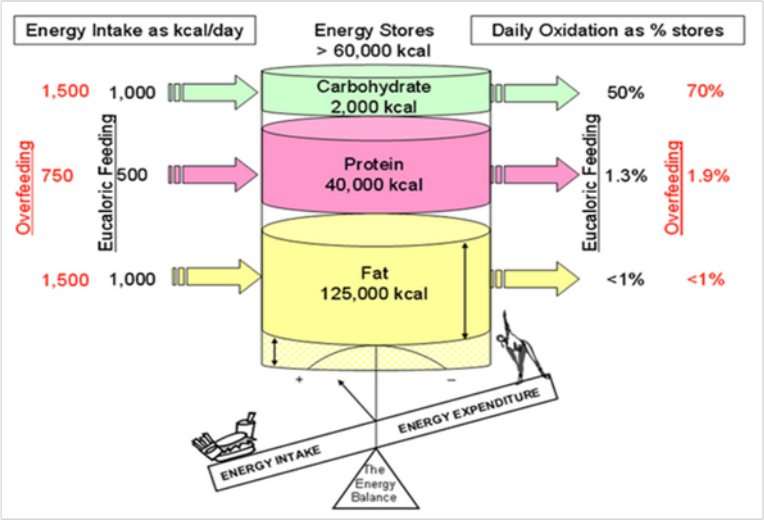

Figure 13. There exists a balance between energy intake and energy expenditure. When the intake exceeds expenditure, such as in the case of over feeding (red), the remaining energy is stored as body fat. The values presented are representative of a 70 kg man with 20% body fat on a 2,500 kcal/day diet. Adopted from [21].

Glucose levels do not remain constant in the blood throughout the course of the day. Immediately after meals, glucose levels are highest, while right before meals, glucose levels will be at their lowest (figure 14). In order to maintain a high enough level of glucose (or fuel) without constant feeding, the body stores some as glycogen after eating when glucose levels are high. As glucose levels decrease in between meals, the glycogen is converted back to glucose to be used in metabolism. A person who is diabetic will have trouble creating insulin, which is used to maintain the appropriate amounts of glucose in the blood. Therefore, a diabetic has to actively monitor their glucose intake [21].

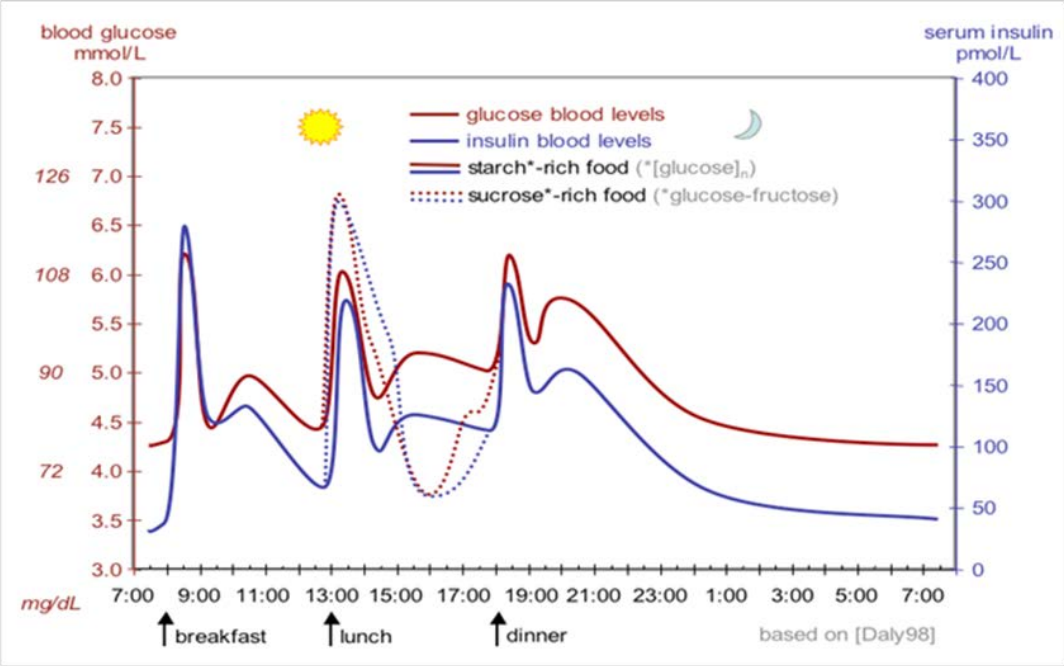

Figure 14. Glucose level increases after dinner and a part of it stored as glycogen in liver; as it gets oxidized its level falls down (in between meals); the glycogen is released as glucose to maintain the level in blood. Adopted from [21].

While the implications of considering the fuel type and amount may be important in real life situations of metabolism, this study assumes a steady state level of glucose such that a rich fuel mixture is obtained. In engineering, a rich mixture refers to the case when there is a higher level of fuel (glucose) than oxygen when compared to the stoichiometric case. This can be easily seen by comparing the chemical reaction equations for the oxidation of glucose (metabolism) as given by equation (2) for a stoichiometric reaction and equation (3) for a rich reaction.

$$C_6H_{12}O_6 + 6O_2 \rightarrow 6CO_2 + 6H_2O \qquad (2)$$

$$2(C_6H_{12}O_6) + 6O_2 \rightarrow 6CO_2 + 6H_2O \quad (3)$$

$C_6H_{12}O_6$ is the chemical formula for glucose. In a rich mixture, such as equation (3), there is more glucose (fuel) than necessary for the reaction, thus there will be leftover glucose and oxygen is the limiting factor as is assumed in the present study.

The flow of blood throughout the body is summarized by figure 15 with oxygen rich vessels represented in red and oxygen poor vessels represented by blue. The heart is located in the center and provides pumping work to move the blood, along with all it carries, throughout the vessels of the circulatory system. As mentioned previously, O_2 diffuses to and from capillaries into the blood stream and these capillaries are located at every organ including the lungs and skeletal muscle.

Currently, it is difficult to create cell cultures that are greater than a couple of layers due to the lack of oxygen reaching the bottom cells [22]. Furthermore, the field of

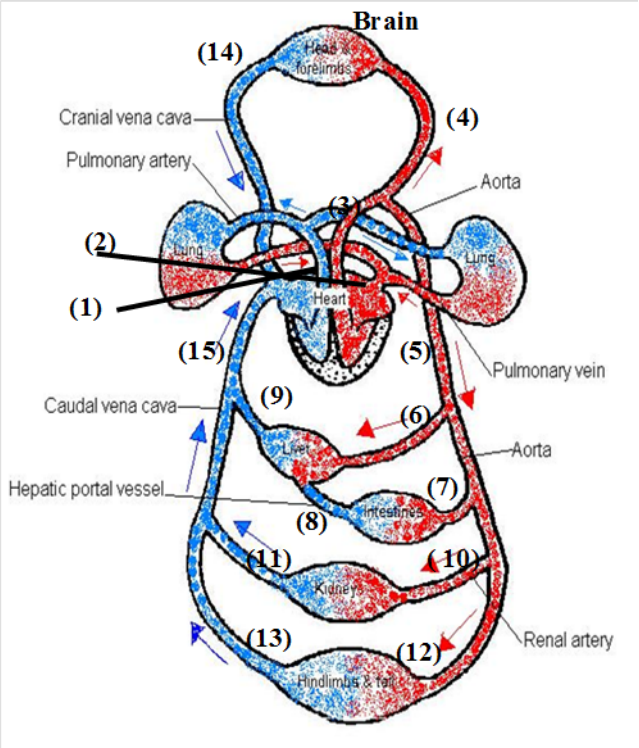

Figure 15. Path of blood flow throughout the body. (1): CO_2 rich blood leaving heart and entering lungs via pulmonary artery; (2): O_2 rich blood entering heart through pulmonary vein; (3): O_2 rich blood leaving heart and then branches into 2 parts; (4): O_2 rich blood to brain (upper part of body: superior); (5): O_2 rich blood to bottom part of body (inferior) via Aorta; (6): O_2 rich blood entering liver through Hepatic portal artery; (7): O_2 rich blood entering intestine to pick up nutrients such as sucrose; (8): Nutrient rich but O_2 poor blood entering liver through hepatic portal vein and mixing with O_2 rich blood in liver; (9) Blood with nutrients (e.g. glucose) and O_2 leaving liver; (10): O_2 rich blood to kidney via renal artery; (11): Kidneys remove toxic substance and excess water and O_2 poor blood leaves kidney via renal vein; (12): blood supply to hind limbs and tail; (13): Blood leaving limbs; (14): Blood leaving brain (superior vena cava); (15): Blood leaving from bottom part or inferior vena cava. Adopted from [23]. Note: Arteries are those blood vessels which carry blood away from heart and veins are those carrying blood into heart.

tissue engineering attempts to artificially create organs and three dimensional tissue cultures for use in research and transplants. In order to do this, cells are extracted from a

donor and a biological scaffold is built for these cells to grow and mature upon. Then oxygen and nutrients must be supplied. Cells continue to grow and dissolve the scaffold, allowing the tissue structure to be strong enough for continued development [24]. In both cases, a better understanding of the oxygen transport process will allow for more efficient oxygen delivery to keep cells alive.

In addition, Chief Perfusionist Gary Grist states that the microvascular delivery of oxygen is as important as the macrovascular theories of perfusion in regards to patient mortalities. He goes on to say that a greater understanding of the oxygen field at the tissue level, can lead to the development of better perfusion techniques by perfusionists like himself [25].

Finally, Warburg has identified that it is irreversible damage to the cells respiration process that causes cancer. This damage could be from respiratory poisons or a lack of oxygen [26]. In situations where it is the latter, a better understanding of the oxygen supply process could lead to preventative treatments in cancer medicine.

II.1 Krogh Model

In 1919, August Krogh developed a way to model capillaries as a cylinder for the purpose of oxygen transport through the tissue of a biological system [27]. This Krogh model has since been used by many scholars with a varying amount of modifications being made as needed [28-30]. Krogh modeled the capillary as a cylinder with another cylinder surrounding it representing the tissue (figure 16). He then calculated the partial pressure of oxygen as a function of the radius, making the assumptions that the axial

diffusion of oxygen through tissue could be neglected and the oxygen is transported evenly over all angles. This reduces the model to one dimension [27]. By joining many Krogh models, like building blocks, one begins to build an idealized organ (figures 17 and 18). The specific metabolic rate of the ideal organ will be the same as for the individual cylinders. While the Krogh model has been the basis for oxygen transport, it has also come under criticism for its simplicity and numerous assumptions [31].

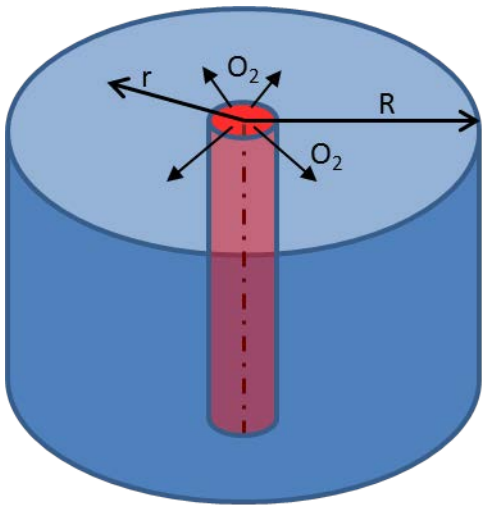

Figure 16. An illustration of a typical Krogh cylinder is shown. The central red cylinder is the capillary, supplying O_2 to the surrounding tissue, blue cylinder. Neglecting axial diffusion and assuming oxygen is transported evenly over all angles simplifies this into one dimensional geometry.

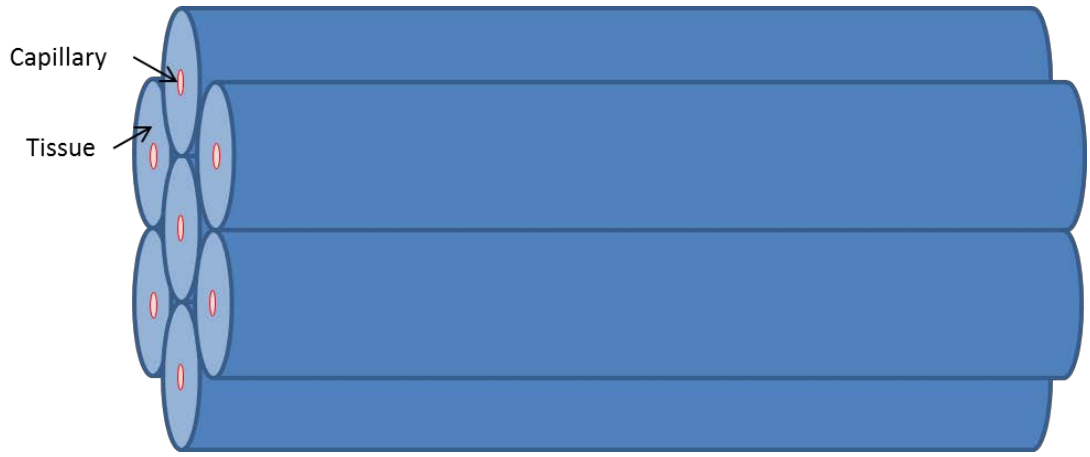

Figure 17. Seven Krogh model cylinders, each consisting of a capillary that is responsible for supplying the tissue surrounding it, are diagramed.

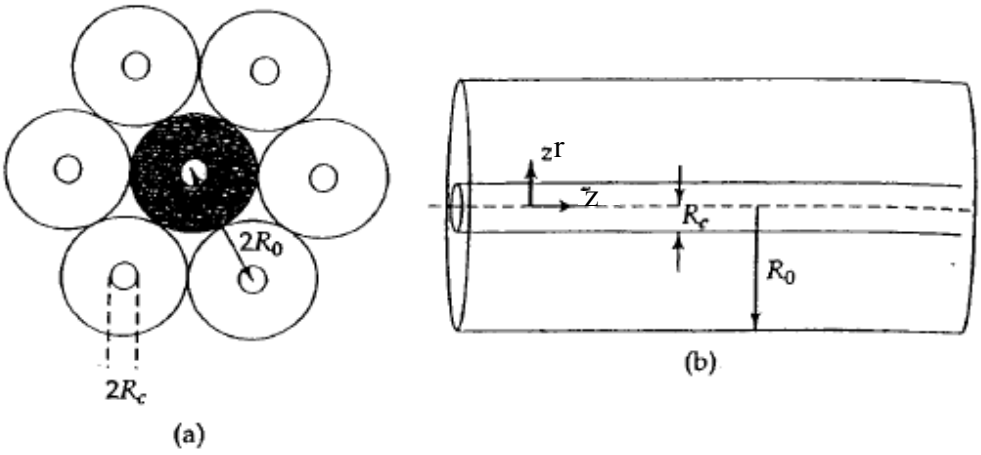

Figure 18. Krogh cylinder model. a) Seven Krogh cylinders with intercapillary distances of 2R0. b) A single Krogh cylinder with the capillary on the axis. Figure adopted from [32].

A solid cylinder model has since been proposed several times [33, 34] including Piiper and Scheid [35]. These model the tissue as a solid cylinder surrounded by

capillaries (figure 19). Piiper and Scheid compare the solid cylinder model to the Krogh model and determine that while both are suitable for modeling capillaries in muscle; the Krogh model is more appropriate. They determine this from experimental comparison and the physiological comparison of the geometries [35]. Piiper and Scheid did not initially account for the fact that capillaries do not completely surround the tissue and there is actually only a fraction of tissue surface area covered by the capillaries. They attempt to remedy this issue later in their study, but in a strange and slightly complex way different from the method used in this paper and to be discussed later.

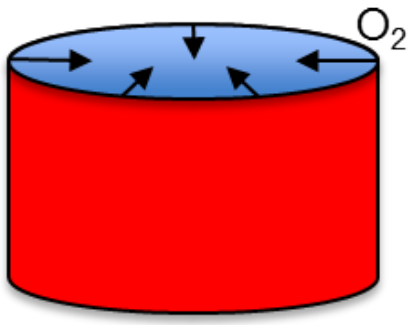

Figure 19. An illustration of the solid cylinder model is shown. The red ring surrounding the cylinder represents the capillaries, completely covering the tissue, blue core cylinder. O_2 is transported radially inwards.

In addition to whether a single capillary is located at the center of the geometry (on the axis) or multiple capillaries are located on the surface of the geometry, there are two different methods for calculating the source term. The first is to assume the consumption rate of oxygen is constant for all cells in the tissue, regardless of distance from the capillaries. This will be referred to as the uniform source (US) model here, but

it may also be called “zero order kinetics” and constant metabolic rate in biological literature. The second method models the oxygen consumption rate as function of the local O_2 concentration. Thus, cells further from the capillaries will have a lower local O_2 concentration and, consequently, a lower oxygen consumption rate when compared to the cells close to the capillaries. This will be referred to as the O_2 dependent (O2) model here, but may also be called “first order kinetics” or linear metabolic rate in biological literature. Typically in biology, including Krogh, the US model is used. Blum has compared the US model and O2 model but did so for general substrates and cannot be applied to the situation for O2 transport [Blum, 1960]. Fletcher also considered “first order kinetics” as well as Michaelis-Menten kinetics which are beyond the scope of the current work [Fletcher, 1978].

There are many causes that lead to oxygen deficiency in the body. The obvious causes include lack of oxygen an oxygen source from problems with air quality or breathing. If the partial pressure of oxygen in the air is reduced by either altitude or pollutants such as smoke or water, then the oxygen concentration will be reduced within the blood. Similarly, the total amount of oxygen in the bloodstream will be reduced if breathing is hindered and the lungs are incapable of filling with air. More specific causes of oxygen deficiency include a lack vitamin B12, affecting the creation of red blood cells, and defects in certain gene coding which can lead to the destruction of red blood cells [19]. Other possible causes are blood clotting, cell wall damage, and blockage from buildup of carcinogens.

The lethal corner is traditionally the portion of the Krogh cylinder that receives no oxygen; located towards the venous end of the capillary and further away radially from said capillary. Grist states that a greater understanding of the oxygen pressure field and the associated lethal corner "helps perfusionists to design successful perfusion strategies more apt to result in favorable outcomes for patients" [25].

Warburg found that it is the damage to cellular respiration that causes cancerous cell development. He claims that carcinogens, radiation, lack of oxygen and all other so called causes of cancer, are actually sources for the damage to cellular respiration [26]. This study examines the lack of oxygen component only and not the other sources as hypotheses are made with regards to cancer development.

II.2 Group Combustion

Similar to metabolism in biology is combustion in engineering; both processes utilize oxygen to burn fuel and produce energy. The biology literature uses Krogh cylinder model assumes uniform sink of oxygen and looks at oxygen transport process between oxygen carrying capillaries located at center of a cylinder with diffusion of oxygen progressing radially outward towards the surrounding tissue. On the other hand the engineering literature contains more exact models but with oxygen radially diffusing from cloud surface towards the axis of the cylindrical cloud.

Similar to metabolism in biology is combustion in engineering; both processes utilize oxygen to burn fuel and produce energy. Combustion is a series of exothermic reactions involving a fuel and oxidant, which may be oxygen. One example is the

burning of a spray of liquid fuel drops in air. When analyzing a cloud of closely gathered fuel drops, it becomes necessary to treat them with group combustion theory. Interactions between drops prevent treating the cloud as a sum of the individual drops. These interactions affect many aspects of the combustion process as the drops will be competing for oxygen amongst themselves [11].

Combustion is a series of exothermic reactions involving a fuel and oxidant, which may be oxygen. For example, the combustion of a single carbon particle is given as

$$C + O_2 \rightarrow CO_2 \tag{4}$$

For this reaction the heating value (HV), or the amount of heat released per unit mass of fuel, is about 32,800 kJ per kg of carbon. In comparison, the HV of glucose (from equation (2)) is about 15,630 kJ per kg glucose [36].

Figure 20 illustrates the burning of a single particle utilizing the resistance concept. O_2 is consumed and CO_2 is produced and both processes face chemical and diffusion resistances. Focusing on the O_2 transport, $Y_{O2\infty}$ is the ambient mass fraction of O_2 (g O_2 / g air) far from the burning particle, Y_{O2w} is the mass fraction of O_2 at the wall of the particle, and the Y_{O2} inside the particle is zero. $\dot{m}_{O2}''$ is the mass flow rate of oxygen per unit surface area of the particle and is the process of interest. There are two resistances controlling the process: the diffusion resistance, $R_{diff,O2}$, and the chemical resistance, $R_{chem,O2}$. When $R_{diff,O2}$ is very small, then the process becomes controlled by

the chemical kinetics and Y_{O2w} equals $Y_{O2\infty}$. On the other hand, if $R_{chem,O2}$ is small, then the process is diffusion controlled (as is assumed in the present study) and Y_{O2w} equals zero.

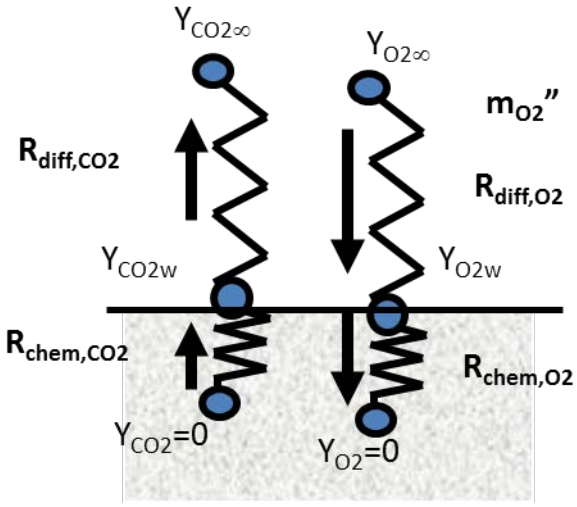

Figure 20. An Illustration of the resistance method for the burning of a single particle is shown. The mass flow rate of oxygen per unit surface area of the particle, m, is a function of both the diffusion resistance, R, and the chemical resistance, R. When diffusion resistance is low, the process is chemically controlled; while if the chemical resistance is low, the process is diffusion controlled (as assumed in the present study) [11]. Adopted from [11].

Now consider a group of particles (or a spray of liquid fuel drops) instead of just one. When analyzing a cloud of closely gathered particles, it becomes necessary to treat them with group combustion theory, as described previously in the candle example. Interactions between drops prevent treating the group as a sum of the individual particles. These interactions affect many aspects of the combustion process as the drops will be competing for oxygen amongst themselves [11].

The group combustion number, G, is the characteristic O_2 consumption rate divided by O_2 transport rate to the cloud. G is proportional to fuel volume fraction times the cloud surface area divided by the particle surface area. Expressing the volume fraction as fuel particle size and number density yields

$$G = 2\pi n d_{particle} R^2 \tag{5}$$

where n is the particle number density, $d_{particle}$ is the diameter of the particle, and R is the cloud radius. Since n and $d_{particle}$ are typically constant, G is function of R only and becomes a measure of the size of the cloud [Annamalai, something something].

Returning to the group, or cloud, of particles, in which the particles are densely packed, the specific burn rate (SBR) can be plotted versus the size of the cloud, or the G number (figure 21). SBR is simply SERR divided by the HV. At small cloud sizes, isometric law applies and SBR is relatively constant as G increases (region A of figure 21). However, as cloud size continues to increase, the SBR decreases (regions B and C of figure 21). Large clouds have an aerobic shell receiving oxygen, and an anaerobic core which receives no oxygen (region D of figure 21). CO_2 and the bulk gas temperature increase at the inner core with increasing cloud size.

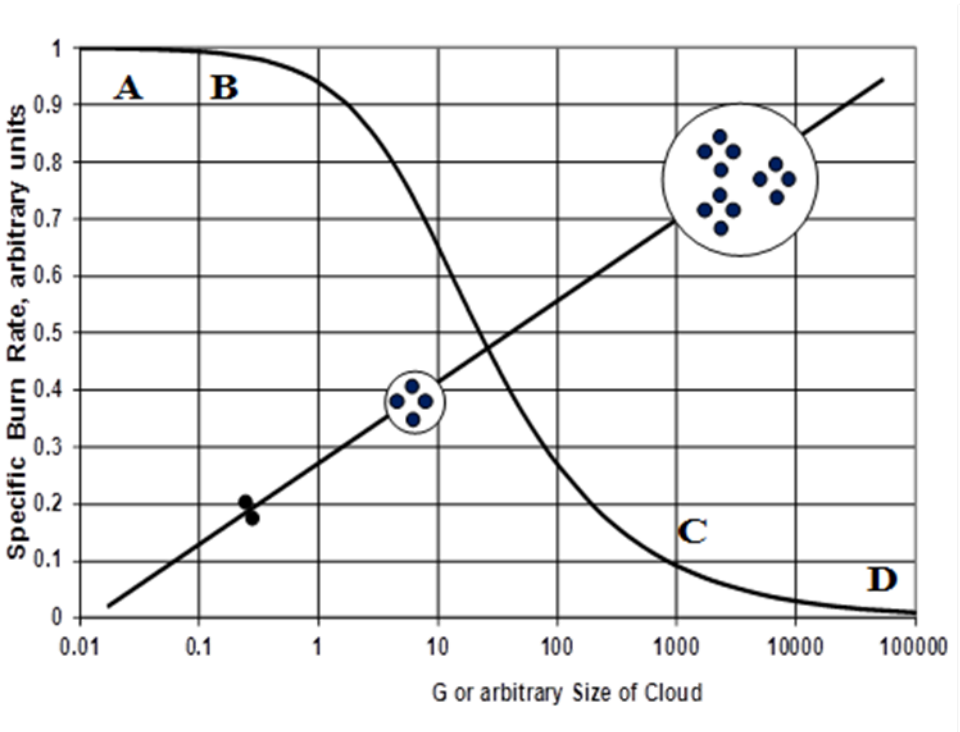

Figure 21. Specific burn rate in arbitrary units versus the arbitrary size of the cloud, or G number (described in the text), is plotted. Region A represents small cloud sizes which follow isometric law and specific burn rate is constant. As cloud size increases, it enters region B and follows non-isometric law, or allometric law. Regions C and D represent very large cloud sizes which form an aerobic shell, where particles receive oxygen, forms around the outside, and an anaerobic core, where no oxygen reaches. Figure adopted from [11].

The results of figure 21 are incredibly similar to the work done by Singer in a separate study on the specific metabolic rate versus the radius of a tissue sphere (figure 22). Singer's qualitative plot shows the influence of sample size on metabolic rate. He modeled the tissue as spheres with an aerobic shell of constant thickness, δ, around the outside of an anaerobic core. The anaerobic core was assumed to use glycolysis with an SMR of 10% compared to the aerobic tissue. As he increased the size of the sphere, the

radius of the anaerobic tissue grew, but the thickness of the aerobic shell was kept constant. He found that small tissue sizes demonstrated isometric behavior as they grew, while larger tissues followed non-isometric behavior [Singer, 2006]. Since whole body metabolic rate is a sum of metabolic rate of small to large organs, then whole body specific metabolic rate must follow a similar behavior (figure 23). As mentioned, there is a striking similarity between figure 21 and figure 22, which raises interest as to why this is.

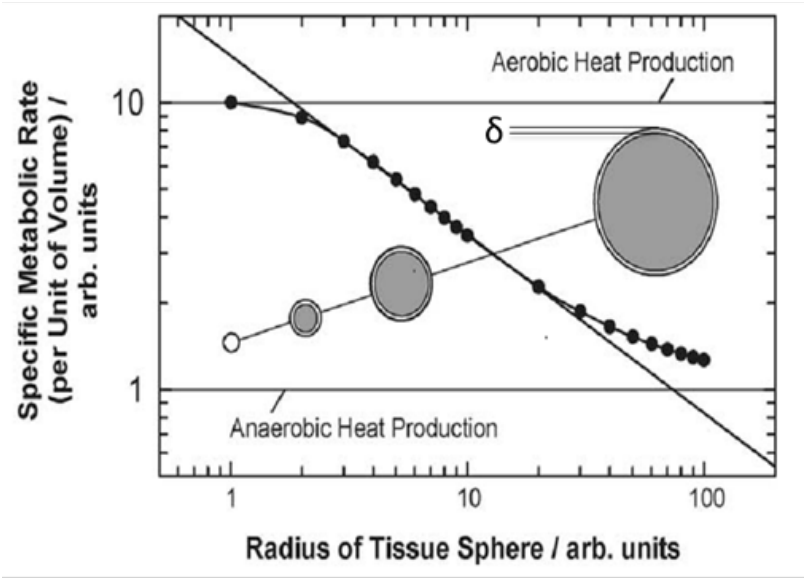

Figure 22. Singer developed this qualitative plot showing the influence of sample tissue size on the metabolic rate for spheres. Tissue spheres consist of an anaerobic core, with a specific metabolic rate of 10% compared to the aerobic shell of constant thickness, δ, surrounding the anaerobic core. Small tissue sizes exhibit isometric behavior, whereas larger tissue sizes exhibit non-isometric behavior. Adopted from [12].

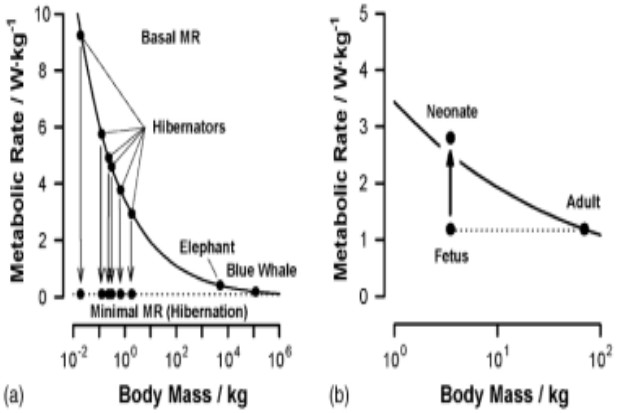

Figure 23. As body mass increases, metabolic rate per unit mass of body decreases following organ behavior; a large organ has lower specific metabolic rate compared to smaller organs. Figure adopted from [12].

Figure 24 illustrates the group behavior of cells within a spherical / cylindrical tissue of radius R. The core (large distance from capillary) has lower oxygen concentration while cells near capillaries receive abundant oxygen.

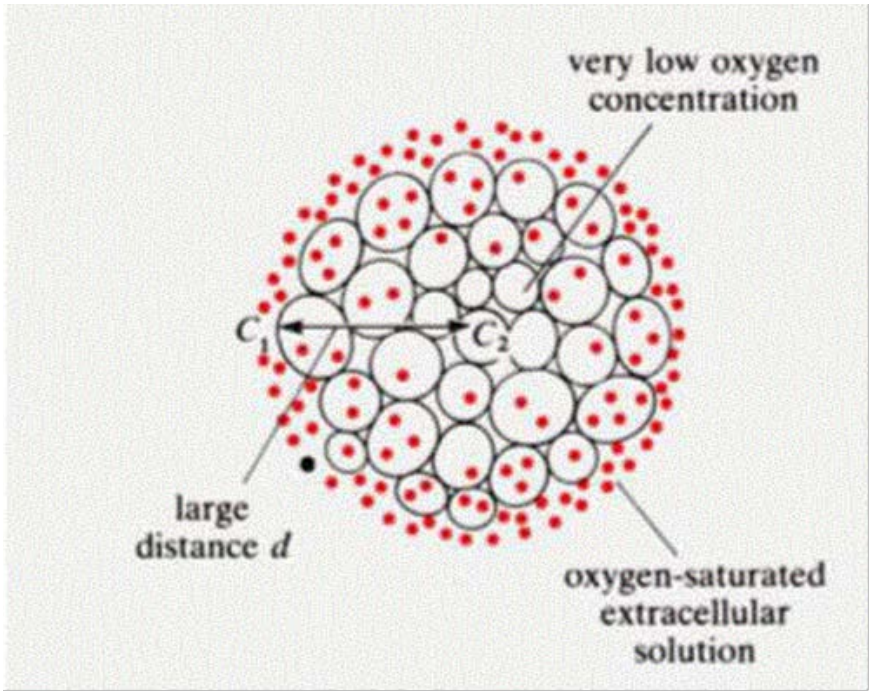

Figure 24. C1 is concentration of dissolved O2 in the IF near capillary-IF interface while C2 is concentration far from interface. Smaller the "d", larger the gradient, faster the O2 transfer. The red spots represent dissolved O2. Sometimes the inner core may not receive enough O2; if so, it is called anaerobic core. Figure adopted from [37].

An important difference between biology and engineering is the use of partial pressure. In biology partial pressure is used as manner of conveying the oxygen concentration either in the blood or tissue. On the other hand, in engineering, partial pressure only applies to gasses such as the partial pressure of oxygen in the air. The partial pressure can then be related to the mass fraction of a gas in a liquid such as blood by Henry's law. This law states that the mass fraction is directly proportional to the partial pressure and can be easily explained using soda as an example. By increasing the pressure of the air surrounding the beverage, one can dissolve more carbon dioxide into

the carbonated beverage. Conversely, when the surrounding air pressure is decreased, the dissolved carbon dioxide diffuses out of the soda. This same principle applied between the air in the lungs and surrounding blood of the capillaries, thus the origin of the use of partial pressure as a way to measure oxygen concentration.

In the present study, the biological cells are compared to particle drop characteristics. The drops are the living cells and the air surrounding the drops now becomes the interstitial fluid with an oxygen source, capillaries, on the outside. Each of the cells is like oxygen sinks and contributes to the local oxygen concentration levels.

II.3 Allometric Laws

Allometric laws are commonly used in the biological community to relate two parameters in various animals, and were described previously by equation (1). Allometric laws can be sorted into the two categories of interspecific allometry and intraspecific allometry. The former applies to the relationship between different species of animals while the latter describes the relationship between the organs of a single species [36].

The general form of allometric equations is given as

$$y = a\, x^{b} \tag{6}$$

where y is the parameter of growth in biology dependent on x which is typically a parameter of size such as body or organ mass. The constant a is the allometric constant

while b is the allometric exponent and is more important. Biology literature compares parameters of growth in living organisms using allometric laws. Equation (1) gives the allometric law for specific metabolic rate of organ k vs the mass of organ k. Converting equation (4) to its logarithmic form yields

$$\ln(y) = \ln(a) + b\ln(x) \tag{7}$$

Thus, by plotting ln(y) vs ln(x) the slope, b, can be determined as well as the y-axis intercept, ln(a) [36].

In 1932, Max Kleiber developed a relationship between an animal's body mass and its metabolic rate. In 1961, Kleiber published all his findings in his book, The Fire of Life. He found the exponential power to be 0.739, which he rounded to 0.75, leading to the terming of his relationship as the three-fourths law or Kleiber's law [38]. Kleiber made this approximation because it was a much simpler calculation at a time when there were no pocket calculators available [39].

In 1984, Schmidt-Nielsen continued on Kleiber's work as he gathered data on different groups of animals including mammals, reptiles, birds, amphibians and fish. His comparative analysis of a wide variety of data showed that while some species deviated from the typical three-fourths power, most species still fell into this range when comparing body mass to metabolic rate [39].

Since Kleiber, there have been many studies and theories about this allometric law as well as other allometric laws. Silva et al. gathered each theory looking at them

critically in 2006. They concluded for metabolic rates, there is no one universal allometric exponent but they believe "there seems to be a common origin for the allometric scaling laws of metabolic rates" [40]. In other words, there is believed to be a single reason for the allometric behavior in biological systems.

Singer continues to look at the works of Schmidt-Nielsen and Kleiber as he looks toward oxygen availability to explain the reason for metabolic rate decrease with an increase in body size. Stating that in larger animals, there is a larger amount of tissue between capillaries, Singer claims the living cells will decrease their metabolism to accommodate the lower supply of oxygen. In contrast, smaller animals will increase their cellular metabolism so as to decrease the higher oxygen concentration and reduce the toxic effects of excess oxygen. Therefore, the cells are actually using the oxygen concentration to identify whether they are in a large or small organism [12].

To summarize, biology models typically presume an uniform source within the tissue. We will analyze and compare both uniform source (US) and O_2 dependent source (O2) models. The Krogh model will be adopted to estimate energy release rate. Also, the Krogh model does not include capillary diffusion limits, which will be imposed here. There is currently no work on energy release rate based on O_2 diffusion limiting the energy release rate of cells. Group combustion solutions are based on models for which O_2 is supplied from the surface; these need modifications for when O_2 is supplied from the center. These issues will be addressed by the present study.

CHAPTER III

OBJECTIVES AND TASKS

The ultimate goal of this project is to gain a better understanding of oxygen transport as related to metabolism in biological systems by using an "unconventional" method which is not normally associated with biology. This is the first time combustion concepts have been applied to metabolism. The extensive group (oxygen deficient) combustion literature in engineering for slab, cylinder and sphere containing millions of micro-oxygen sinks (micron sized carbon particles) is applied to metabolism in organs by replacing carbon particles with metabolic cells which serve as oxygen sinks and compared and validated with a previously accepted biological model for the oxygen transport problem in a biological system. However group combustion models in engineering deal with oxygen transfer from surface of the cloud of slab, cylinder and sphere with O2 radially transport occurring towards the core.

The current objective is to use the group combustion (also known as oxygen deficient combustion) concept for cylindrical geometry , modify it for application to vital organs (brain, kidney, liver, heart), estimate oxygen supply and energy release rate and compare the results with a traditional biological model, the Krogh cylinder, as well as experimental data. The problem assumes a steady state, diffusion controlled process In order to achieve the objective, the following tasks must be performed.

1. Review biology literature, gather biological data and information for use in the subsequent models.

2. Create mathematical models to simulate the diffusion of oxygen from capillaries through the tissue for generalized geometry (slab, cylinder and sphere) different geometries and conditions.
3. Modify the group combustion model and obtain solutions with oxygen supply either from capillaries on surface (COS) or from capillary on axis of cylinder (COA).
4. Compute the oxygen concentration at the capillary (CAP) -interstitial fluid (IF) interface.
5. Obtain oxygen profiles within IF and specific metabolic rates for each of the models.
6. Compare the oxygen concentration profiles for COA and COS
7. Define a lethal corner when oxygen concentrations drop below the level necessary for complete cell functioning and obtain lethal volume fraction defined as ratio of lethal volume to total volume of organ.
8. Conduct parametric studies to simulate possible biological and environmental changes.
9. Determine the validity of the group combustion concept by comparing with experimental data. If valid, attempt to link group combustion to intraspecific allometry.

III.1 Significance

The necessity of this research is evident in the emerging biological technology including tissue engineering, perfusion techniques and its relation to patient mortalities, and myriad of diseases including cancer attributed to oxygen deficiency [26]. The oxygen deficiency is related to cancer cell growth according to Warburg [26].

CHAPTER IV

MATHEMATICAL MODELING

This chapter details the mathematical modeling and formulation used in the analysis of oxygen transport from the capillaries to the metabolic cells. First, saturation curves are modeled for hemoglobin and myoglobin based on thermodynamics. Then, the formulation of mathematical models used is explained in detail. Next, the calculation of metabolic rate for the different models is covered. Finally, the lethal volume is defined and discussed.

IV.1 Blood Oxygen Content, Oxygen Saturation, and Saturation Curves

Fresh air enters the lungs with a partial pressure of oxygen at 160 mmHg. The moisture of the lungs causes this to drop to 104 mmHg once it reaches the alveoli (small air sacks in the lungs). The alveoli are surrounded by capillaries which are only two microns away from the alveoli. Blood enters from the arterial side of the capillaries surrounding the alveoli with a partial pressure of oxygen at 40 mmHg and it exits at the venous end with a partial pressure of oxygen at 104 mmHg [41].

The O_2 transported from alveoli enters blood as dissolved O_2 (a physical process). The dissolved O_2 then reacts with Hb in red blood cells of blood which oxidizes to HbO_2, $Hb(O_2)_2$, $Hb(O_2)_3$, and $Hb(O_2)_4$. Generally it is denoted as $Hb(O2)_n$ where "n" ranges from 1 to 4. Hence, dissolved oxygen (called aqueous O_2) decreases as more oxidized Hb (called chemical O_2) appears; but it is made up by transport of

oxygen from alveoli thus maintaining complete thermodynamic equilibrium (physical and chemical).

IV.1.1 Mass Fraction and Partial Pressure

The oxygen transported from alveoli dissolves into the blood (a physical process) by Henry's law:

$$[O_2(aq)],\ \frac{\text{mL of } O_2}{\text{L of Blood}} = H_{O2}\ p_{O_2}(\text{mm Hg}) \tag{8}$$

where H_{O2} is Henry's constant for O_2 dissolving in a liquid , p_{O2} is the partial pressure of oxygen in mm of Hg , and $[O_2(aq)]$ is the amount of aqueous oxygen in mL (Typically CST standard) per L of blood. Henrys constant, α_{O2} or H_{O2}, equals 0.031 mL of O_2 per mm of Hg per unit L of blood. To convert from pO_2 (mmHg) to the mass fraction (g O_2 / g blood), the ratio of oxygen density over blood density is multiplied by $[O_2(aq)]$ as given by

$$Y_{O2} = [O_2(aq)]\ \frac{\rho_{O2}\left(\frac{\text{kg}}{\text{mL of CST gas}}\right)}{\rho_{bl}\left(\frac{\text{kg}}{\text{L}}\right)} = H_{O2}\left(\frac{\text{mL of } O_2}{\text{L of blood} * \text{mm Hg}}\right) p_{O_2}\ \frac{\rho_{O2}}{\rho_{bl}} \tag{9}$$

where Y_{O2} is the mass fraction of O_2 in g O_2 per g blood, ρ_{O2} is the density of O_2 (at CST standard) and equals 0.001423 kg/L or 1.423×10^{-6} kg/mL or 1.423 mg per mL of O_2 at CST, and ρ_{bl} is the density of blood and equals 1.060 kg/L. By combining the constants, equation (9) simplifies to

$$Y_{O2} = [O_2(aq)]\frac{\rho_{O2}}{\rho_{bl}} = H_{O2}\ p_{O_2}\ \frac{\rho_{O2}}{\rho_{bl}} \tag{10}$$

$$Y_{O2} = 0.031\left(\frac{\text{mL of } O_2}{\text{L of blood mm Hg}}\right) p_{O_2}(\text{mm Hg}) \frac{1.423 \times 10^{-6}\left(\frac{\text{kg}}{\text{mL of CST gas}}\right)}{1.06\left(\frac{\text{kg}}{\text{L}}\right)} \tag{11}$$

$$= 4.162 \times 10^{-8}\ \frac{\text{kg of } O_2}{\text{kg blood*mm Hg}}\, p_{O_2}(\text{mm Hg})$$

$$Y_{O2} = \gamma_{O2} * p_{O2} \tag{12}$$

where

$$\gamma_{O2} = H_{O2}\ \frac{\rho_{O2}}{\rho_{bl}} \tag{13}$$

Here, γ_{O2} is Henry's constant times the ratio of densities and is equal to 4.18E-08 g of O_2 per g blood per mm of Hg with Henry's constant included. Using equation(10), it is easy to go from partial pressure to mass fraction and thus, the dissolved oxygen mass fraction in the capillary, $Y_{O2,cap}$, can be calculated. When converting from pO_2 to Y_{O2} or vice versa using equation (12), the solubility is presumed to be the same everywhere.

IV.1.2 Saturation Curves

Saturation curves for Hb and Mb were developed based on thermodynamics. Each Hb molecule can bind with up to four O_2 molecules with each additional O_2 increasing Hb's affinity for another O_2. The chemical reactions are given as

$$\begin{aligned} &Hb + O_2 \rightleftharpoons HbO_2 \\ &HbO_2 + O_2 \rightleftharpoons Hb(O_2)_2 \\ &Hb(O_2)_2 + O_2 \rightleftharpoons Hb(O_2)_3 \\ &Hb(O_2)_3 + O_2 \rightleftharpoons Hb(O_2)_4 \end{aligned} \tag{14}$$

where O_2 molecules are added one at a time. Equilibrium is written as

$$K_n^{\,0} = \frac{X_{Hb\text{-}nO2}}{X_{Hb}\; X_{O2(aq)}^{\;n}} \tag{15}$$

Where n= 1, 2, 3, and 4 and K_n is dimensionless equilibrium constant. With Henry's constant it can be written in terms of partial pressure

$$K_n{}^0(\text{dimensionless}) = \frac{X_{\text{Hb-nO2}}}{X_{\text{Hb}}\, X_{O2(aq)}} = \frac{[\text{Hb - (O2)}_n][\text{N}]^n}{[\text{Hb}][\text{O2(aq)}]^n} = \frac{X_{\text{Hb-nO2}}[\text{N}]^n}{X_{\text{Hb}}\, H_{O2}{}^n p_{O2}{}^n} = \frac{[\text{Hb - (O2)}_n][\text{N}]^n}{[\text{Hb}][\text{O2(aq)}]^n} \tag{16}$$

$$K_n{}^0 = \frac{[\text{Hb-(O2)}_n][\text{N}]}{[\text{Hb}]\, H_{O2}{}^n\, p_{O2}{}^n} \tag{17}$$

Define

$$K'_n{}^0 = \frac{K_n{}^0 H_{O2}{}^n}{[\text{N}]},\ \frac{1}{(\text{mm Hg})^n} \tag{18}$$

Then equilibrium relation (15) becomes

$$K'_n{}^0 \left(\frac{1}{\text{mm Hg}^n}\right) = \frac{[\text{Hb-(O2)}_n]}{[\text{Hb}]\, p_{O2}{}^n},\ p_{O2} \text{ in mm Hg} \tag{19}$$

Here, $K^0{}_n$', where n=1-4, are the dimensional equilibrium constants and are affected by the pH, temperature, and various inhibitors. Note that units for Kn' is 1/ (mm Hg} ^{n}.

For e.g. with n=1, $\text{Hb} + \text{O}_2 \rightleftharpoons \text{HbO}_2$,

$$K'_1{}^0 \left(\frac{1}{\text{mm Hg}}\right) = \frac{[\text{Hb-O2}]}{[\text{Hb}]\, p_{O2}} \tag{20}$$

Similarly one can define for all other three reactions.

$$K'^{0}_{2}\left(\frac{1}{mm\,Hg^{2}}\right)=\frac{[Hb(O_2)_2]}{[Hb]p_{O2}{}^{2}}$$

$$K'^{0}_{3}\left(\frac{1}{mm\,Hg^{3}}\right)=\frac{[Hb(O_2)_3]}{[Hb]p_{O2}{}^{3}} \qquad (21)$$

$$K'^{0}_{4}\left(\frac{1}{mm\,Hg^{4}}\right)=\frac{[Hb(O_2)_4]}{[Hb]p_{O2}{}^{4}}$$

One can solve for [Hb-O_2] , [Hb-O_2]$_2$….in terms [Hb] and pO_2. Subject to conditions total [Hb] must be equal to a sum of Hb, Hb in oxidized Hb, one can obtain [Hb] under chemical equilibrium. See Technical report on Bio-burn by Kalyan Annamalai (2014).

Hb saturation is defined as the actual amount of O_2 bound to Hb divided by the total possible amount of O_2 that could be bound to Hb. This is mathematically explained by equation (22). Here, K^0_n', where n=1-4, are the dimensional equilibrium constants and are affected by the pH, temperature, and various inhibitors.

$$S_{O2,Hb}=\frac{\text{actual } O_2}{\text{maximum } O_2}=\frac{1*[HbO_2]+2*[Hb(O_2)_2]+3*[Hb(O_2)_3]+4*[Hb(O_2)_4]}{4*[Hb_{total}]} \qquad (22)$$

Using chemical equilibrium, equation (23) is derived, of which the full derivation, as developed by Atkins and De Paula, can be found in Appendix B [42].

$$S_{O2} = \frac{K^0_1'(p_{O2}) + 2K^0_1'K^0_2'(p_{O2})^2 + 3K^0_1'K^0_2'K^0_3'(p_{O2})^3 + 4K^0_1'K^0_2'K^0_3'K^0_4'(p_{O2})^4}{4\left\{1 + K^0_1'(p_{O2}) + K^0_1'K^0_2'(p_{O2})^2 + K^0_1'K^0_2'K^0_3'(p_{O2})^3 + K^0_1'K^0_2'K^0_3'K^0_4'(p_{O2})^4\right\}} \quad (23)$$

The equilibrium constants are given by Atkins and De Paula and with a known pO_2 value, the saturation percent can easily be calculated [42].

Mb (smaller molecule with M=16,000 g/mol) is essentially one fourth of Hb (large molecule with M=64,000 g/mol) and can only bind one O_2 molecule at a time. The resulting chemical reaction is given as

$$Mb + O_2 \rightleftharpoons MbO_2 \quad (24)$$

and the resulting saturation percent is simply

$$S_{O2,Mb} = \frac{K'_{Mb}(p_{O2})}{\left\{1 + K'_{Mb}(p_{O2})\right\}} \quad (25)$$

where K'_{Mb} is the equilibrium constant for Mb. The blood with dissolved O_2 and $Hb(O_2)_n$ in equilibrium reaches the tissue via capillaries, dissolved O_2 is then transferred across the capillary (Cap) walls to interstitial fluid (IF) and finally to metabolic cells for use in oxidation of nutrients with O_2. As dissolved O_2 concentration in capillary decreases (thus decreasing mass fraction of O_2 or partial pressure), the oxygenated Hb compound discharges O_2 to maintain chemical equilibrium. If this tissue is skeletal

muscle or heart tissue, then Mb in the IF captures the O_2, forms MbO_2 compounds, reach chemical equilibrium within IF; here MbO_2 is transported due to diffusive processes. Thus Mb results in increased transport rate of O_2 to cells.

IV.2 Mass Transfer Across Capillaries

The O_2 rich blood travels from the heart to several organs via the aorta. The aorta branches into several arterioles near the organ of interest and further branches out as pre-capillaries and capillaries supplying oxygen to metabolic cells in the space between capillaries (figure 25 and figure 26).

In biology, permeability, K' (cm/s), is used to describe the transport process. Consider the oxygen consumption rate per unit area given by

$$\dot{m}_{O2}''\left(\frac{g}{cm^2}\right)=\frac{(\rho D)_{cap}}{\delta_{cap}}\left(Y_{O2,cap}-Y_{O2,cap\text{-}IF}\right)=\rho K'_{cap}\left(Y_{O2,cap}-Y_{O2,cap\text{-}IF}\right) \tag{26}$$

where D is the diffusion coefficient in cm^2 per second, δ_{cap} is the capillary thickness in cm, and K'_{cap} is the capillary permeability coefficient given by

$$K'_{cap}=\frac{D_{cap}}{\delta_{cap}} \tag{27}$$

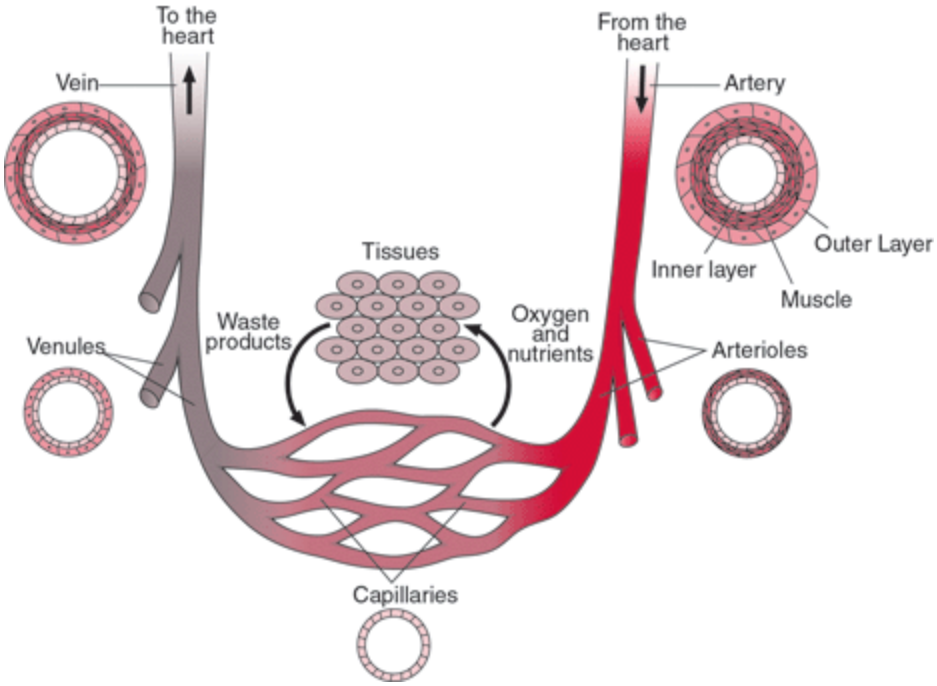

Figure 25. Blood flows from the heart through arteries which branch into arterioles which branch into capillaries, the smallest unit of blood vessel. Capillaries deliver oxygen and nutrients to the tissue cells in between the capillaries. Cross sections of each blood vessel are also shown, with capillaries having the thinnest walls. Adopted from [17].

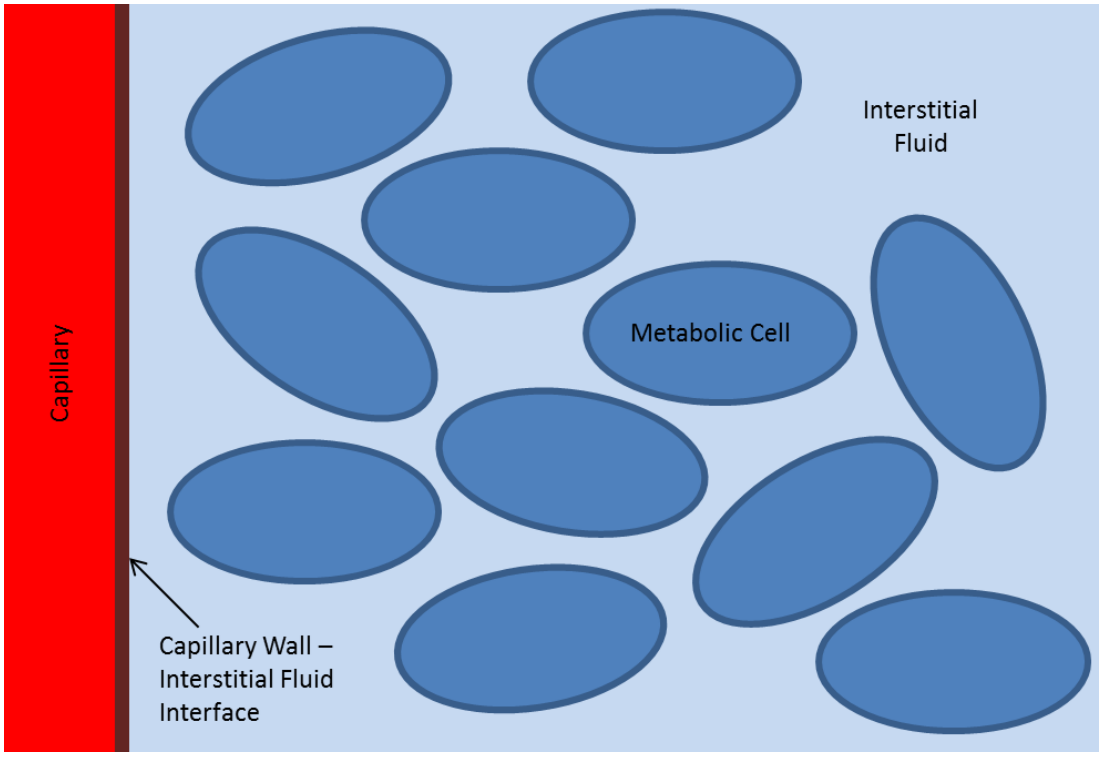

Figure 26. Illustration of capillary supplying oxygen to tissue consisting of metabolic cells suspended in interstitial fluid.

IV.3 Intercell Spacing and Number Density of Cells

Another property to be used in the forthcoming models is the number density of cells, n, given in cells per cm^3 of tissue. Considering a cube with sides ℓ, and one cell with diameter d_{cell} located on each corner, there is a total of eight cells. From this, n can be calculated as

$$n = \frac{\text{No of cells}}{\ell^3} = \frac{8}{\ell^3} \tag{28}$$

and ℓ, which is also the distance from the center of one cell to the next, must be

$$\ell = \frac{2}{n^{(1/3)}} \tag{29}$$

This is also called the intercellular spacing and must be greater than the radius of two adjacent cells. If the cells are of equal size, as is assumed here, then the intercellular spacing must be greater than the diameter of the cell. Thus,

$$\frac{\ell}{d_{cell}} >> 1, \text{ or } \left(\frac{2}{d_{cell}\ n^{(1/3)}}\right) >> 1 \tag{30}$$

Not only does this assure that cells are not overlapping, but it also plays a role in the mass transfer boundary layer. The boundary layer is typically about the same length as the radius of the particle, or in this case, the cell. Therefore, to avoid boundary layer issue, ℓ should be at least twice as large as the cell diameter.

IV.4 Conservation Equations

Following engineering literature on oxygen deficient or group combustion [11], the differential equation governing the transport of O_2 through the tissue is (see figures 27, 28, and 29)

$$\frac{1}{r^s}\frac{d}{dr}\left(r^s \frac{dY_k}{dr}\right) = -\frac{\dot{m}_k'''}{(\rho D)_{eff}} \tag{31}$$

where, r is the distance from the center of the geometry, s is the geometric constant as described below, Y_k is the mass fraction of species k, $\dot{m}_k'''$ is the volumetric mass flow rate of species k, and $(\rho D)_{eff}$ is the effective density and diffusion coefficient. The geometric constant s will be 0, 1, or 2 for slab, cylinder, or sphere geometries respectively. Oxygen is the species of interest here, but carbon dioxide may also be used.

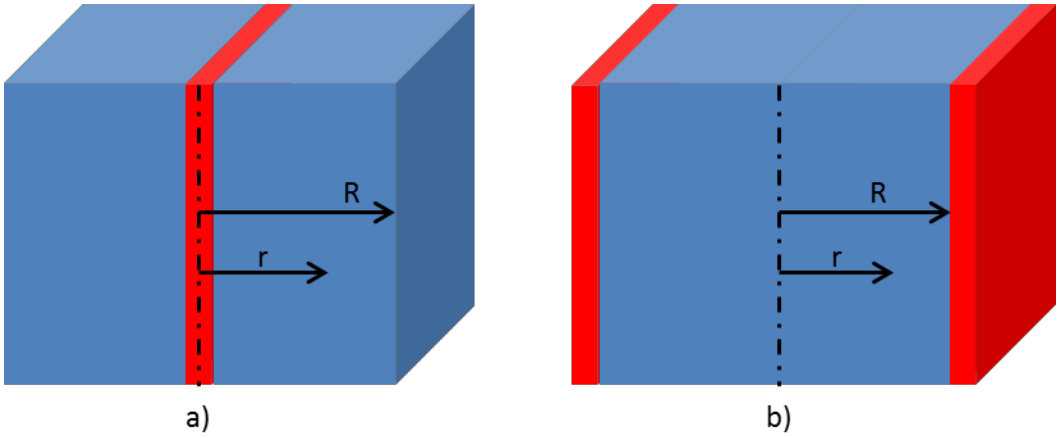

Figure 27. Illustrations of a) the COA model and b) the COS model, both in slab geometry. Red slabs represent the capillaries while the blue slabs represent the tissue.

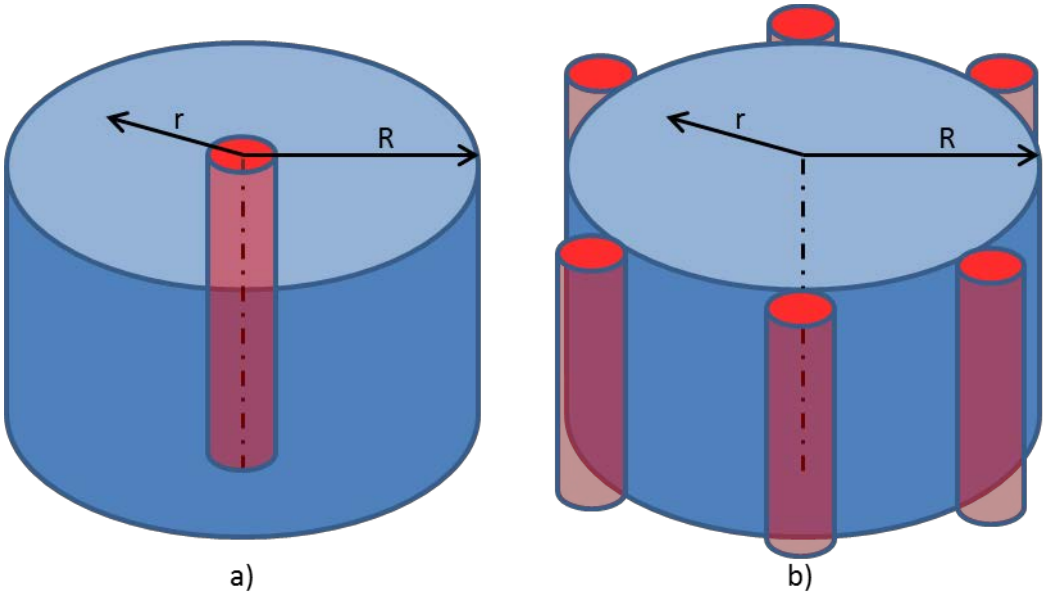

Figure 28. Illustrations of a) the COA model and b) the COS model, both in cylindrical geometry. Red cylinders represent the capillaries while the blue cylinders represent the tissue.

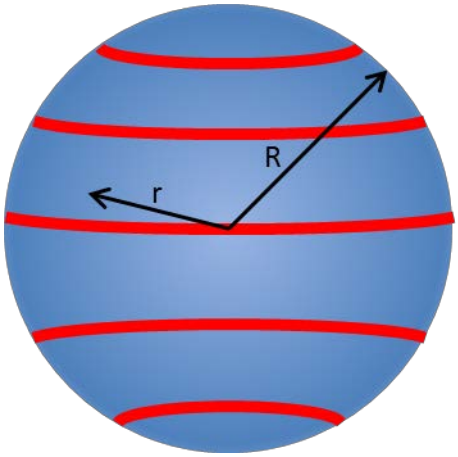

Figure 29. Illustrations of the COS model in spherical geometry. The red lines represent the capillaries surrounding the blue sphere which represents the tissue.

For oxygen, the volumetric mass flow rate is negative and given by Equation (32). This flow rate is positive when carbon dioxide is the species of interest.

$$\dot{m}_{O2}'''(r) = -\dot{m}_{O2,p}(g/s \text{ per cell}) * n \text{ (cells/cm}^3) = -2\pi(\rho D)_{bp} d_{cell} Y_{O2}(r) n \qquad (32)$$

Where the cell consumption rate under diffusion control from bulk IF fluid at "r" to the cells located at "r".

$$\dot{m}_{O2,p}\left(\frac{g}{s}\right) = -2\pi\left\{\rho\left(\frac{g}{cm^3}\right) D\left(\frac{cm^2}{s}\right)\right\}_{bp} d_{cell}(cm) Y_{O2}(r) \qquad (33)$$

Here, n is the number of cells per volume in the tissue (typically constant), $\dot{m}_{O2}$ is the sink rate of O_2 species per cell, $(\rho D)_{bp}$ is the bulk gas to particle density and diffusion coefficient, d_{cell} is the diameter of the cells in the tissue (typically constant for most species), and Y_{O2} is the mass fraction of O_2 species at location "r".

The following explains the difference between the bulk fluid to particle and effective diffusion. In between the cells there is interstitial fluid. The bulk fluid to particle applies to the diffusion from IF to cell; for CO_2, it is diffusion from cell to IF. The effective diffusion is from the capillary-IF interface to the cells. The simplifying assumption is made that all of the diffusion coefficients of O_2 into IF consisting of many components are equal.

The typical engineering literature treats combustion of carbon to be diffusion controlled and hence volumetric sink rate (g/cm3/s), or oxygen consumption rate is the source term in equation (31) is proportional to the mass fraction of O_2 called diffusion controlled combustion in engineering but called as first order kinetics in biology. Engineering uses the term "kinetics" only for Arrhenius type of equations. Similar formulation for biology presumes diffusion control of O_2 transport rate from IF to each cell which assumes that cells contain enough enzymes to oxidize the nutrient. Thus, volumetric sink rate is a function of "r" and hence source is O_2 dependent. The biology literature and more particularly Krogh cylinder model assumes uniform sink rate throughout the tissue and is independent of "r" called as "zero order kinetics" in biology. Thus, the source term for O_2 will decrease moving away from the capillary. For quantitative comparisons, uniform source will be evaluated using an averaged mass fraction computed from O_2 profiles for "O2" dependent source term. Krogh assumed a uniform oxygen consumption rate [27]. Thus, solutions for equation (31) will be obtained for uniform source (US) and O2 dependent source. Solutions require two boundary conditions for second order differential equation.

Prior to presenting the boundary conditions for equation (31), two models, each subjected to two source term conditions are considered. The first has the capillary located at the central axis with a surrounding layer of tissue (Capillary on Axis – COA, figure 28a) with transport of O_2 proceeding from axis towards the surface of cylinder while the second has a layer of tissue surrounded by a multitude of capillaries on the surface (Capillary on Surface – COS, figure 28b, called as solid model in biology) with

transport of O_2 proceeding from surface towards the axis of cylinder. In both models, the capillaries supply oxygen to tissue which consists of metabolic cells suspended in interstitial fluid (figure 21). The two source term conditions are a uniform oxygen consumption rate (US) and an oxygen consumption rate that is dependent on the oxygen concentration at the given location (O2). Together, these make up four scenarios: COA-US, COA-O2, COS-US and COS-O2.

Each scenario can be applied to up to three geometries: slab, cylinder, and sphere. The slab geometry consists of a slab of capillaries between two slabs of tissue for the COA model and is reversed for the COS model (figure 27). Next, the cylindrical geometry is the traditional choice because it is the shape of the capillaries and simplest to visualize (figure 28). Finally, the spherical geometry is only applied to the COS model (figure 29) because its use in the COA model is impractical. The capillaries are part of a connected cardiovascular system and cannot be isolated by completely encasing them with in the tissue. ***This paper focuses only on the cylindrical geometry which can be seen in figure 28.*** For the COS model, the oxygen is supplied evenly from the surface of the tissue cylinder such that angular equilibrium is maintained.

IV.5 Boundary Conditions

COA: As stated previously, the COA model consists of the capillary at the center of the geometry and on the axis surrounded by the tissue. The capillary supplies the tissue in a radial direction from the center. Boundary conditions for this model are gives as follows:

$$\frac{dY_{O_2}(r = R)}{dr} = 0 \tag{34}$$

$$Y_{O_2}(r = r_{cap}) = Y_{O_2,\text{Cap-IF}} \tag{35}$$

Here, r_{cap} is the distance from the center that marks the boundary of the capillary and the tissue. In cylindrical geometry it is the radius of the capillary cylinder. Y_{O_2} is the mass fraction of oxygen at a given location and $Y_{O_2,\text{Cap-IF}}$ is the mass fraction of oxygen at the boundary between the capillary wall and interstitial fluid of the tissue. Equation (34) indicates the flux is zero or an impermeable boundary of the tissue geometry, R. Therefore, no mass can transfer between the two sets of tissue. O_2 diffuses from the core of the geometry towards the surface. Equation (35) specifies the mass fraction will be specified at the interface between the capillary wall and the interstitial fluid. Later $Y_{O2capi\ IF}$ will be related to Y_{O2cap} through interface species balance equation.

COS: The COS model is similar to the combustion model in engineering, where fuel particles are surrounded by the oxygen source. Similarly, the tissue here is surrounded by capillaries which supply the oxygen in an inwards direction (e.g. skeletal muscles). The boundary conditions for this model are given as follows:

$$\frac{dY_{O_2}(r = 0)}{dr} = 0 \tag{36}$$

$$Y_{O_2}(r = R) = Y_{O_2,\text{Cap-IF}} \tag{37}$$

These conditions are similar to those for the COA model except the flux is zero at the axis of the geometry and the mass fraction of oxygen is set at the outer edge of the tissue, R. O_2 diffuses from R toward the core of the geometry.

IV.6 Oxygen Profiles

Following combustion literature for COS problems and modifying solution for COA problems, solutions can be obtained for all four cases. Details are given in Technical Report by Annamalai (2014). Each of the scenarios previously described were solved and the solutions have been collected and presented in table 1. Larger the radius of organ, larger is G value.

Table 1. Solutions for tissue radius, oxygen profiles, effectiveness factor, r_{cap}/R, and $Y_{O2,cap\text{-}IF}/Y_{O2,cap}$ for the four models.

$$\xi=\frac{r}{R}, \quad G= 2\ \pi\ n\ d_{cell}\ R^2, \quad G_{cap}= G\xi_{cap}^{\ 2}, \quad \sqrt{G_{cap}}= \sqrt{G}\ \ \xi_{cap}$$

By setting $Y_{O2}= Y_{O2lethal}$, ξ_{lethal} can be solved.

Model	Tissue Radius, R
COS-O2	$\frac{R_{COS}}{r_{cap}} = \left(\frac{2\ F_{COS}}{S_{cap,m}\ \rho\ r_{cap}}\right) \approx \left(\frac{2}{S_{cap,m}\ \rho\ r_{cap}}\right)$, capillaries cover surface (38)
COA-O2	$\frac{R_{COA}}{r_{cap}} = \sqrt{\left\{1+\frac{2}{r_{cap}\ S_{cap,m}\ \rho}\right\}} \approx \sqrt{\frac{2}{r_{cap}\ S_{cap,m}\ \rho}}$, for $\frac{r_{cap}}{R_{COA}} \ll 1$ (39)
COS-US	Equivalent to COS-O2
COA-US	Equivalent to COA-O2

Table 1 (continued).

Model	O2 Profiles (ξ=r/R Form)	
COS-O2	$\frac{Y(r)}{Y(r=R)} = \frac{I_0\left(\sqrt{G}\ \xi\right)}{I_0\left(\sqrt{G}\right)}$	(40)
COA-O2	$\frac{Y(r)}{Y(r=r_{cap})} = \frac{\left[\left\{\frac{K_1\left(\sqrt{G}\right)}{I_1\left(\sqrt{G}\right)}\right\} I_0\left(\sqrt{G}\ \xi\right) + K_0\left(\sqrt{G}\,\xi\right)\right]}{\left\{\frac{K_1\left(\sqrt{G}\right)}{I_1\left(\sqrt{G}\right)}\right\} I_0\left(\sqrt{G}\ \xi_{cap}\right) + K_0\left(\sqrt{G}\ \xi_{cap}\right)}$	(41)
COS-US	$\frac{Y(r)}{Y(r=R)} = 1 - \frac{G}{4}\left(\frac{Y_{O2,avg}}{Y_{O2,cap\text{-}IF}}\right)\left(1-\xi^2\right)$	(42)
COA-US	$\frac{Y(r)}{Y(r=r_{cap})} = 1 - \frac{G}{4}\left(\frac{Y_{O2,avg}}{Y_{O2,cap\text{-}IF}}\right)\left(\left(\xi^2 - \xi^2_{cap}\right) + 2\ln\left(\frac{\xi_{cap}}{\xi}\right)\right)$	(43)
Model	**O2 Profiles ($y=r/r_{cap}$ Form)**	
COS-O2	$\frac{Y(r)}{Y(r=R)} = \frac{I_0\left(\sqrt{G_{cap}}\ y\right)}{I_0\left(\frac{\sqrt{G_{cap}}}{\xi_{cap}}\right)}$	(44)
COA-O2	$\frac{Y(r)}{Y(r=r_{cap})} = \frac{\left\{\frac{K_1\left(\frac{\sqrt{G_{cap}}}{\xi_{cap}}\right)}{I_1\left(\frac{\sqrt{G_{cap}}}{\xi_{cap}}\right)}\right\} I_0\left(\sqrt{G_{cap}}\ y\right) + K_0\left(\sqrt{G_{cap}}\ y\right)}{\left\{\frac{K_1\left(\frac{\sqrt{G_{cap}}}{\xi_{cap}}\right)}{I_1\left(\frac{\sqrt{G_{cap}}}{\xi_{cap}}\right)}\right\} I_0\left(\sqrt{G_{cap}}\right) + K_0\left(\sqrt{G_{cap}}\right)}$	(45)
COS-US	$\frac{Y(r)}{Y(r=R)} = 1 - \frac{G}{4}\left(\frac{Y_{O2,avg}}{Y_{O2,cap\text{-}IF}}\right)\left(1-y^2\xi^2_{cap}\right)$	(46)
COA-US	$\frac{Y(r)}{Y(r=r_{cap})} = 1 - \frac{G}{4}\left(\frac{Y_{O2,avg}}{Y_{O2,cap\text{-}IF}}\right)\left\{\xi^2_{cap}\left(y^2-1\right) - 2\ln\left(y\right)\right\}$	(47)

Table 1 (continued).

Model	Effectiveness Factor, η_{eff}
COS-O2	G form: $\eta_{eff} = \frac{2}{\sqrt{G}} \frac{I_1\left(\sqrt{G}\right)}{I_0\left(\sqrt{G}\right)}$ (48) G_{cap} form: $\eta_{eff} = \frac{2}{\left(\frac{\sqrt{G_{cap}}}{\xi_{cap}}\right)} \frac{I_1\left(\frac{\sqrt{G_{cap}}}{\xi_{cap}}\right)}{I_0\left(\frac{\sqrt{G_{cap}}}{\xi_{cap}}\right)}$ (49)
COA-O2	G form: $\eta_{eff} = \frac{2\ \xi_{cap}}{\left(1-\xi_{cap}^{\ 2}\right)\sqrt{G}} \left\{ \frac{\left\{\frac{I_1\left(\sqrt{G}\right)}{K_1\left(\sqrt{G}\right)}\right\} K_1\left(\sqrt{G}\,\xi_{cap}\right) - I_1\left(\sqrt{G}\ \xi_{cap}\right)}{I_0\left(\sqrt{G}\ \xi_{cap}\right) + K_0\left(\sqrt{G}\ \xi_{cap}\right)\left\{\frac{I_1\left(\sqrt{G}\right)}{K_1\left(\sqrt{G}\right)}\right\}} \right\}$ (50) G_{cap} form: $\eta_{eff} = \frac{2\ \xi_{cap}^{\ 2}}{\left(1-\xi_{cap}^{\ 2}\right)\left\{\sqrt{G_{cap}}\right\}} \left\{ \frac{\left\{\frac{I_1\left\{\left(\frac{\sqrt{G_{cap}}}{\xi_{cap}}\right)\right\}}{K_1\left\{\left(\frac{\sqrt{G_{cap}}}{\xi_{cap}}\right)\right\}}\right\} K_1\left\{\left(\frac{\sqrt{G_{cap}}}{\xi_{cap}}\right)\right\} - I_1\left\{\left(\frac{\sqrt{G_{cap}}}{\xi_{cap}}\right)\right\}}{I_0\left\{\left(\frac{\sqrt{G_{cap}}}{\xi_{cap}}\right)\right\} + K_0\left\{\left(\frac{\sqrt{G_{cap}}}{\xi_{cap}}\right)\right\}\left\{\frac{I_1\left\{\left(\frac{\sqrt{G_{cap}}}{\xi_{cap}}\right)\right\}}{K_1\left\{\left(\frac{\sqrt{G_{cap}}}{\xi_{cap}}\right)\right\}}\right\}} \right\}$ (51)
COS-US	Typically 1, but $Y_{O2avg}/Y_{O2capIF} = \eta_{eff}$ for COS assumed in current work
COA-US	Typically 1, but $Y_{O2avg}/Y_{O2capIF} = \eta_{eff}$ for COA assumed in current work

Table 1 (continued).

Model	$Y_{O2,cap-IF} / Y_{O2,cap}$	
COS-O2	$\frac{Y_{O2,cap-IF}}{Y_{O2,cap}} = \frac{1}{\left\{1+\eta_{eff}\frac{1}{F_{COS}}\left(\frac{V_{reac}}{V}\right)\left(\frac{D_{IF-cell}}{K'_{cap}d_{cap}}\right)\sqrt{GG_{cap}}\right\}}$	(52)
COA-O2	$\frac{Y_{O2,cap-IF}}{Y_{O2,cap}} = \frac{1}{\left(1+\eta_{eff}\left(\frac{V_{reac}}{V}\right)\frac{D_{IF-cell}}{K'_{cap}d_{cap}}\left\{G-G_{cap}\right\}\right)} \approx \frac{1}{\left(1+\eta_{eff}\left(\frac{V_{reac}}{V}\right)\frac{D_{IF-cell}}{K'_{cap}d_{cap}}G\right)}$ when $G_{cap} \ll G$	(53)
COS-US	$\frac{Y_{O2,cap-IF}}{Y_{O2,cap}} = \frac{1}{\left\{1+\eta_{eff}\left(\frac{D_{IF-cell}}{K'_{cap}d_{cap}}\right)\left(\frac{1}{F_{COS}}\right)\sqrt{GG_{cap}}\right\}}$	(54)
COA-US	$\frac{Y_{O2,cap-IF}}{Y_{O2,cap}} = \frac{1}{\left(1+\eta_{eff}\frac{D_{IF-cell}}{K'_{cap}d_{cap}}\left\{G-G_{cap}\right\}\right)}$	(55)

In equations (40) – (43), G is termed as the group combustion number in engineering, ξ is the dimensionless radius given by r/R and ξ_{cap} is the dimensionless capillary radius given by r_{cap}/R.

IV.7 Average Mass Fraction of O_2

Defining

$$Y_{O2,avg} = \frac{\int_0^R Y_{O2}(r)\, 2\pi\, r\, dr}{\int_0^R 2\pi\, r\, dr} = \frac{2}{R^2}\int_0^R Y_{O2}(r)\ r\, dr\,, \quad \text{COS model} \tag{56}$$

If non-dimensional profiles are used

$$\frac{Y_{O2,avg}}{Y_{O2,cap\text{-}IF}} = \frac{2}{R^2}\int_0^R \frac{Y_{O2}(r)}{Y_{O2,cap\text{-}IF}}\ r\, dr = 2\int_0^1 \frac{Y_{O2}(\xi)}{Y_{O2,cap\text{-}IF}}\ \xi\, d\xi\,, \quad \text{COS model} \tag{57}$$

Similarly

$$Y_{O2,avg} = \frac{\int_{r_{cap}}^R Y_{O2}(r)\, 2\pi\, r\, dr}{\int_{r_{cap}}^R 2\pi\, r\, dr} = \frac{2}{R^2 - r_{cap}^{\ 2}}\int_{r_{cap}}^R Y_{O2}(r)\ r\, dr, \quad \text{COA model} \tag{58}$$

$$\frac{Y_{O2,avg}}{Y_{O2,cap\text{-}IF}} = \left(\frac{2}{R^2 - r_{cap}^{\ 2}}\right)\int_{r_{cap}}^R \frac{Y_{O2}(r)}{Y_{O2,cap\text{-}IF}}\, r\, dr = \left(\frac{2}{1-\xi_{cap}^{\ 2}}\right)\int_{\xi_{cap}}^1 \frac{Y_{O2}(\xi)}{Y_{O2,cap\text{-}IF}}\, \xi\, d\xi\,, \quad \text{COA model} \tag{59}$$

Thus the O_2 sink rate per metabolic cell under transport control from IF to cell is given as

$$\dot{m}_{O2,cell,avg} = 2\pi(\rho D)_{IF\text{-}cell}\, d_{cell}\, Y_{O2,avg} \tag{60}$$

Multiplying by number of cells per unit volume yields uniform sink rate of O_2 ($g/cm^3/s$). Thus, average O_2 sink rate per unit volume is given as

$$\dot{m}_{O2,avg}''' = \dot{m}_{O2,cell,avg}\; n \tag{61}$$

The metabolic rate for whole tissue is given as

$$\dot{m}_{O2} = \dot{m}_{O2,cell,avg}\; n\; V_{reac} \tag{62}$$

Where $V_{reac} = V_{cyl}$ for COS models when oxygen concentration is above lethal level. The above can be used in COA and COS models with uniform source. Details are provided in Chapter V: Results and Discussion.

IV.8 Tissue Oxygen Consumption Rate, Effectiveness Factor and Metabolic Energy Release Rate

Knowing the O2 profiles and using equation (32) for $\dot{m}_{O2}'''$, the volumetric sink rate is computed as function of "r". Integrating over the volume gives the oxygen consumption rate for the whole volume

$$\dot{m}_{O2} = \int_0^R \dot{m}_{O2}'''(r)\, 2\pi\, r\, dr\, L, \quad \text{COS model} \tag{63}$$

Which presumes that whole tissue of radius R consists of metabolic cells; if part of tissue of radius r_{Lethal} is lethal (i.e. $Y_{O2} < Y_{O2\ lethal}$), then these cells undergo only glycolysis.

IV.8.1 Lethal Volume Fraction

The V represents the geometric volume. When organ is large, it is possible a part of organ may have $Y_{O2} < Y_{O2\ lethal}$ below which there is no metabolism. The region which contains below $Y_{O2\ lethal}$ is called lethal or anaerobic volume. The lethal volume fraction (LVF) is defined as

$$LVF = \frac{\text{Lethal Volume}, V_{lethal}}{\text{Geometrical Volume}, V} \tag{64}$$

Thus, metabolic volume fraction or reaction or reaction volume fraction (RVF)

$$RVF = \frac{\text{Reaction Volume}, V_{reac}}{\text{Geometrical Volume}, V} = 1\text{-}LVF \tag{65}$$

IV.8.2 O2 Sink Rate and Metabolic Rate

Knowing the O profiles and using equation (32) for $\dot{m}_{O2}'''$, the volumetric sink rate is computed as function of "r". Integrating over the volume gives the oxygen consumption rate for the whole volume

$$\dot{m}_{O2} = \int_0^R \dot{m}_{O2}'''(r)\, 2\pi\, r\, dr\, L, \quad \text{COS model} \tag{66}$$

$$\dot{m}_{O2} = \int_{r_{cap}}^R \dot{m}_{O2}'''(r)\, 2\pi\, r\, dr\, L, \quad \text{COA model} \tag{67}$$

Where L is the length of the cylinder. Thus, with

$$\dot{m}_{O2,cell} = 2\pi\, (\rho D)_{bp}\, d_{cell}\, Y_{O2} \tag{68}$$

$$\dot{m}_{O2}''' = n\ \dot{m}_{O2,cell} = n\ 2\pi\, (\rho D)_{bp}\, d_{cell}\, Y_{O2} \tag{69}$$

$$\dot{m}_{O2} = \int_{r_{Lethal}}^R \dot{m}_{O2}'''(r)\, 2\pi\, r\, dr\, L = \int_{r_{Lethal}}^R \left\{ n \left(2\pi\, (\rho D)_{bp}\, d_{cell}\ n\ Y_{O2} \right) \right\} 2\pi\, r\, dr\, L, \quad \text{COS model} \tag{70}$$

where

$$\dot{m}_{O2}'''(r)=\left\{n\left(2\pi\ (\rho D)_{bp}\ d_{cell}\ n\ Y_{O2}\right)\right\} \tag{71}$$

Then expressing in terms of O2 profiles, integrating and normalizing,

$$\begin{aligned}\frac{\dot{m}_{O2}}{\left\{2\pi\ (\rho D)_{bp}\ d_{cell}\ nL\pi R^2 L Y_{O2,cap\text{-}IF}\right\}} &= 2\int_{\xi_{Lethal}}^{1}\left(\frac{Y_{O2}(\xi)}{Y_{O2,cap\text{-}IF}}\right)\ \xi\, d\xi\,, \quad \text{COS model} \\ &= 2\int_{0}^{1}\left(\frac{Y_{O2}(\xi)}{Y_{O2,cap\text{-}IF}}\right)\xi\, d\xi - 2\int_{0}^{\xi_{Lethal}}\left(\frac{Y_{O2}(\xi)}{Y_{O2,cap\text{-}IF}}\right)\xi\, d\xi\end{aligned} \tag{72}$$

$$\begin{aligned}\frac{\dot{m}_{O2}}{\left\{2\pi\ (\rho D)_{bp}\ d_{cell}\ n\ V\ Y_{O2,cap\text{-}IF}\right\}} &= \left(\frac{Y_{O2avg}}{Y_{O2,cap\text{-}IF}}\right) - \xi_{Lethal}^{\,2}\,\frac{Y_{O2,lethal}}{Y_{O2,cap\text{-}IF}}\,\frac{Y_{O2,avg\ lethal}}{Y_{O2,lethal}} \\ &= \left(\frac{Y_{O2avg}}{Y_{O2,cap\text{-}IF}}\right) - \xi_{Lethal}^{\,2}\,\frac{Y_{O2,avg\ lethal}}{Y_{O2,cap\text{-}IF}}, \quad \text{COS model}\end{aligned} \tag{73}$$

Where

$$\frac{Y_{O2,avg,Lethal}}{Y_{O2,cap\text{-}IF}} = 2\int_{0}^{\xi_{Lethal}}\left(\frac{Y_{O2}(\xi)}{Y_{O2,cap\text{-}IF}}\right)\ \xi\, d\xi\,, \quad \text{COS model} \tag{74}$$

and

$$\left(\frac{Y_{O2avg}}{Y_{O2,cap\text{-}IF}}\right) = 2\int_{0}^{1}\left(\frac{Y_{O2}(\xi)}{Y_{O2,cap\text{-}IF}}\right)\ \xi\, d\xi \tag{75}$$

Using the profiles given in table 1 for COS-O2, the term ($Y_{O2,avg}/Y_{O2,cap-IF}$) can be determined. In the current thesis it has been assumed that for COS-O2 models, $Y_{O2,avg,Lethal} = Y_{O2,avg}$ in order to get simplified expressions for $Y_{O2,cap-IF}/Y_{O2,cap}$; however as seen in figure 30, the better assumption will be to assume $Y_{O2,avg,Lethal} = Y_{O2,lethal}$ rather than $Y_{O2,avg}$. Future work will consider the effect of having $Y_{O2,avg,Lethal} \neq Y_{O2,avg}$.

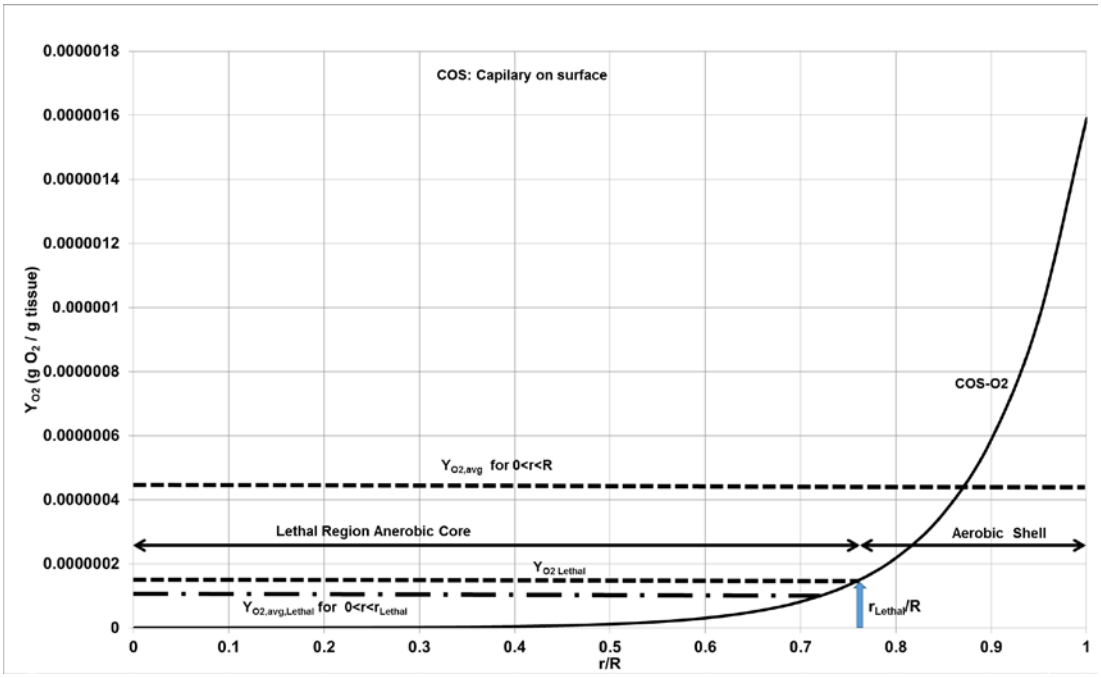

Figure 30. Illustration of $Y_{O2,avg}$, $Y_{O2,Lethal}$, $Y_{O2,avg,Lethal}$, and r_{Lethal}/R.

If $Y_{O2,avg\ lethal} = Y_{O2,avg}$, then

$$\frac{\dot{m}_{O2}}{\left\{2\pi\ (\rho D)_{bp}\, d_{cell}\ n\ V\ Y_{O2,cap\text{-}IF}\right\}} = \left(\frac{Y_{O2avg}}{Y_{O2,cap\text{-}IF}}\right) - \xi_{Lethal}^{\ 2}\ \frac{Y_{O2,avg}}{Y_{O2,cap\text{-}IF}}$$

$$= \left(\frac{Y_{O2avg}}{Y_{O2,cap\text{-}IF}}\right)\left(1-\xi_{Lethal}^{\ 2}\right) \qquad (76)$$

$$= \left(\frac{Y_{O2avg}}{Y_{O2,cap\text{-}IF}}\right)(1\text{-LVF}) \quad \text{COS model}$$

Dividing the numerator and denominator by tissue mass

$$\frac{\dot{m}_{O2,m}}{\left\{2\pi\ (\rho D)_{bp}\, d_{cell}\ nLY_{O2,cap\text{-}IF}/\rho\right\}} = \frac{\text{specific act O2 sink rate,(g/s per g tissue)}}{\text{O2 sink rate if each cell is at}Y_{O2,cap\text{-}IF}\text{,(g/s,per g tissue)}}$$

$$= \left(\frac{Y_{O2avg}}{Y_{O2,cap\text{-}IF}}\right)(1\text{-LVF}), \quad \text{COS model}$$

(77)

IV.8.3 Energy Release Rate

Since energy released per unit mass of oxygen consumed (HHV_{O2}) is relatively constant for most fuels and nutrients (CH, fat, protein), the metabolic energy release rate of whole cylinder and volumetric energy release rate is given as

$$\dot{q}_{O2} = \dot{m}_{O2} HHV_{O2}, \qquad \dot{q}_{O2}''' = \dot{m}_{O2}''' HHV_{O2} \qquad (78)$$

where $\dot{q}$ is the metabolic rate and L is the length of the cylinder. Thus metabolic rate of whole tissue can be estimated. Equation (76) becomes

$$\frac{\dot{m}_{O2}*HHV_{O2}}{\left\{2\pi\ (\rho D)_{bp}\ d_{cell}\ nL\pi R^2 LY_{O2,cap\text{-}IF}*HHV_{O2}\right\}}= \\ =\frac{\text{actual energy release rate (J/s)}}{\text{Energy release rate if each cell is at}Y_{O2,cap\text{-}IF},\text{(J/s)}},\quad \text{COS model} \tag{79}$$

or

$$\frac{\dot{m}_{O2,m}}{\left\{2\pi\ (\rho D)_{bp}\ d_{cell}\ nLY_{O2,cap\text{-}IF}/\rho)\right\}}= \\ =\frac{\text{specific energy release rate,(g/s per g tissue)}}{\text{specific energy release rate if each cell is at}Y_{O2,cap\text{-}IF},\text{(g/s,per g tissue)}} \\ =\left(\frac{Y_{O2avg}}{Y_{O2,cap\text{-}IF}}\right)(1\text{-LVF}),\quad \text{COS model} \tag{80}$$

IV.8.4 Effectiveness Factor (η_{eff}) and Solutions in Terms of η_{eff}

In engineering literature there is no lethal volume fraction (LVF=0) since O2 dependent model for source will not lead to negative value for YO2 and the particle still releases energy even at low concentrations; thus for engineering studies

$$\frac{\dot{m}_{O2}}{\left\{2\pi\ (\rho D)_{bp}\ d_{cell}\ nL\pi R^2 L Y_{O2,cap\text{-}IF}\right\}} = \frac{\text{act O2 sink rate}}{\text{O2 sink rate if each cell is at} Y_{O2,cap\text{-}IF}} = \left(\frac{Y_{O2avg}}{Y_{O2,cap\text{-}IF}}\right), \quad \text{COS model} \tag{81}$$

The effectiveness factor in engineering literature is defined as

$$\eta_{eff} = \frac{\dot{m}_{O2}}{\dot{m}_{O2}\ \text{with each cell exposed to}\ Y_{O2,Capil\text{-}IF}} = \frac{\dot{m}_{O2,m}}{\dot{m}_{O2,m}\ \text{with each cell exposed to}\ Y_{O2,Capil\text{-}IF}} = \frac{\dot{q}_m}{\dot{q}_m \text{with each cell exposed to}\ Y_{O2,Capil\text{-}IF}} = \left(\frac{Y_{O2avg}}{Y_{O2,cap\text{-}IF}}\right) \tag{82}$$

where

$$\left(\frac{Y_{O2avg}}{Y_{O2,cap\text{-}IF}}\right) = 2\int_0^1 \left(\frac{Y_{O2}(\xi)}{Y_{O2,cap\text{-}IF}}\right)\ \xi\, d\xi \tag{83}$$

Using the profiles given in Table 1 for COS-O2, the term ($Y_{O2,avg}/Y_{O2,cap\text{-}IF}$), and hence η_{eff}, can be determined. From equation (75)

$$\eta_{eff,COS} = \left(\frac{Y_{O2avg}}{Y_{O2,cap\text{-}IF}}\right) = \frac{2}{\sqrt{G}}\ \frac{I_1\left(\sqrt{G}\right)}{I_0\left(\sqrt{G}\right)}, \quad \text{COS-O2} \tag{84}$$

Similarly for COA

$$\eta_{eff,COA} = \frac{Y_{O2avg}}{Y_{O2cap-IF}} = \frac{2\ \xi_{cap}}{\left(1-\xi_{cap}^{\ 2}\right)\sqrt{G}} \left\{ \frac{\left[K_1\left(\sqrt{G}\,\xi_{cap}\right) - \left\{ \frac{K_1\left(\sqrt{G}\right)}{I_1\left(\sqrt{G}\right)} \right\} I_1\left(\sqrt{G}\ \xi_{cap}\right) \right]}{\left\{ \frac{K_1\left(\sqrt{G}\right)}{I_1\left(\sqrt{G}\right)} \right\} I_0\left(\sqrt{G}\ \xi_{cap}\right) + K_0\left(\sqrt{G}\ \xi_{cap}\right)} \right\}, \quad \text{COA - O2} \tag{85}$$

Equation (79) for COS becomes

$$\frac{\dot{m}_{O2}}{\left\{2\pi\ (\rho D)_{bp}\, d_{cell}\ n\ Y_{O2,cap\text{-}IF} V)\right\}} = \eta_{eff}\left\{1\text{-LVF}\right\}, \quad \text{COS model} \tag{86}$$

or

$$\frac{\dot{m}_{O2,m}}{\left\{2\pi\ (\rho D)_{bp}\, d_{cell}\ nY_{O2,cap\text{-}IF}/\rho)\right\}} = \eta_{eff}\left\{1\text{-LVF}\right\}, \quad \text{COS model} \tag{87}$$

One can interpret the actual sink rate to be O_2 consumption in case each cell is exposed to $Y_{O2,avg}$.

$$\dot{m}_{O2,cell,avg} = \text{avg O2 rate per cell} = \left\{2\pi\ (\rho D)_{bp}\ d_{cell} Y_{O2,avg}\right\}$$

$$\text{number of cells, N} = n*V,\quad V=\left\{n\ \pi R^2 L\right\},\quad \text{COS model}$$

$$\dot{m}_{O2} = \left\{2\pi\ (\rho D)_{bp}\ d_{cell} Y_{O2,avg}\right\} * \left\{n\ \pi R^2 L\right\},\quad \text{COS model} \tag{88}$$

$$\text{number of cells, N} = n*V,\quad V=n\ \pi\left\{R^2 - r_{cap}^{\ 2}\right\} L,\quad \text{COA model}$$

$$\dot{m}_{O2} = \left\{2\pi\ (\rho D)_{bp}\ d_{cell} Y_{O2,avg}\right\} * n\ \pi\left\{R^2 - r_{cap}^{\ 2}\right\} L,\quad \text{COA model}$$

Then $Y_{O2avg\ lethal} < Y_{O2lethal}$ since it covers a region for $0< Y_{O2}< Y_{O2,lethal}$; thus lowest values for metabolic rate is obtained by setting $Y_{O2avg\ lethal} = Y_{O2lethal}$.

$$\frac{\dot{m}_{O2,m}}{\left\{2\pi\ (\rho D)_{bp}\ d_{cell}\ nLY_{O2,cap\text{-}IF}/\rho)\right\}} = \eta_{eff}\left\{1\text{-}LVF\right\},\quad LVF=\xi_{Lethal}^{\ 2},\quad \text{COS model} \tag{89}$$

Where ξ_{Lethal} is solved from oxygen profiles.

For COA models, one can show that

$$\frac{\dot{m}_{O2}}{\left\{2\pi\ (\rho D)_{bp}\ d_{cell}\ n\ \ V\ Y_{O2,cap\text{-}IF}/\rho)\right\}} = \eta_{eff}\left\{1\text{-}LVF\right\},\quad LVF=\left(1\text{-}\xi_{Lethal}^{\ 2}\right),\quad \text{COA model} \tag{90}$$

$$\frac{\dot{m}_{O2,m}}{\left\{2\pi\ (\rho D)_{bp}\ d_{cell}\ n\ \ Y_{O2,cap\text{-}IF}/\rho)\right\}} = \eta_{eff}\left\{1\text{-}LVF\right\},\quad LVF=\left(1\text{-}\xi_{Lethal}^{\ 2}\right),\quad \text{COA model} \tag{91}$$

For COA model

$$\dot{m}_{O2} = \left\{2\pi\ (\rho D)_{bp}\, d_{cell} Y_{O2,avg}\right\}\ \left\{n\ \pi\ \left(R^2 - r_{cap}^{\ 2}\right) L\right\},\ \text{COA model}$$
$$\text{number of cells, } N = nV,\quad V = \left\{n\ \pi\ \left(R^2 - r_{cap}^{\ 2}\right) L\right\},\quad \text{COA model} \tag{92}$$

For uniform source model of Krogh cylinders, the US can be evaluated with two options: i) each cell is exposed to $Y_{O2,avg}$ so that total metabolic rate for whole tissue remains the same for both COS-O2 and COS-US models, ii) each cell is exposed to $Y_{O2,cap\text{-}IF}$ or $\eta_{eff} = 1$. For the second option, the US will yield a very high sink rate for O2. COA-US is calculated with COA –O2 average mass fraction and COS-US is calculated with COS-O2 average mass fraction.

IV.9 Capillary-IF Interface Oxygen Mass Fraction

So far the profiles were presented in terms of $Y_{O2cap\text{-}IF}$ which is related to Y_{O2cap} through interface O_2 concentration. Aqueous oxygen in the capillaries is assumed to have a relatively high mass fraction or partial pressure. Oxygen concentration will then be less on the other side of the capillary wall, at the capillary-interstitial interface, due to the permeability ($K_{cap} = \rho D$/thickness of capillary wall) of the capillary wall. The mass transport rate of O_2 across the capillary wall is given as

$$\dot{m}_{O2}\left(\frac{g}{s}\right) = K'_{cap}\rho\left(Y_{O2,cap} - Y_{O2,cap\text{-}IF}\right)A_{cap} = \eta_{eff} * 2\pi\left(\rho D\right)_{IF\text{-}cell}\, d_{cell}\, Y_{O2,Cap\text{-}IF}\, n\, V \tag{93}$$

where $\dot{m}_{O2}$ is the mass flow rate in grams per second across the capillary wall and V is the volume of tissue cylinder $V=\pi R^2 L$ for COS model, $V=\pi R^2 L-\pi r_{cap}^2 L$ for COA model and

$$\frac{Y_{O2,Cap\text{-}IF}}{Y_{O2,Cap}}=\frac{K'_{cap}\rho A_{cap}}{\left\{\eta_{eff}*2\pi(\rho D)_{IF\text{-}cell}\, d_{cell}\ n\ V+K'_{cap}\rho A_{cap}\right\}}=\frac{1}{\left\{1+\frac{\eta_{eff}*2\pi n d_{cell}R^2(\rho D)_{IF\text{-}cell}\, V}{K'_{cap}\rho A_{cap}R^2}\right\}} \quad (94)$$

Using equation (88) and solving for $Y_{O2,cap\text{-}IF}$ yields for all four models

$$\frac{Y_{O2,Cap\text{-}IF}}{Y_{O2,Cap}}=\frac{1}{\left\{1+\eta_{eff}G\left[\frac{(\rho D)_{IF\text{-}cell}\, V}{K'_{cap}\rho A_{cap}R^2}\right]\right\}} \quad (95)$$

It is noted that equation (93) presumed whole geometric volume containing metabolic cells is available for O_2 sink. Equation (95) could be modified as

$$\frac{Y_{O2,Cap\text{-}IF}}{Y_{O2,Cap}}=\frac{1}{\left\{1+\eta_{eff}G\left[\frac{(\rho D)_{IF\text{-}cell}\, V(1\text{-}LVF)}{K'_{cap}\rho A_{cap}R^2}\right]\right\}} \quad (96)$$

if cells within V_{Lethal} are not available for oxidation assuming lethal volume is at average $Y_{O2,avg}$. The term (1-LVF) represents the ratio of reaction volume or aerobic volume to total volume of tissue.

$$\frac{V_{reac}}{V} = 1-\alpha\frac{V_{lethal}}{V} = 1-\alpha*LVF \tag{97}$$

By setting α=0, we assume no LVF or we do not account for LVF and when α=1, we assume LVF or we do account for LVF.

For COS-US (uniform source model of Krogh cylinders), the US can be evaluated with two options: i) each cell is exposed to Y_{O2avg} so that metabolic rate for whole tissue remains the same for both COS-O2 and COS-US models in equation (95), ii) each cell is exposed to $Y_{O2,cap-IF}$ or η_{eff} =1 in equation (95). For the second option, the US will yield a very high sink rate for O_2. COA-US is calculated with COA-O2 average mass fraction and COS-US is calculated with COS-O2 average mass fraction.

If lethal volume or ξ_{Lethal} is zero, then

$$\frac{Y_{O2,cap-IF}}{Y_{O2,cap}} = \frac{1}{\left\{1+2\pi\eta_{eff}\ \frac{D_{IF-cell}}{K'_{cap}}\frac{n\ d_{cell}}{\rho\ S_{cap,m}}\right\}}, \quad \text{COS} \tag{98}$$

Similarly for COA models

$$\frac{Y_{O2,cap\text{-}IF}}{Y_{O2,cap}} = \frac{1}{\left\{1 + 2\pi\eta_{eff}\ \frac{D_{IF\text{-}cell}}{K'_{cap}}\frac{n\ d_{cell}}{\rho\ S_{cap,m}}\right\}},\quad \text{COA, LVF=0,}\ \ \eta_{eff,COA} \neq \eta_{eff,COS} \qquad (99)$$

Even though expressions for both COA and COS seem similar, $\eta_{eff,COA} \neq \eta_{eff,COA}$ due to different boundary conditions.

IV.10 Correction Factor (η)

In order to compute the tissue sink rate for O_2 and hence tissue metabolic rate, $Y_{O2,cap}$ must be specified and then $Y_{O2,cap\text{-}IF}$ is calculated using equation (95). Then the definition for effectiveness can be invoked and use charts for η_{eff} vs G and compute metabolic rate. If each cell is exposed to $Y_{O2,cap}$, one can determine the tissue O_2 sink rate as though each cell is isolated. For both COA and COS

$$\eta = \frac{\dot{m}_{O2}}{\dot{m}_{O2}\ \text{with each cell exposed to}\ Y_{O2,Cap}} = \frac{\dot{m}_{O2}}{\dot{m}_{O2}\ \text{with each cell exposed to}\ Y_{O2,Cap\text{-}IF}}\frac{Y_{O2\ cap\text{-}IF}}{Y_{O2,cap}}$$

$$= \frac{\dot{m}_{O2,m}}{\dot{m}_{O2,m}\ \text{with each cell exposed to}\ Y_{O2,Cap}} = \frac{\dot{m}_{O2,m}}{\dot{m}_{O2,m}\ \text{with each cell exposed to}\ Y_{O2,Cap\text{-}IF}}\frac{Y_{O2\ cap\text{-}IF}}{Y_{O2,cap}}$$

$$= \frac{\dot{q}_m}{\dot{q}_m \text{with each cell exposed to}\ Y_{O2,Capil\text{-}IF}}\frac{Y_{O2\ cap\text{-}IF}}{Y_{O2,cap}}$$

$$\eta = \eta_{eff}\ \left(\frac{Y_{O2\ cap\text{-}IF}}{Y_{O2,cap}}\right) \qquad (100)$$

Thus,

$$\eta = \eta_{eff}\,(1\text{-LVF})\left(\frac{Y_{O2\ cap\text{-}IF}}{Y_{O2,cap}}\right) \quad \text{COS, COA} \tag{101}$$

The term η is similar to η_{eff}, except $\dot{m}_{O2}$ or $\dot{q}$ is calculated using $Y_{O2,cap}$ instead of $Y_{O2cap\text{-}IF}$ for each cell. Thus, η is found by simply multiplying η_{eff} by $Y_{O2,cap\text{-}IF} / Y_{O2,cap}$. As noted earlier, even though expressions for η for COA and COS seem similar, the $\eta_{COA} = \eta_{COS}$ and

$$\left(\frac{Y_{O2\ cap\text{-}IF}}{Y_{O2,cap}}\right)_{COS} \neq \left(\frac{Y_{O2\ cap\text{-}IF}}{Y_{O2,cap}}\right)_{COA} \tag{102}$$

Using equations (101) and (95), η can be determined and plotted. First compute as though each cell is isolated at $Y_{O2,cap}$, obtain single cell sink rate, multiply by number of cells within aerobic part of tissue, then apply correction factor η, and finally compute actual sink rate of O_2 and hence actual metabolic rate.

IV.11 Energy Release Rate

The energy release rate (ERR) expressions are now summarized. ERR can be calculated for each cell as though each cell is isolated at an O_2 concentration of $Y_{O2,cap\text{-}IF}$, then ERR can be calculated for the whole tissue. For isolated cells, equation (103) is used, while for the whole tissue, equation (104) is used.

$$ERR_{cell}(W/cell) = 2\pi \rho D\, d_{cell}\, Y_{O2,cap\text{-}IF}\, HHV_{O2} \quad (103)$$

$$ERR(W/cm^3_{tissue}) = 2\pi \rho D\, d_{cell}\, Y_{O2,cap\text{-}IF}\, HHV_{O2}\, n\, \eta_{eff} \quad (104)$$

η_{eff} is given by equations (84) and (85) for COS-O2 and COA-O2 models respectfully. As mentioned previously, for US models, η_{eff} can be found through two methods. One is to simply assume η_{eff} is equal to one and the second is to use the average mass fraction calculated from the corresponding O2 model (COA vs COS). Both methods have been tried in this study. ERR can also be calculated at the dissolved O_2 mass fraction in the capillary using

$$ERR_{cell}(W/cell) = 2\pi \rho D\, d_{cell}\, Y_{O2,cap}\, HHV_{O2} \quad (105)$$

$$ERR(W/cm^3_{tissue}) = 2\pi \rho D\, d_{cell}\, Y_{O2,cap}\, HHV_{O2}\, n\, \eta \quad (106)$$

where $Y_{O2,cap\text{-}IF}$ is changed to $Y_{O2,cap}$ and η_{eff} is changed to η. Specific energy release rate, SERR (W/g), can be found by dividing equation (104) or (106) by the tissue density. SERR is equivalent to the specific metabolic rate, SMR.

The ERR is equivalent to the metabolic rate per unit volume which can also be calculated for each model from the local mass fraction by using

$$\dot{q}'''(r) = 2\pi (\rho D)\, d_{cell}\, Y_{O2}(r)\, HHV_{O2}\, n \quad (107)$$

where $\dot{q}'''$ is the metabolic rate per unit volume and $Y_{O2}(r)$ is the local oxygen mass fraction. Integrating over the volume gives the metabolic rate for the model and in the case of the cylindrical geometry, it is given as

$$\dot{q} = \int_0^R \dot{q}'''(r)\, 2\pi\, r\, dr\, L \;, \quad \text{COS model} \tag{108}$$

where $\dot{q}$ is the metabolic rate and L is the length of the cylinder. The integration is from zero to R, the outer tissue radius, for the COS model and from r_{cap}, the capillary radius, to R for the COA model. Dividing equation (108) by the mass of the model gives the specific metabolic rate, $\dot{q}_m$. The specific metabolic rate is the same for the whole organ as it is for the individual model cylinders.

IV.12 Results for Large and Small G

IV.12.1 Very Large G (e.g. large tissue radius)

As tissue becomes larger or as number of cells serviced by capillary increase, the $Y_{O2,cap\text{-}IF}$ decreases and reaches very low value compared to $Y_{O2,cap}$ (typically $pO_{2,cap}$ = 45-95 mm of Hg and recall $Y_{O2} = \gamma_{O2}\, pO_2$). The maximum transport rate is achieved when the difference between the mass fraction of dissolved O_2 in the capillary and the mass fraction of O_2 at the capillary – interstitial fluid interface is greatest. This occurs as the $Y_{O2,cap\text{-}IF}$ tends to a very low value compared to $Y_{O2,cap}$. When $Y_{O2cap\text{-}IF} << Y_{O2cap}$,

$$\dot{m}_{O2,max}\left(\frac{g}{s}\right)= K'_{cap}\ \rho\ Y_{O2,cap}\ S_{cap}\ ,\ \text{COS or COA, Large G} \qquad (109)$$

or

$$\frac{\dot{m}_{O2,max}}{m}\left(\frac{g}{g\ \text{of tissue}}\right)= \frac{K'_{cap}\ \rho\ Y_{O2,cap}\ S_{cap}}{m},\ \text{COS or COA, large G} \qquad (110)$$

Where S_{cap} is the total capillary surface area available for tissue of mass "m".

For COS

$$S_{cap}\left(cm^2\right)= 2\ \pi\ R_{cos}\ L = 2\ \pi\ R_{cos}{}^2\left(\frac{L}{R}\right),\ \text{COS} \qquad (111)$$

Since mass "m" $\propto R^3$, it is apparent from equation (108) that

$$\dot{m}_{O2,max}\ \text{ or }\ \dot{q}_{max} \propto\ m^{(2/3)}\ ,\ \text{COS} \qquad (112)$$

and

$$\dot{m}_{O2,m,\ max}\ \text{or}\ \dot{q}_{m,\ max} \propto\ m^{\ (-1/3)},\quad \text{COS} \qquad (113)$$

and hence specific metabolic rate for large tissues is proportional to mass to the (-1/3) power for COS tissues.

Similarly for COA

$$S_{cap} = 2\pi\, r_{cap}\, L = 2\ \pi\, r_{cap}\, R \left(\frac{L}{R}\right),\ \text{COA} \tag{114}$$

thus

$$\dot{m}_{O2,max} \text{ or } \dot{q}_{max} \propto m^{(1/3)},\ \text{COA} \tag{115}$$

and

$$\dot{m}_{O2,m,\,max} \text{ or } \dot{q}_{m,\ max} \propto m^{(-2/3)},\ \text{COA} \tag{116}$$

and hence specific O_2 consumption rate or specific metabolic rate for large tissues is proportional to mass to the (-2/3) power for COA tissues.

IV.12.2 Very Small G (e.g. small tissue radius)

Recalling from the previously given equation (106) for ERR of the tissue

$$ERR(W / cm^3_{tissue}) = 2\pi\, \rho D\, d_{cell}\, Y_{O2,cap}\, HHV_{O2}\, n\, \eta \tag{106}$$

For small tissue with very few cells, $\eta \approx 1$; thus

$$ERR(W) = 2\pi \rho D \, d_{cell} \, Y_{O2,cap} \, HHV_{O2} \, n \, V \tag{117}$$

$$ERR(W / cm^3_{tissue}) = 2\pi \rho D \, d_{cell} \, Y_{O2,cap} \, HHV_{O2} \, n \tag{118}$$

which shows that specific metabolic rate is independent of tissue radius or

$$\dot{m}_{O2} \text{ or } \dot{q} \propto m \text{ , COA or COS} \tag{119}$$

and

$$\dot{m}_{O2,m,} \text{ or } \dot{q}_{m,} \propto m^{(0)} \text{ , COA} \tag{120}$$

and hence, they follow isometric laws.

IV.12.3 General Law

Writing the previously derived relationships as a general proportional equation yields

$$\dot{q}_{m,} \propto m^{b} \tag{121}$$

and one finds the exponent “b” in allometric law satisfies the following inequality

$$\begin{aligned} &\text{For COS}, \quad -1/3 < b < 0 \\ &\text{For COA}, \quad -2/3 < b < 0 \end{aligned} \tag{122}$$

Thus, small organs will follow isometric law while large organs follow allometric (non-isometric law).

IV.13 Tissue Cylinder Radius (R)

The radius of tissue cylinder can be determined by two methods: i) inter-capillary distance and ii) surface area of capillaries per unit mass ($S_{cap,m}$).

IV.13.1 Intercapillary Distance

There are many capillaries serving the tissue; many of them are active during exercise in order to supply energy needs and a few are closed under sedentary conditions. Thus, intercapillary distance between active capillaries vary (figure 31). Half of “active” intercapillary distance is assumed to be cylinder radius.

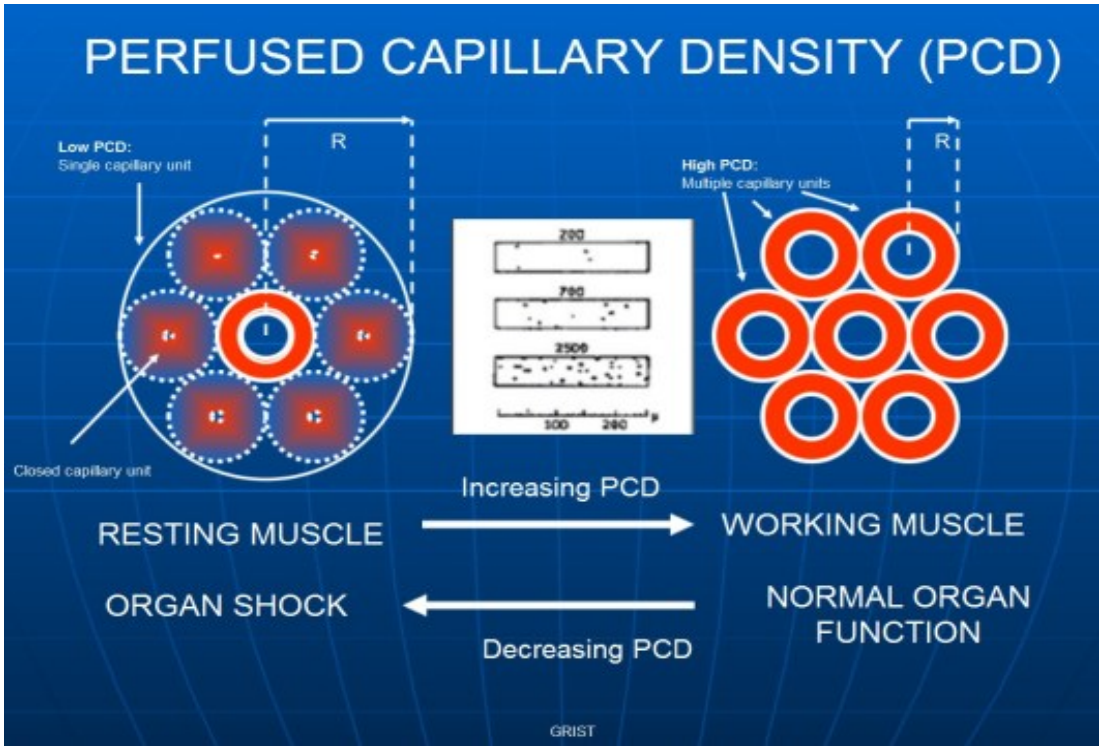

Figure 31. This diagram shows the Krogh cylinder radius when muscles are resting and working. With increased activity, more capillaries open and the radius of the Krogh cylinder (or capillary unit) decreases. Figure adopted from [43].

IV.13.2 Surface Area of Capillaries per Unit Mass ($S_{cap,m}$)

Tissue radius, R, is determined from $S_{cap,m}$, which is the same for both COS and COA models.

a) COS: Considering COS and assuming capillaries cover the surface area completely, then

$$S_{cap,m} = \frac{2\pi R_{COS} L}{\pi R_{COS}^2 L \rho} = \frac{2}{R_{COS} \rho}, \quad \text{COS} \tag{123}$$

Therefore, R will be larger for COS model unless the fraction of area covered by capillaries, F, is accounted for. If indeed only a fraction of the surface area is covered by capillaries for the COS model, then $S_{cap,m}$ is given by

$$S_{cap,m} = \frac{2\pi R_{COS} L F_{COS}}{\pi R_{COS}^2 L \rho} = \frac{2F_{COS}}{R_{COS} \rho} \tag{124}$$

where R_{COS} is the radius of the COS model cylinder, L is the length of the cylinder, ρ is the density of the tissue, and F_{COS} is the fraction of cylinder area covered by capillaries. Solving equation (124) for R_{COS} and non-dimensionalizing by dividing by the capillary radius, r_{cap}, yields

$$\frac{R_{COS}}{r_{cap}} = \left(\frac{2 F_{COS}}{S_{cap,m} \rho r_{cap}} \right) \tag{125}$$

When F_{COS} equals one, R_{COS} will always be higher since it has many capillaries surrounding the cylinder and hence mass needs to be increased so that $S_{cap,m}$ remains the same. Recall the group combustion number G, a measure of the size of the cloud, as given by

$$G = 2\pi d_{cell} n R^2 \tag{126}$$

Substituting equation (124) into equation (126) yields G_{COS}, given as

$$G_{COS} = 2\, S_{cells,m} \frac{\rho R_{COS}^2}{d_{cell}} = G_{cap} \frac{R_{COS}^2}{r_{cap}^2} = G_{cap} \left(\frac{2\, F_{COS}}{r_{cap}\, S_{cap,m}\, \rho} \right)^2 \tag{127}$$

where G_{cap} is defined as

$$G_{cap} = 2\pi\, d_{cell}\, n\, r_{cap}^2 = 2 \left(\frac{\rho\, s_{cell,m}}{d_{cell}} \right) r_{cap}^2 \tag{128}$$

Here, $s_{cell,m}$ is the surface area of all metabolic cells per unit mass of any organ (cm^2/g)

b) <u>COA</u>: For COA models, F_{COA} is always equal to one because the entire area of the capillary is in contact with the tissue. $S_{cap,m}$ is therefore given as

$$S_{cap,m} = \frac{2\pi\, r_{cap} L}{\pi \left(R_{COA}^2 - r_{cap}^2 \right) L\, \rho} = \frac{2\, \xi_{cap}^2}{r_{cap} \left(1 - \xi_{cap}^2 \right) \rho} \tag{129}$$

where

$$\xi_{cap} = \frac{r_{cap}}{R_{COA}} \tag{130}$$

and R_{COA} is the radius from the center of the cylinder to the edge of the tissue in the COA model. To calculate R_{COA}, equation (129) is solved for RCOA and non-dimensionalized by dividing by the capillary radius. This yields

$$\frac{R_{COA}}{r_{cap}} = \sqrt{\left\{1 + \frac{2}{r_{cap}\ S_{cap,m}\ \rho}\right\}} \tag{131}$$

The G number can now be written in a modified form for the COA model of

$$G_{COA} = 2\left(\frac{\rho\ s_{cells,m}}{d_{cell}}\right)\ R_{COA}{}^{2} = 2\ \left(\frac{\rho\ s_{cells,m}}{d_{cell}}\right) r_{cap}{}^{2} \left(\frac{R_{COA}{}^{2}}{r_{cap}{}^{2}}\right) = G_{cap}\left\{1 + \frac{2}{r_{cap}\ S_{cap,m}\ \rho}\right\} \tag{132}$$

where G_{cap} is given as

$$G_{cap} = 2\ \left(\frac{\rho\ s_{cells,m}}{d_{cell}}\right) r_{cap}{}^{2} \tag{133}$$

Where $S_{cap,m}$ is the capillary surface area per unit mass of any organ. It will be seen later that when capillary surface area is very low (e.g. sedentary person with more capillaries closed), Krogh cylinder radius is increased, G is very large, oxygen may not reach all metabolic cells, particularly those far away from capillaries, and specific energy release rate follows allometric law (non-isometric). During exercise most capillaries are open, Krogh cylinder radius is decreased, and hence $S_{cap,m}$ is very high and G is low and oxygen reaches almost all cells and specific energy release rate follows isometric law.

IV.13.3 FCOS

As discussed before, COA has single capillaries while COS may have many capillaries. For COS, each capillary provides half the area to the cylinder of radius R. Considering N_{COS} capillaries on surface of COS, the F_{COS} can be expressed as

$$F_{COS} = \frac{N_{COS} \; \frac{2 \pi r_{cap} \; L}{2}}{2 \pi R_{COS} \; L} = \frac{N_{COS} \; r_{Cap}}{2 \; R_{COS}} \tag{134}$$

In order for COS to have the same surface area as COA, the number of capillaries for COS must be two with each providing half the area to the cylinder of radius R. Using this in equation (134) yields

$$F_{COS} = \frac{N_{COS} \; r_{cap}}{2 \; R_{COS}} = \frac{r_{cap}}{R_{COS}} \tag{135}$$

and substituting equation (125) into equation (135) and solving for F_{COS} gives

$$F_{COS} = \sqrt{\left(\frac{S_{cap,m} \; \rho \; r_{Cap}}{2} \right)} \tag{136}$$

for when capillary surface area of COS equals the capillary surface area of COA. It is assumed that there is no mass transfer along the angular direction.

IV.14 Lethal Corner and Lethal Volume Fraction (LVF)

The lethal corner is traditionally defined as any section of anaerobic tissue; tissue that receives no oxygen (figure 32 for Krogh cylinder). For the models presented here, this definition can only be applied to the uniform source situations as the oxygen dependent model will never approach zero. Therefore, a modified version of the lethal corner is used where if the oxygen concentration percent relative to the oxygen concentration at the capillary-interstitial fluid interface is less than 3.6 mmHg (1.5E-07 g O_2/g blood), then that section of tissue will be deemed a part of the lethal corner [44]. The radius where oxygen concentration falls below the lethal concentration is deemed the lethal radius, r_{Lethal}. All tissue from this location to the capillary is aerobic tissue, receiving adequate oxygen for metabolic function. On the other hand, tissue further from the capillary than the lethal radius is anaerobic and thus, this constitutes the lethal volume.

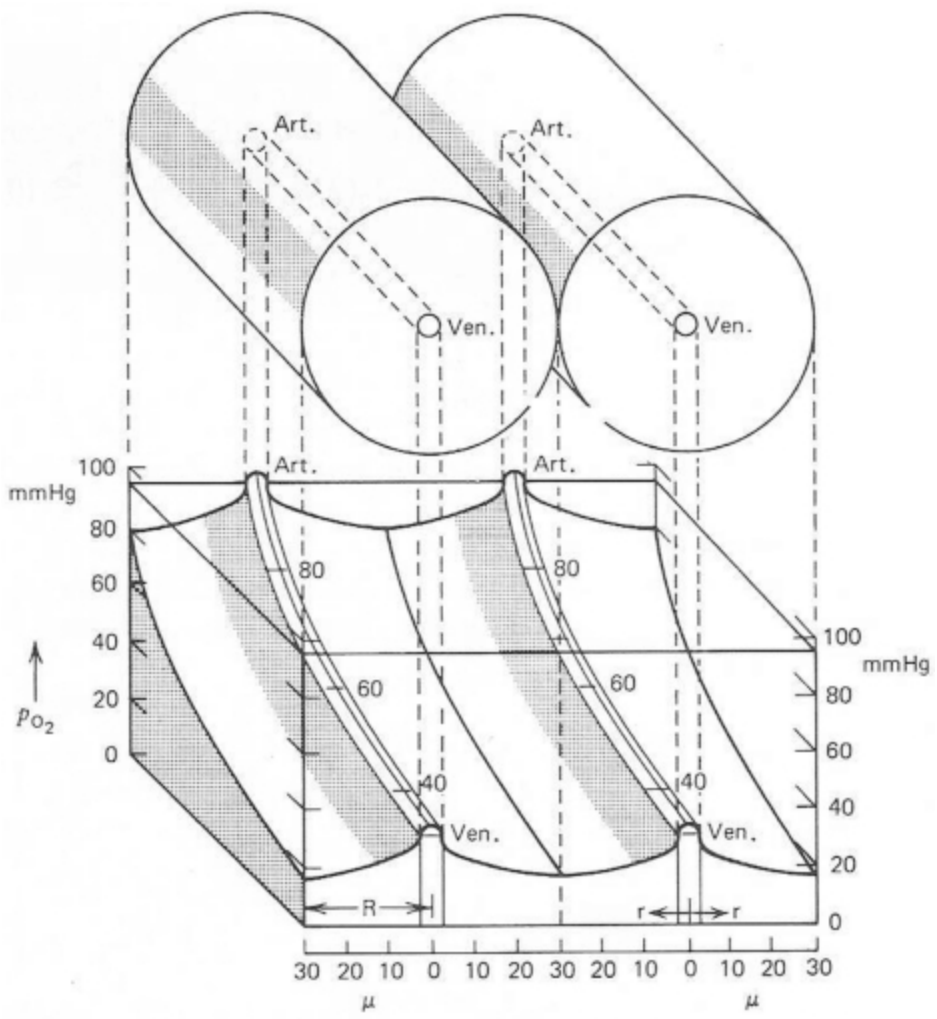

Figure 32. Schematic of two dimensional Krogh cylinder model with O_2 profiles along the capillary axis. The pO_2 decreases from the arterial beginning to a low value at the venous end. At any axial location along the capillary, pO_2 falls in the radial direction in the tissue. The lethal corner here would be located at the venous end, furthest away from the capillary (distance R). Figure adopted from [45].

In order to find the lethal radius, an iterative procedure called the "sandwich method" is used. From the oxygen profile solutions given in table 1, the oxygen concentration is calculated at each point radially from the capillary until the value falls

below the set lethal limit. The program then interpolates the lethal radius value from the last two radii recorded; one in the aerobic tissue and one in the anaerobic tissue.

Lethal volume divided by the total tissue volume is equal to the lethal volume fraction, LVF, as mentioned previously. The LVF of the COA model is given as

$$\mathrm{LVF} = \frac{\left(1 - \xi_L^{\,2}\right)}{\left(1 - \xi_{cap}^{\,2}\right)} \tag{137}$$

where ξ_L is the dimensionless lethal radius and defined as the lethal radius divided by the tissue radius. For the COS model, the LVF is given as

$$\mathrm{LVF} = \xi_{lethal}^{\,2} \tag{138}$$

CHAPTER V

RESULTS AND DISCUSSION

This chapter presents results and discussion based on formulation presented in Chapter IV. Firstly, the methodology of solution is presented followed by i) equilibrium results for Hb and Mb saturation of blood are presented. Next it is followed by presentation of input data used in obtaining the result followed by presentation of ii) oxygen profiles, iii) interface concentration of O2, iv) specific tissue metabolic rate ,v) exponents "b_k" in allometric laws describing the relation between $SERR_k$ or $\dot{q}_{m,k}$ (W/g organ k, also called as specific metabolic rate, SMR, in biology) and mass of organ k, m_k

$$\dot{q}_{m,k}\left(\frac{W}{kg\ of\ k}\right) = a_k\ m_k(kg)^{\ b_k} \tag{1}$$

where a_k and b_k are allometric constants.

V.1 Methodology of Solution

1. Using Henry's law, relate mass fraction of O_2, which is typically used, to partial pressure of O_2 (Equation (12) in Chapter IV).
2. Obtain saturation curve for O_2 using Hb as carrier of O_2 (Using Equation (23) in Chapter IV), and Mb as carrier of O_2 (Equation (25) in Chapter IV), relate pO_2 in

terms of mass fraction, indicate Y_{O2} at arteriole and venule (Equation (12) in Chapter IV).

3. Obtain non dimensional O_2 profiles ($Y_{O2}(r)/Y_{O2,capi\text{-}IF}$)with G as parameter for COS (Equations (40) and (42) in Chapter IV) and G and (r_{cap}/R) as parameters for COA (Equations (41) and (43) in Chapter IV).
4. Using O_2 profile, estimate the ERR of whole cloud (Equations (103) in Chapter IV) and obtain effectiveness factor η_{eff}, as function of G for COS (Equation (84) in Chapter IV) and G and ξ_{cap} ($=r_{cap}/R$) for COA (Equation (85) in Chapter IV).
5. Determine capillary-interstitial fluid (Cap-IF) interface mass fraction of O_2 by matching O_2 consumption by cells within cylinder R to mass transfer rate of O_2 through capillary of thickness δ_{cap}. (Equations (96) in Chapter IV).
6. Obtain correction factor η as function of G for COS and G and ξcap (=rcap/R) for COA (Equation (101) in Chapter IV);this s is very useful relation since organ metabolic rate can be obtained with a knowledge of η, and Y_{O2cap}.
7. Determine cylinder radius from known a) inter-capillary distance or b) $S_{cap,m}$ specific capillary surface area (cm^2/g) (Equations (123) and (129) in Chapter IV) since $S_{cap,m}$ equals capillary surface area within cylinder radius R divided by cylinder tissue mass for either COS or COA.
8. Using η, estimate cylinder metabolic rate of radius R (W) and hence calculate specific metabolic rate (SMR, W/g).

9. Conduct parametric studies for the effect of $S_{cap,\,m}$ which varies from low values for sedentary person (or cylinder radius is large) to a high value (or cylinder of radius is small) of a person exercising.
10. Compare i) capillary-Interstitial fluid (Cap-IF) interface pO_2 , ii) specific metabolic rate and iii) allometric exponents b_k with experimental data.

V.2 Blood O_2 Content and Saturation Percent

V.2.1 O2 Saturation Percent

As O_2 is transferred from alveoli to blood, it gets dissolved due to Henry's law. The dissolved O_2 reacts with red blood cell (RBC or Hb) and produces $Hb(O_2)$, $Hb(O_2)_2$, $Hb(O_2)_3$, and $Hb(O_2)_4$. As Hb is oxidized, the dissolved concentration will decrease, but the alveoli transfer more O_2 and maintain physical and chemical equilibrium. Similarly, Mb (which is not present in blood) is typically present in the IF of heart and skeletal muscle tissue and reacts with dissolved O_2 in IF to produce $Mb(O_2)$ and reach local chemical equilibrium with O_2.

Instead of YO2, biology uses pO_2 to indicate the concentration of O_2 in blood even though O_2 is not gas. For example, the pO_2 at 40 mm of Hg in venule represents a hypothetical alveoli at 40 mm of Hg maintaining chemical and physical equilibrium with a hypothetical capillary around alveoli receiving O_2; the pO_2 is related to Y_{O2} through Henry's law (Equation (12) in Chapter IV). The Hb and Mb saturation curves were modeled based on thermodynamics and used to identify what percentage of the total Hb or Mb is oxygenated. Using the data from Atkins and De Paula, presented in table 2,

and equation (19), one can determine the saturation O_2 percent as well as equilibrium concentrations of various oxidized Hb compounds. Once concentrations of $Hb(O_2)$, $Hb(O_2)_2$, $Hb(O_2)_3$, and $Hb(O_2)_4$ are determined, the saturation O_2 percent (=100*O_2 moles with Hb / (4*Total Hb) versus pO_2 can be obtained (Equation (22)).

Table 2. Equilibrium constants used to model Hemoglobin and Myoglobin saturation curves. Data taken from Atkins and De Paula [42].

Equilibrium Constant	Value	Units
K^0_1'	0.01	1/mm of Hg
K^0_2'	0.02	1/mm of Hg
K^0_3'	0.04	1/mm of Hg
K^0_4'	0.08	1/mm of Hg
K'_{Mb}	0.4	1/mm of Hg

Figure 33 shows the percent concentration (Hb with each oxidized compound / total Hb in blood) vs pO_2. At pO_2=0, only Hb is present. At higher pO_2, $Hb(O_2)_4$ is the dominant form of Hb, while at lower concentrations, deoxygenated Hb is dominant. The reason none of the other oxygenated forms of Hb reach high concentrations is because Hb undergoes conformational changes as each O_2 molecule bonds. These changes result in a higher affinity of Hb for the next O_2 molecule. Therefore, HbO_2 relatively quickly becomes $Hb(O_2)_4$. As the pO_2 level, and thus oxygen concentration, increases, $Hb(O_2)_4$ concentration dominates. At low pO_2 of the order of 40 mm of Hg (typical venule

pressure), 40% is due to $Hb(O_2)_4$, 10% due to $Hb(O_2)_3$, 10% due to $Hb(O_2)_2$, 10% due to $Hb(O_2)$, 30% due to Hb. The blood in the vein at this pO_2 returns to the lungs via the heart for the next cycle.

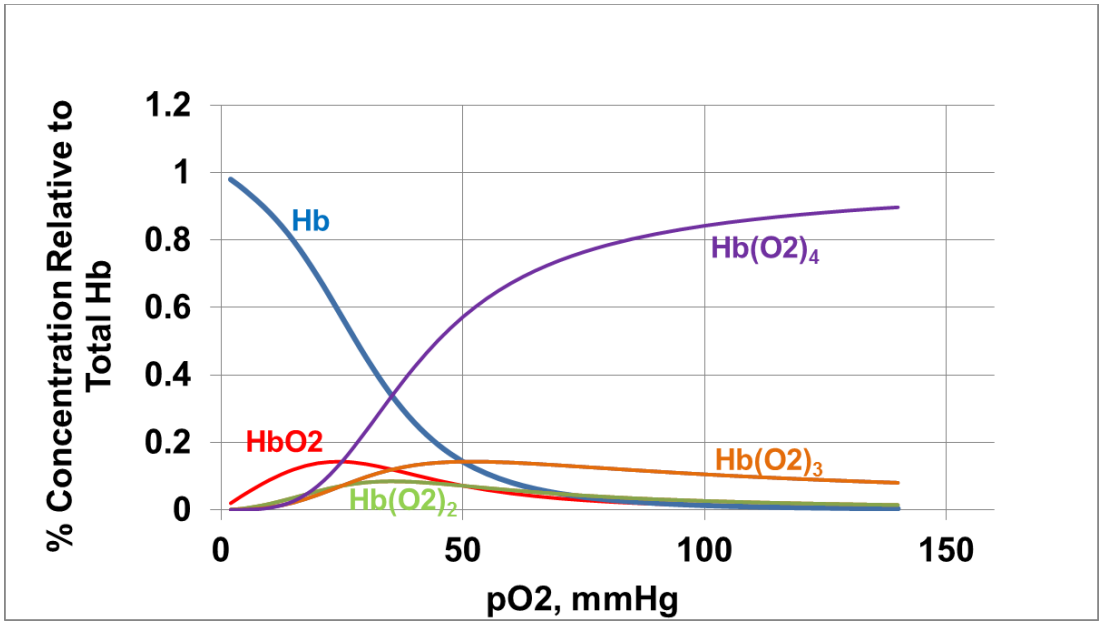

Figure 33. Concentrations of hemoglobin as well as the four forms of oxygenated hemoglobin are plotted as percentages relative to the total hemoglobin vs pO_2 levels. As the pO2 level, and thus oxygen concentration, increases, $Hb(O_2)_4$ concentration dominates.

Once concentrations of $Hb(O_2)$, $Hb(O_2)_2$, $Hb(O_2)_3$, and $Hb(O_2)_4$ are determined, the saturation O_2% (chemical O_2 content expressed as percent of O_2 content when all Hb in blood is oxidized to $Hb(O_2)_4$) versus pO_2 can be obtained (see equation (22) in Chapter IV). The Hb and Mb saturation curves were modeled based on thermodynamics

and used to identify what percentage of the total Hb or Mb is oxygenated. The saturation curves were plotted and can be seen in figure 34.

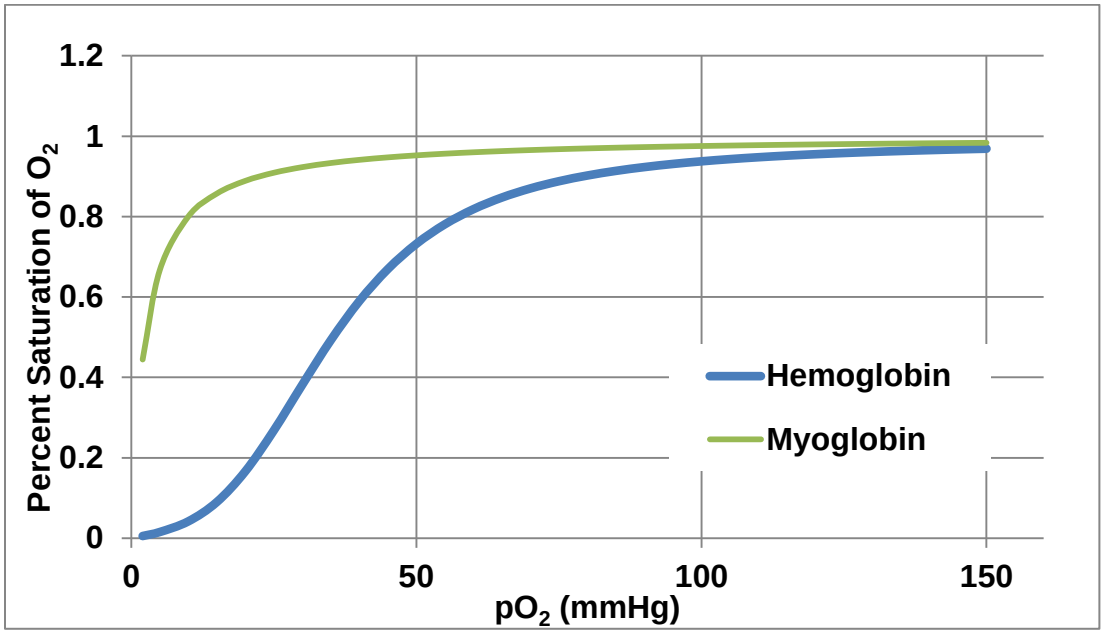

Figure 34. Hemoglobin and Myoglobin saturation curves calculated from equation (14) as derived by Atkins and De Paula [42]. The shape of the Hb curve is due to the conformational changes it undergoes as O_2 molecules bind. These curves can shift left or right depending on pH, temperature, and other factors.

V.2.2 O_2 Content in the Blood

As mentioned earlier the total blood O_2 content is a sum of dissolved O_2 (physical or aqueous O_2) and O_2 associated with oxidized Hb (chemical O_2). In combustion science, the O_2 content is given as mass fraction of O_2 while the biology literature presents total O_2 as gas volume in mL of O_2 per L of blood. Biology uses CST standard gas (0°C, 1.013 bar; and hence, 1 g mole occupies 22.4 Liters of gas or density =1.429 g/L of gas). Total O_2 content in blood in mL of O_2/L of blood = mL of

dissolved O_2/L of blood + (22400 mL/CST mole)(Saturation%/100)*4* $[Hb]_{total}$ (g/L of blood) /M_{Hb}(g/mole). Typically, total O_2 content is about 200 mL per L of blood of density 1.06 g/cm^3. It can be easily converted into mass of O_2 per unit mass of blood by using Y_{O2} (g of O_2 / g blood) = (O_2 in mL/L) * $1.0x10^{-3}$ (L/mL)*1.429 (g/L) / (1.06 (g/cm3)*(1000 cm3/L)) = (O_2 in mL/L) * γ_{O2} where $\gamma_{O2} = 1.348x10^{-6}$.

Similarly, Mb (which is not present in blood) present in tissues which receive dissolved O_2 from capillaries gets oxidized to MbO_2 and reached equilibrium with O_2. The variation of chemical, aqueous, and total O_2 in mL per L of blood vs pO_2 is plotted in Figure 35. It is apparent that the concentration of chemical O_2 is almost 50-60 times that of O_2(aq) bonded to Hb as seen in figure 35. It can also be seen, that raising pO_2 levels beyond 100 mmHg, as done in oxygen treatments, primarily increases the dissolved O_2 in the blood, while the amount of O_2 bonded to Hb does not increase quite as much.

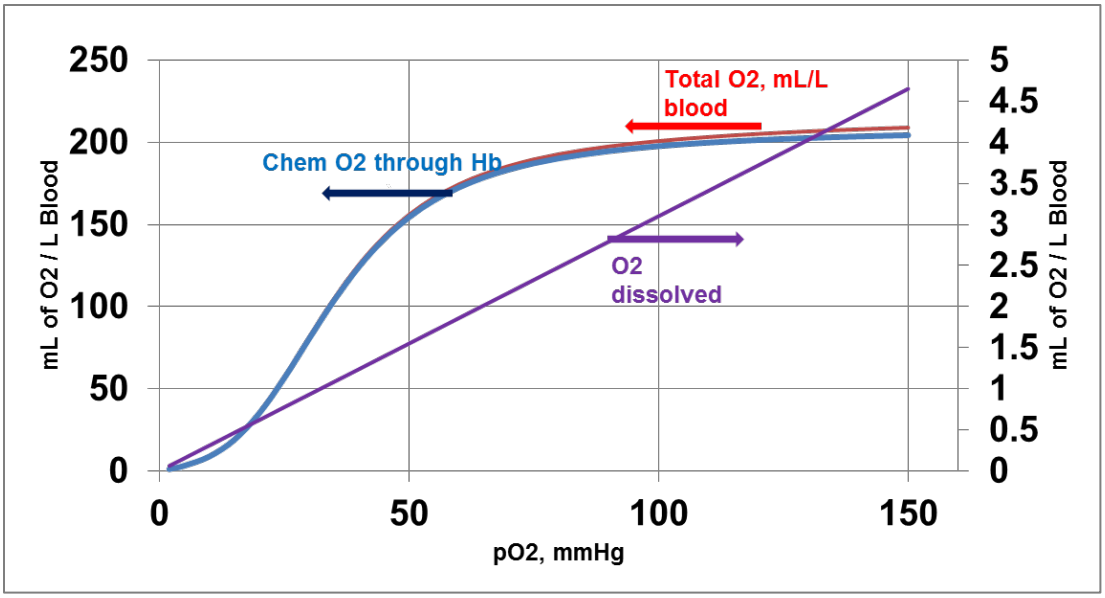

Figure 35. Comparison between the amount of O2 chemically bound to Hb (blue line) and the amount of O2 dissolved in the blood stream (purple line). The red line represents the total amount of O2 in the blood. The ordinate is in mL of O2 (CST gas equivalent). As oxygen is consumed, dissolved O2 decreases in organs due to consumption, and then it decreases total O2 indicating delivery of O2 to the tissue from capillaries in the organ.

Figure 35 can also be plotted as the mass fraction versus pO_2 as seen in figure 36. This plot also allows us to see the parts per million (ppm) of O2 in the blood. For example, at 100 mmHg, there is approximately 4 ppm of dissolved O2 in the blood stream. The right hand side of this plot was used to convert from partial pressure to mass fraction for the models.

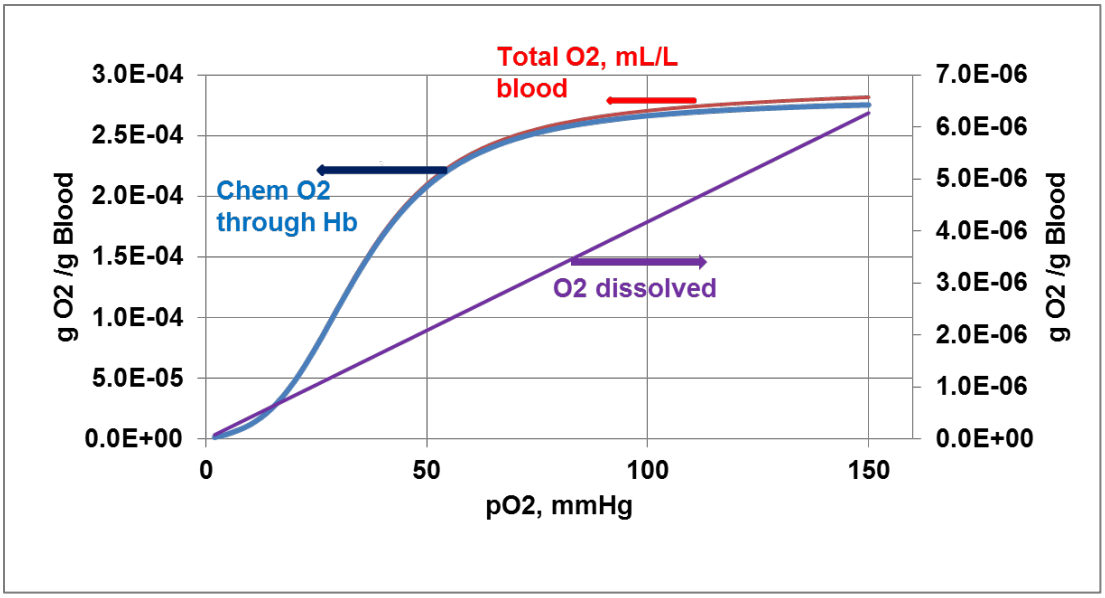

Figure 36. Comparison between the mass fraction of O2 chemically bound to Hb (blue line) and the mass fraction of O2 dissolved in the blood stream (purple line). The red line represents the total mass fraction of O2 in the blood. One part per million (1 ppm) of O2 = 1 g of O2 per million g of blood. At 100 mm Hg, we have 5 ppm of dissolved blood and 250 ppm of chemically bound O2 indicating almost 70 times that of dissolved blood.

V.3 Input Data for Quantitative Calculations

Biological values for the solutions were obtained from various literature sources and presented in table 3 for capillary values and table 4 for tissue values. The units have been converted on some values for consistency. All values are listed along with the literature reference they have been taken from. If no reference is given, then the value was calculated from the other biological values.

Table 3. Biological values for capillaries used in the oxygen transport models. 1 mL of O_2 at CST = 1.43 g/mL.

Variable	Meaning	Value	Units	Reference
$Y_{O2,cap}$	Dissolved oxygen concentration in capillary	$3.97x10^{-6}$	g O2/g blood	
pO_2,cap		95	mmHg	[46]
ρ_{blood}	Blood density	1.06	g/cm^3	[47]
r_{cap}	Capillary radius	0.0003	cm	[46]
t_{cap}	Capillary wall thickness	0.0001	cm	[48]
K'_{cap}	Oxygen permeability across capillary	0.2	cm/s	
$S_{cap,L}$	Total capillary surface area of liver	$2.1x10^5$	cm^2	[49]
$S_{cap,m,L}$	Specific capillary surface area of liver	135	cm^2/g	
F_{COS}	Surface area fraction covered by capillaries	0.1447		

Table 4. Biological values for tissue (interstitial fluid and cells) used in the oxygen transport models.

Variable	Meaning	Value	Units	Reference
D_{O2}	Diffusion coefficient of oxygen	0.00002	cm^2/sec	[46]
ρ_{tissue}	Tissue density	1.06	g/cm^3	[50]
d_{cell}	Cell diameter	0.002	cm	[51]
n	Number of cells per volume	$1.69x10^8$	cells/cm^3	[52]
pO_2 lethal	Lethal oxygen concentration	3.6	mmHg	[44]
HHV_{O2}	Higher heating value per unit mass of stoichiometric oxygen	14200	J/g	[36]
HHV_{O2}'	Higher heating value per unit mass of stoichiometric oxygen	20310	J/cm3	Calculated based on CST standard

Remarks: inter-cell spacing (ℓ)/d_{cell}>1; $\ell = \left(\frac{6}{\pi * n}\right)^{1/3} = 0.0022$, ($\ell$)/$d_{cell}$=1.1>1;

estimation based on a sphere of diameter ℓ equal to volume per cell (1/n); further the distance from capillary must be greater than d_{cell} to accommodate cell.

1 mL of O2 consumed per L = 1.0×10^{-3}* 32 (g/mol)*14200 J/g / (22.4 L per mol) = 0.00143 g per L=20.29 J/per L of blood

V.4 Oxygen Profiles

Utilizing the values from tables 3 and 4 with the solutions presented in table 1, the resulting oxygen profiles were plotted using Excel. Figure 37 shows the oxygen concentration profiles for COS-O2 and COA-O2 models; from the profiles the volume averages YO2 can be calculated and the ratio $Y_{O2avg}/Y_{O2cap\text{-}IF}$ which is same as η_{eff} can be obtained for both COS-O2 and COA-O2 models. Then using this average YO2avg, the uniform sink of O_2 is evaluated for the Krogh model. For comparison, figure 38 shows the oxygen profiles where η_{eff} for the US models is equal to one; i.e. US model is evaluated using $Y_{O2cap\text{-}IF}$. Once again, all results shown are for cylindrical geometry, as that is the primary focus of this paper.

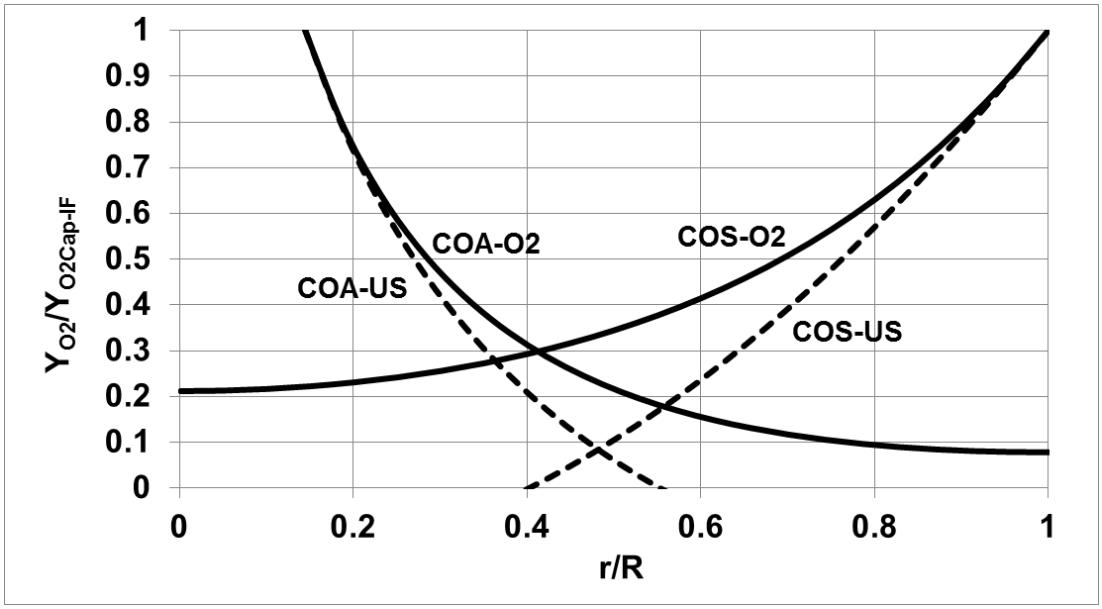

Figure 37. Oxygen concentration profiles for the four models in cylindrical geometry where COA is capillary on axis, COS is capillary on surface, US is uniform source, and O2 is oxygen dependent source. The uniform source is calculated using the average mass fraction from the O2 models. G_{COS}=8.75; G_{COA}=9.13; η_{eff} for COS-O2= 0.55; η_{eff} for COA-O2=0.18.

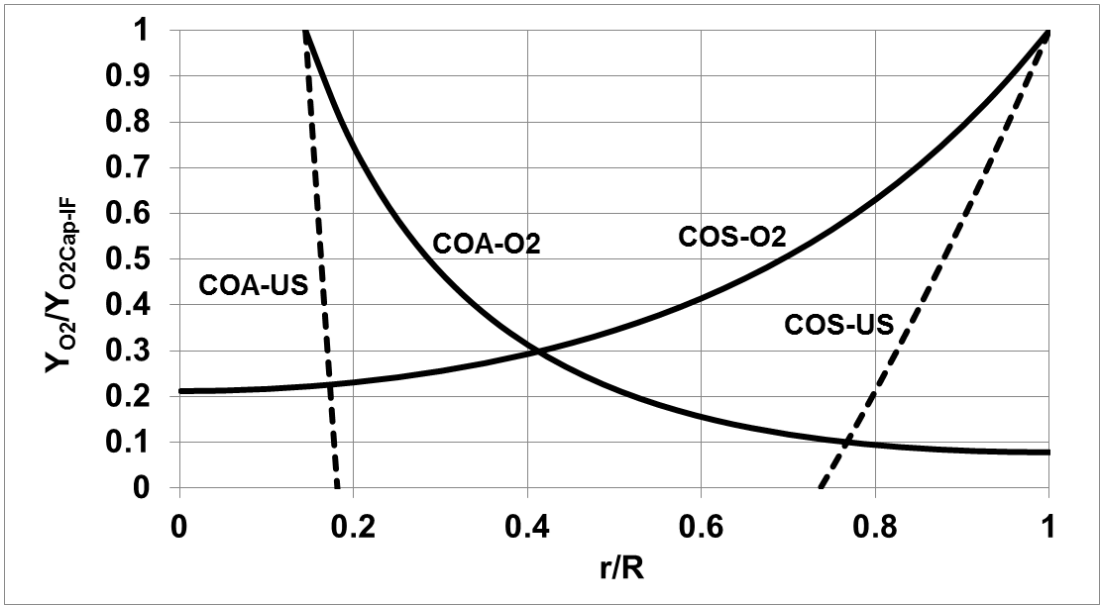

Figure 38. Oxygen concentration profiles for the four models in cylindrical geometry where COA is capillary on axis, COS is capillary on surface, US is uniform source, and O2 is oxygen dependent source. G_{COS}=8.75; G_{COA}=9.13; The uniform source is calculated using η_{eff} equal to one.

Oxygen concentration decreases as the radius, r, increases, moving further from the capillaries. The slope of the curve is zero at the edge of the tissue for COA and at the center for COS as specified by the boundary conditions mentioned earlier. Notice the oxygen dependent models decrease at a slower rate than uniform source the models. This can be explained by the use of the uniform source instead of a varying source. Also, the uniform source models gave negative values after a certain radius. Understandably, a negative oxygen concentration does not make physical sense, therefor the oxygen concentration is set to zero for these situations. On the other hand, because of their varying source term that depends on the local oxygen concentration, the O2

models will never go negative and only approach zero. As the oxygen concentration decreases, the source term also decreases and both go to zero at large radii.

V.5 Capillary – IF Interface Oxygen Concentration

Using Equation (95) for the Cap-IF interface mass fraction, the partial pressure of O_2 at cap-IF interface is estimated. Figure 39 plots the variation of $pO_{2,cap\text{-}IF}$ with pO_2,cap for COA-O2, COA-US, COS-O2, and COS-US for specified $S_{cap,m}$ (cm2/g). It is seen for small $S_{cap,m}$ (at high specific metabolic rate), the $pO_{2,cap\text{-}IF}$ keeps decreasing and reaches almost zero indicating the transport control across capillaries at very low $S_{cap,m}$ (e.g. large organ with same capillary surface area). For large $S_{cap,m}$ (low specific metabolic rate), the $pO_{2,cap\text{-}IF}$ is almost same as $pO_{2,cap}$.

V.6 Lethal Volume Fraction

Once $Y_{O2,cap\text{-}IF}$ is known, the oxygen mass fraction and hence pO_2 in the IF can be determined. Lethal limit for pO_2 was set to 3.6 mmHg (pO_2 lethal). The distance from the oxygen source to the point where the lethal O_2 concentration is reached, δ, is called the aerobic shell for the COS models and the aerobic core for the COA models. This is the section of tissue that receives enough O_2 to be metabolically active. The O2 models never reached the lethal limit for the base study. On the other hand, both US models reach the lethal limit and then quickly go to zero (figure 37) since they evaluate sink (g of O_2 consumed per g of tissue) at higher rate. The anaerobic volume divided by the total volume of the tissue gives the lethal volume fraction, LVF (which is the same as

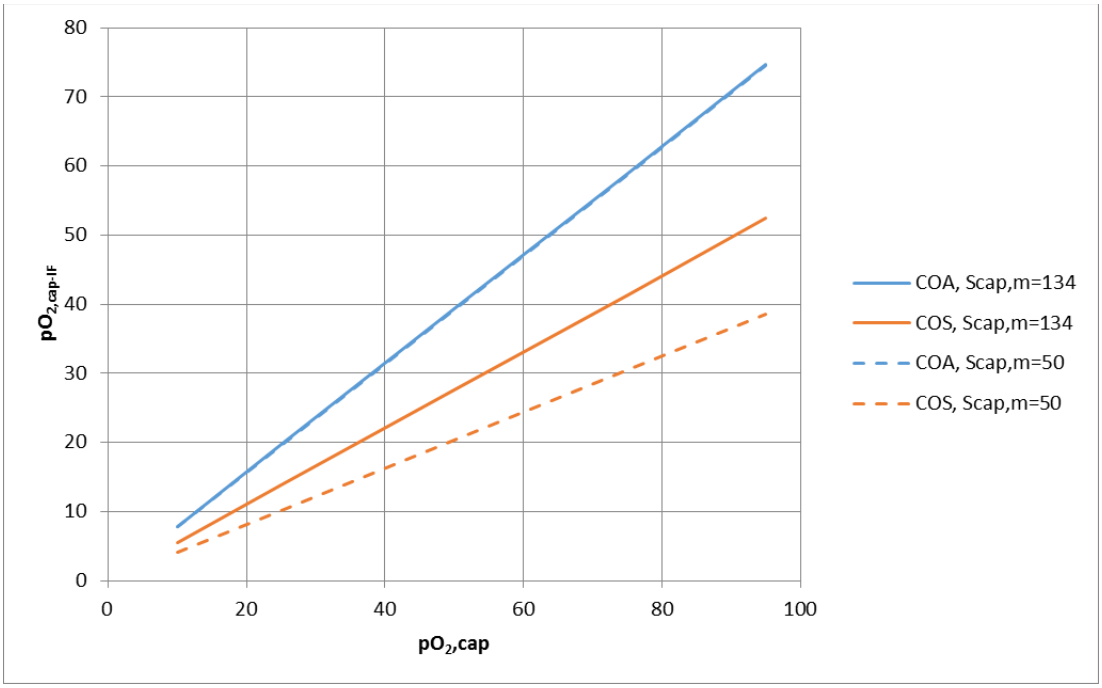

Figure 39. Plot of $pO_{2,cap-IF}$ versus $pO_{2,cap}$ for COS and COA models at two different specified values of $S_{cap,m}$.

the ratio of the number of lethal cells to total number of cells), or the fraction of cells not receiving an adequate supply of O_2. Based on Warburg's hypothesis, the cells located in the anaerobic tissue would be at greater risk for becoming cancer cells [26], or LVF is proportional to fraction of cells being cancerous or carcinogenic. The body periodically flushes out cancerous cells from each organ. Sometimes these cancerous cells drift, escape, and join the blood stream, affecting other parts of the body.

Several parametric studies were conducted to see the effects of various parameters on the LVF. First, pO2 levels were varied and the resulting LVF can be seen in figure 40 for FCOS = 0.1447. The O2 models do not experience any lethal volume until the capillary pO2 drops below 60mmHg for COA and 40 mmHg for COS. Next,

FCOS was set equal to one and the LVF was recalculated and can be seen in figure 41. The LVF is much higher for the COS models now because as FCOS increases, the tissue radius, R_{COS}, also increases to maintain the same specific capillary surface area as the COA models.

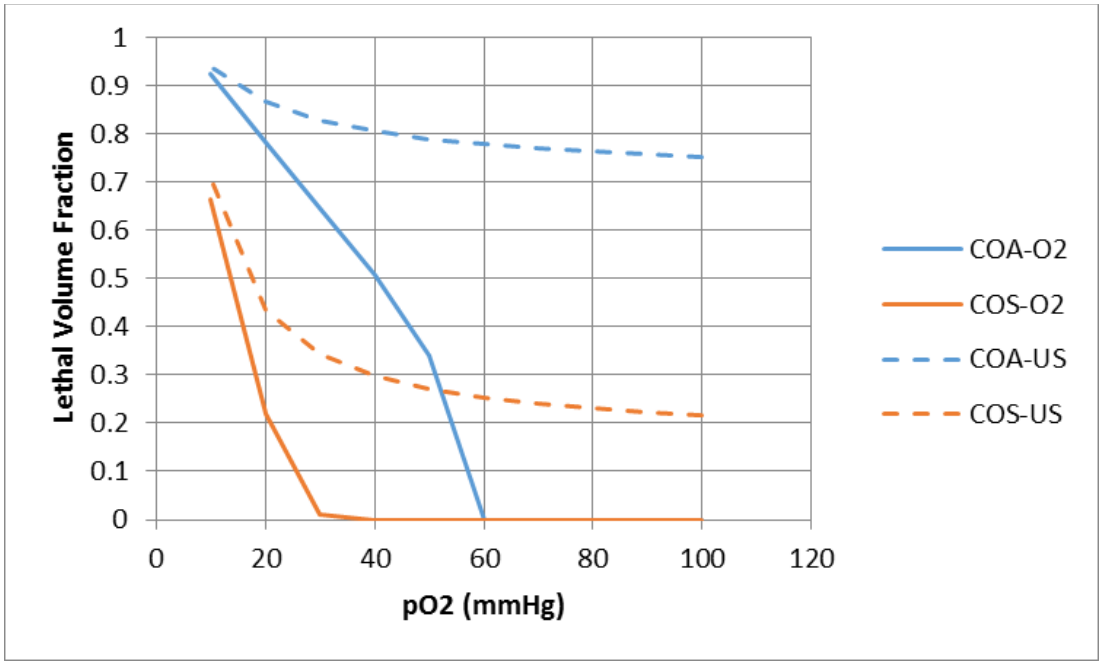

Figure 40. Lethal volume fraction vs the capillary oxygen concentration with FCOS = 0.1447 and α = 0.

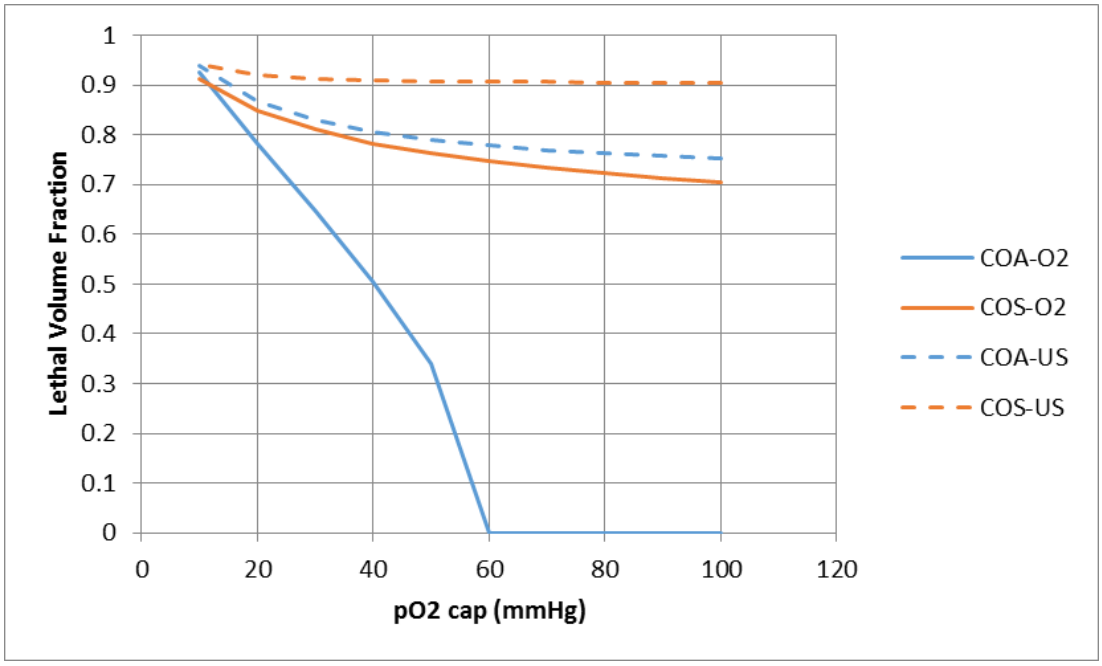

Figure 41. Lethal volume fraction vs the capillary oxygen concentration with FCOS = 1 and α = 0.

$S_{cap,m}$ was also varied to study the effects on LVF for the four models with FCOS = 0.1447 and α = 0. Figure 42 shows the plot of LVF vs $S_{cap,m}$. If $S_{cap,m}$ is small (e.g. resting muscle), possibly from blocked or closed off capillaries, then it has to serve over larger tissue, or the tissue radius will be larger (figure 43). As the tissue radius is increased, the lethal volume also increases. Similarly, as tissue radius is decreased, the LVF decreases (figure 42). The COA models have a higher LVF because of the geometric factor. At a larger radius from the center of the cylinder, there is a larger volume of cells at that particular distance. Thus, there are more cells located further from the capillary than in the COS model and the COA model will have a larger LVF.

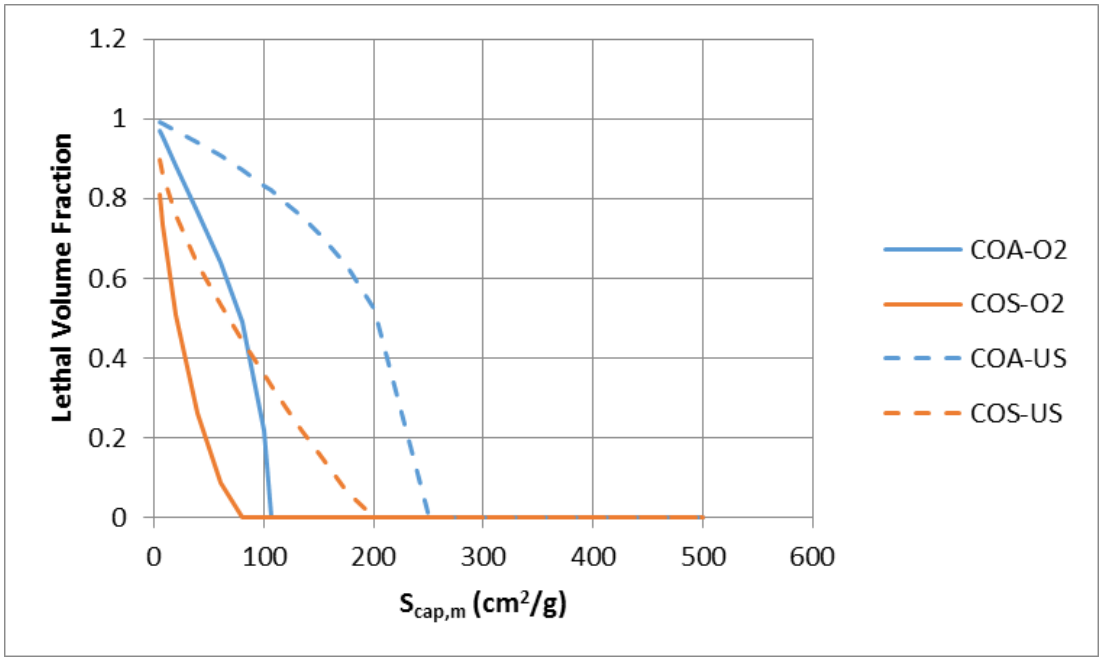

Figure 42. Lethal volume fraction is plotted vs the specific capillary surface area, $S_{cap,m}$ (cm^2/g), for the four models. The uniform source is calculated using the average mass fraction from the O2 models. α=0, FCOS=0.1447.

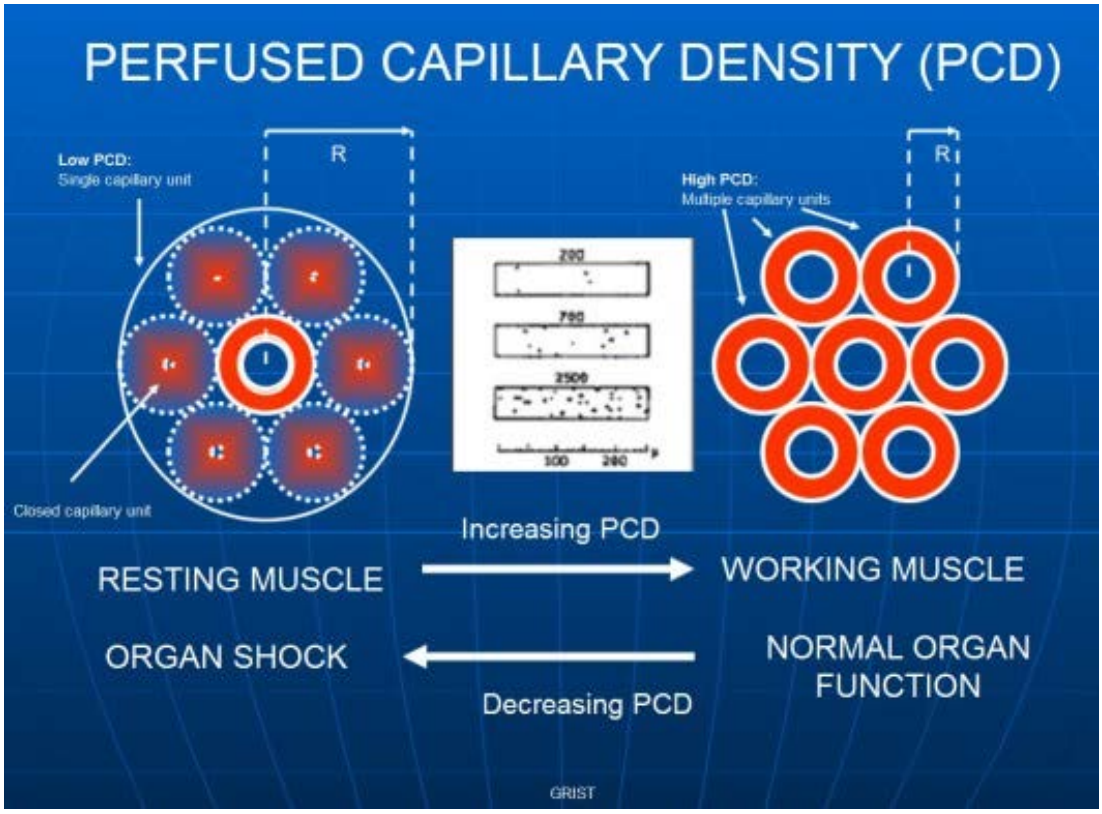

Figure 43. Capillaries can open and close depending on the state of the tissue. For the case of skeletal muscle tissue, during rest, the minimum numbers of capillaries are open. On the other hand, a working muscle will have the maximum number of capillaries open to supply adequate blood flow. Adopted from [43].

The denominator of equation (96) suggests that one must exclude those cells within LVF in estimating O_2 consumption rate and hence $Y_{O2,cap\text{-}IF}$ will increase if effect of LVF is included which will enhance metabolic rates of cells within aerobic region. However, it has been assumed that these cells within lethal region has the same average sink rate as those in aerobic region; $Y_{O2,avg\ lethal}$ is close to $Y_{O2,lethal}$ and as such those cells in lethal region will decrease the whole tissue metabolic rate to a lesser extent and

hence $Y_{O2,cap-IF}$ will be higher than prediction. If LVF = 0, then there is no error involved.

Since it has been assumed that tissue radius is proportional to the organ size, this means that smaller organs would have a smaller occurrence of cancer than larger organs. No evidence has been found to support this claim, but a lack of oxygen is not the only factor to cause damage to the cellular respiration. Respiratory poisons, lack of nutrients, and circulatory problems specific to a certain organ could also contribute to the damaging of the cellular respiration. It is important to remember for cancer, there are many sources that may lead to the fundamental cause of cancer development: damage to cellular respiration and creation of cells without mitochondria: the micro-combustion chamber within the cell.

V.7 Effectiveness Factor, η_{eff} (based on $Y_{O2,cap-IF}$), and Correction Factor, η (based on $Y_{O2,cap}$).

Non-dimensional plots for η_{eff} and η similar to combustion science can be generated as a function of G for COS-O2. Figure 44 shows the results for the η_{eff} versus G for COS model, while figure 45 shows η_{eff} versus G and with G_{cap} as parameter for the COA model. Note that varying G_{cap} does not affect η_{eff} in the COS model.

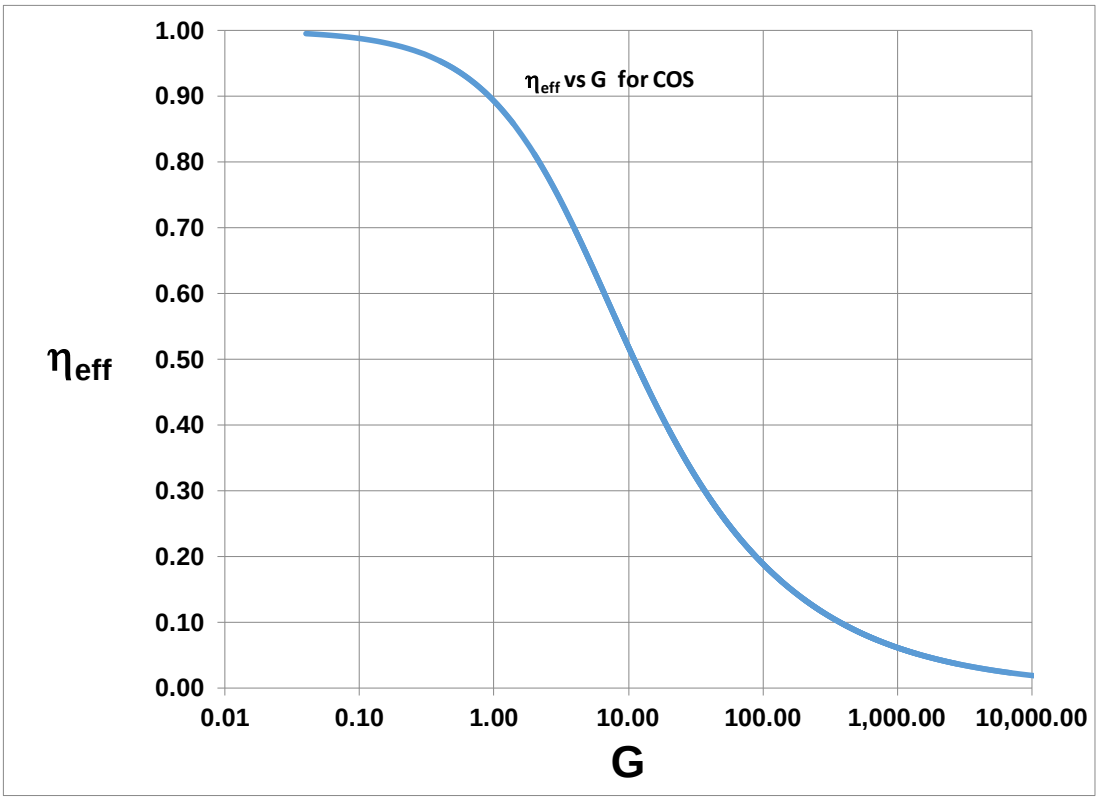

Figure 44. Variation of effectiveness factor with G for COS models. η_{eff} is the ratio of actual metabolic rate over the isolated metabolic rate if all cells were at an oxygen concentration equal to that of cap-IF interface.

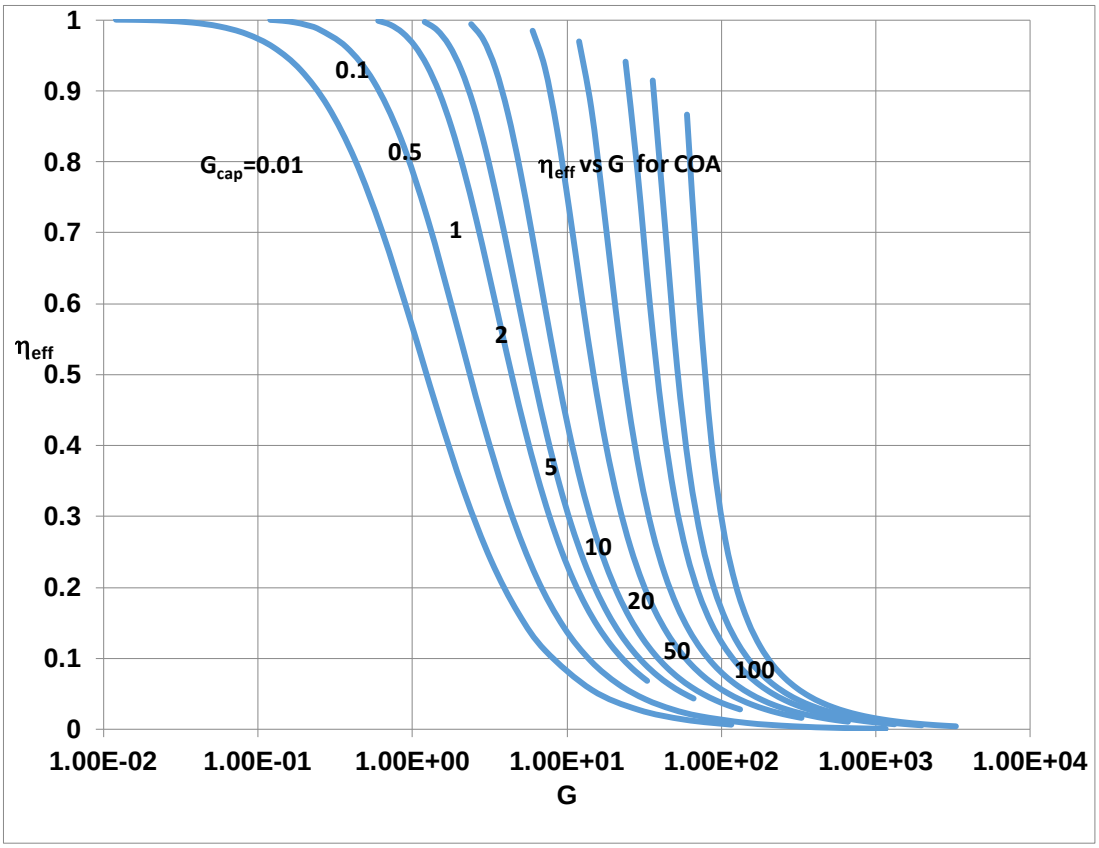

Figure 45. Variation of effectiveness factor with G for COA models with G_{cap} as a parameter ($G_{cap}=2\pi$ n d_{cell} r_{cap}^2). η_{eff}, is the ratio of actual metabolic rate over the isolated metabolic rate if all cells were at an oxygen concentration equal to that of cap-IF interface.

The generation of the plot for η requires a relation between YO2,cap-IF and YO2,cap. For COS-O2 model, the relation is given as

$$\frac{Y_{O2,cap\text{-}IF}}{Y_{O2,cap}} = \frac{1}{\left\{1+\eta_{eff} G \left(\frac{D_{IF\text{-}cell}}{K'_{cap} d_{cap}}\right)\left(\frac{r_{cap}}{F_{COS} R_{COS}}\right)\right\}} = \frac{1}{\left\{1+\eta_{eff} \frac{1}{F_{COS}} \left(\frac{D_{IF\text{-}cell}}{K'_{cap} d_{cap}}\right)\sqrt{GG_{cap}}\right\}} \quad (139)$$

where

$$\left(\frac{D_{IF\text{-}cell}}{K'_{cap}d_{cap}}\right)=\left(\frac{\delta_{cap}}{d_{cap}}\right),\ \left(\frac{r_{cap}}{F_{COS}R_{COS}}\right)=\left(\frac{G_{cap}}{F_{COS}}\right),\ G_{cap}=2\pi\, n\, d_{cell}\, r_{cap}^2 \tag{140}$$

For the COA model, the relation is given as

$$\frac{Y_{O2,cap\text{-}IF}}{Y_{O2,cap}}=\frac{1}{\left(1+\eta_{eff}G\frac{D_{IF\text{-}cell}}{K'_{cap}d_{cap}}\left\{1-\left(\frac{r_{cap}}{R_{COA}}\right)^2\right\}\right)}=\frac{1}{\left(1+\eta_{eff}\frac{D_{IF\text{-}cell}}{K'_{cap}d_{cap}}\left\{G-G_{cap}\right\}\right)} \tag{141}$$

or

$$\frac{Y_{O2,cap\text{-}IF}}{Y_{O2,cap}}\approx\frac{1}{\left(1+\eta_{eff}\frac{D_{IF\text{-}cell}}{K'_{cap}d_{cap}}G\right)}\ \text{when}\ G_{cap}<<G,COA \tag{142}$$

where η_{eff} is a function of G and G_{cap}.

Figure 46 shows the results for η versus G for the COS model for a hypothetical spherical tissue immersed in an infinite plasma having O_2 mas fraction same as $Y_{O2,cap}$. Under this condition $K'_{cap}=D_{IF\text{-}cell}/R$; volume, $V=(4/3)\pi R^3$; surface area $A_{cap}=4\pi R^2$. The result tends to the same relation as in engineering for spherical porous carbon particle. G was varied to see how changing the tissue cylinder size would affect η where η is the

ratio of actual metabolic rate over the isolated metabolic rate if all cells were at an oxygen concentration equal to that of inside the capillary.

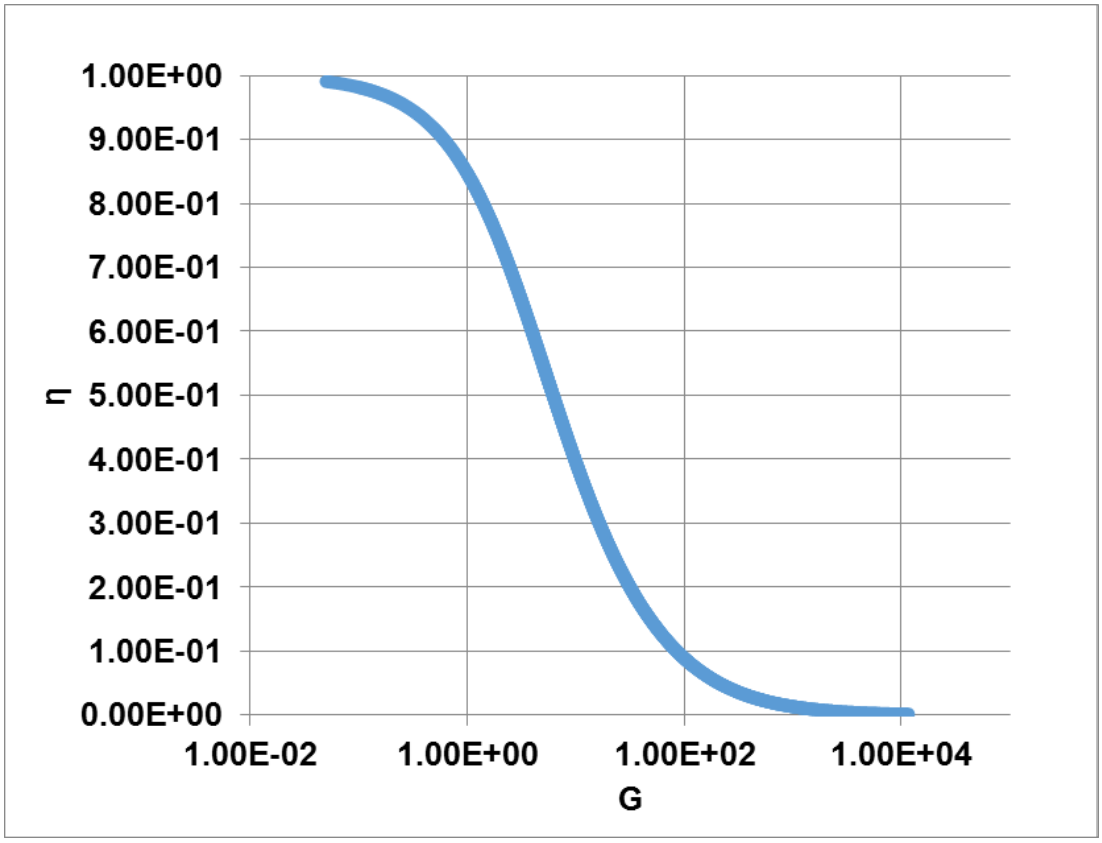

Figure 46. η, the ratio of actual metabolic rate over the isolated metabolic rate if all cells were at an oxygen concentration equal to that of inside the capillary, versus G, the group combustion number for a hypothetical spherical tissue cloud immersed in an infinite plasma having same concentrations YO2,cap for the COS models. For this case $K'_{cap} = D_{IF\text{-}cell}/R$; $V= (4/3)\,\pi R^3$, $A_{cap}=4\,\pi R^2$; see equation (95). When G is small, η behaves isometrically and the allometric exponent, b_k, is approximately zero. On the other hand, when G becomes large, b_k approaches -1/3 for COS models. G is based RCOS.

When G is very low, η behaves isometrically and the allometric exponent, b_k, is approximately zero. On the other hand, when G becomes very large, there is a thin layer

of cells near the capillary receiving O_2 and mass transfer controls metabolic rate. Therefore, b_k approaches -1/3 for COS models

Figure 47 shows a comparison of the results for η_{eff} versus G for COS and COA with G_{cap} as a parameter. At fixed G_{cap}, decreasing R (e.g. reduction in inter-capillary distance with exercise), cause η_{eff} to increase and more cells get O_2. At given G of 10, η_{eff} =0.52 for COS while at same G (same cylinder radius R), η_{eff} is almost same as 0.52 at G_{cap}=6.3 but 0.75 if G_{cap} is set at 10. If r_{cap} is increased, G_{cap} increases and η_{eff} increases since more capillary area is provided.

As in COS models, when G is very low, η behaves isometrically and the allometric exponent, b_k, is approximately zero. On the other hand, when G becomes very large, there is a thin layer of cells near the capillary at axis receiving O_2 and mass transfer controls metabolic rate. Therefore, b_k approaches -2/3 for COA models.

If, in a given capillary network, one capillary was to become blocked, then $S_{cap,m}$ would decrease and the tissue cylinder radius, R, would increase. This would cause an increase in G and thus a decrease in η. On the other hand, if more capillaries were opened, then $S_{cap,m}$ would increase. This would cause R, and thus G, to decrease leading to an increase in η. Also, with a higher $S_{cap,m}$, the LVF would also decrease. Therefore, one can see the importance of healthy living so as to prevent O_2 deficiency in the tissues.

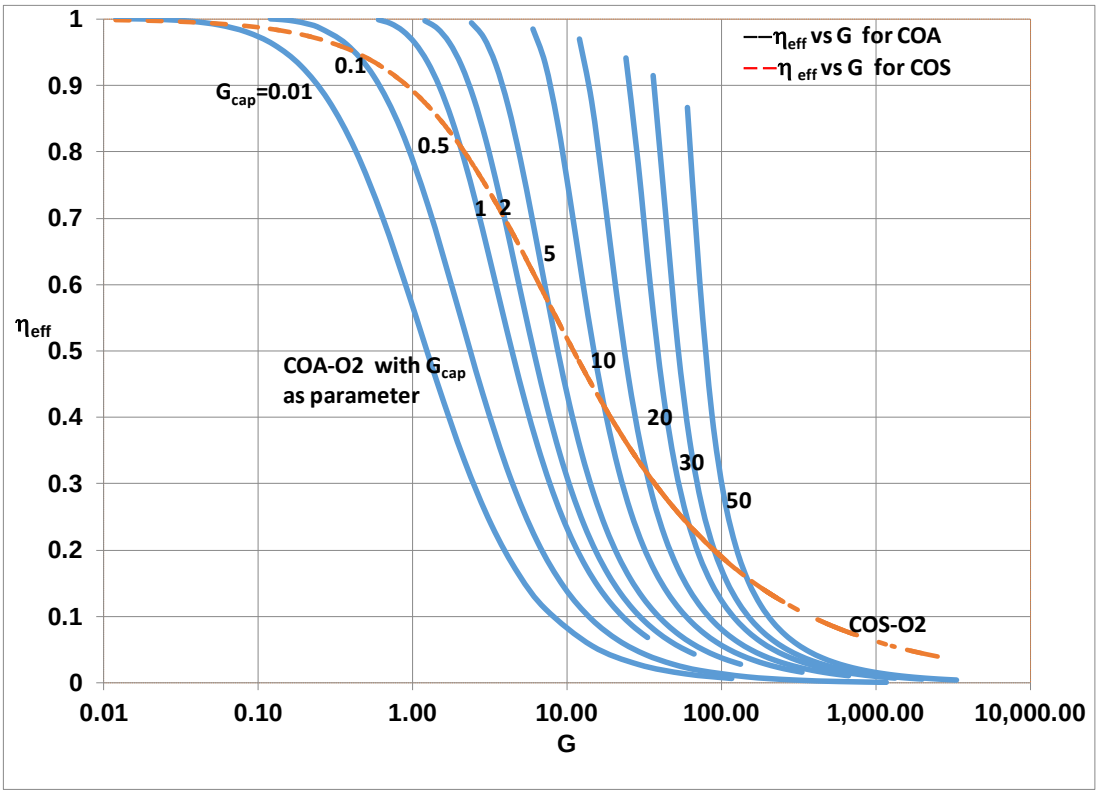

Figure 47. A comparison of the effectiveness factor vs G for COS and COA models. The ratio of actual metabolic rate over the isolated metabolic rate if all cells were at an oxygen concentration equal to that of inside the capillary, versus G, the group combustion number and a measure of the size of the tissue, for the COA models with G_{cap} as a parameter. When G is small, η behaves isometrically and the allometric exponent, b_k, is approximately zero. On the other hand, when G becomes large, b_k approaches -2/3 for COA models. G is based on RCOA.

V.8 Specific Energy Release Rate (SERR, W/g) or Specific Metabolic Rate (SMR, W/g)

First, specific energy release rate is calculated as though each cell is exposed pO_2 = $pO_{2,cap}$ and by multiplying number of cells per g, one can estimate the isolated metabolic rate per unit mass (W/g). Then, multiplying tissue density isolate metabolic rate per unit volume (W/cm^3) can also be obtained. Knowing n, d_{cell}, R, r_{cap}, for COS

and COA, G and G_{cap} can be calculated and hence the correction factor η (Figures 46 and 47) is evaluated. Applying η, the actual oxygen consumption rate per unit mass (W/g) or (W/cm^3) is calculated. Since 1 cm^3 of O_2 consumed = $1.0x10^{-3}$* 32 (g/mole)*14200 (J/g) / (22.4 L per mol) = 0.00143 g per L = 20.29 J then actual specific tissue metabolic rate is estimated.

SERR or SMR (W/g) was calculated for each model under the conditions of the base study and found to be 0.238 W/g and 0.499 W/g for COA and COS models respectively. The SERR, given in parentheses, is equivalent to the specific metabolic rate, SMR in biology. LVF for both of the O2 models was 0. For the COA-US model, the LVF was 0.78 (78%), and the LVF of the COS-US model was 0.25 (25%). The reason for such drastic differences between the COA and COS models, with regards to both SMR and LVF, is due to the geometric conditions imposed by the cylindrical geometry. For example, if δ (the aerobic shell thickness) was equivalent between the two models, then because of the cylindrical geometry, the COS model would have a lesser anaerobic volume (V-2 πR* δ L) than the anaerobic volume of the COA model (V-2 πr_{cap}* δ L) (figure 48). The greater anaerobic volume means a higher LVF and lower SMR.

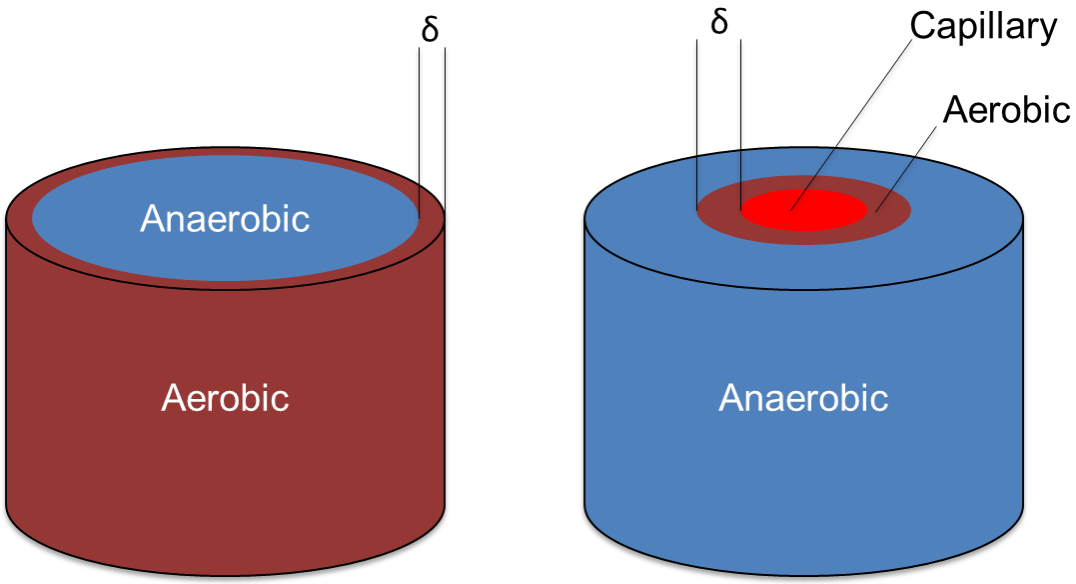

Figure 48. COS model on the left with an aerobic shell surrounding the anaerobic core. The COA model on the right has an anaerobic shell surrounding the aerobic core. Assuming δ is equal between the two models, the aerobic volume will be larger for the COS model than the COA model.

The thickness δ has been calculated for each model under the conditions of the base study and found to be 20.7 µm for COA-O2 and COS-O2 and 10.1 µm for COA-US and COS-US. Based on the specific capillary surface area used in the base study of 134.5 cm^2/g, the tissue radius is 20.7 µm. Since the O2 models never drop below the lethal limit, their δ is equal to the tissue radius and the entire tissue cylinder is considered aerobic. Singer et. al. used a constant aerobic shell thickness of 100 µm, which they admit is just a rough assumption [13]. Our values vary because δ is calculated from the lethal radius of a given model.

Since it is assumed no metabolic activity takes place within the lethal volume (typically energy release due to glycolysis ≈ 10% of energy release due to oxidation), a factor was introduced (α) to account for the reactive volume versus total volume.

$$V_{reactive} = V_{total} - \alpha V_{lethal} \tag{142}$$

When α is set to zero, the reacting volume is equal to the total tissue volume, but when α is set to one, the reacting volume is less than the total tissue volume. When α=1, reacting volume is less and hence O2 consumption rate will decrease since reaction volume decreases affecting the interface cap-IF concentration. Thus

$$\frac{Y_{O2,cap\text{-}IF}}{Y_{O2,cap}} = \frac{1}{\left\{1+\eta_{eff}\frac{1}{F_{COS}}\left(\frac{V_{reac}}{V}\right)\left(\frac{D_{IF\text{-}cell}}{K'_{cap}d_{cap}}\right)\sqrt{GG_{cap}}\right\}}, COS \tag{143}$$

$$\frac{Y_{O2,cap-IF}}{Y_{O2,cap}} = \frac{1}{\left(1+\eta_{eff}\left(\frac{V_{reac}}{V}\right)\frac{D_{IF-cell}}{K'_{cap}\,d_{cap}}\left\{G-G_{cap}\right\}\right)}, \; COA \tag{144}$$

By using this factor, the anaerobic portion of the tissue is assumed to not be reacting with the O_2. This will cause a decrease in SMR, resulting in new values of 0.006 W/g and 0.032 W/g respectively, while COA-US and COS-US yields 0.003 W/g and 0.022 W/g. The SMRs for the O2 models remained the same.

V.9 Parametric Studies

Next, several parametric studies were conducted to see the effects of various parameters on SMR. Parameters to be examined include capillary pO_2 levels, capillary permeability (K'_{cap}), specific capillary surface area($S_{cap,m}$), and cell interspacing (ℓ). Similar to before, the two cases of effectiveness factor were considered and compared. When the US models used η_{eff} (= $Y_{O2avg}/Y_{o2cap\text{-}IF}$) calculated from the O2 models, then the US and O2 models had the same SMR indicating the source term does not affect the calculation of SMR. If η_{eff} is set equal to one for the US models, then both US models will have the same SMR as long as FCOS for COS is such that $S_{cap,m}$ is the same for COA and COS. But, SMR will be higher than the O2 models. This indicates the boundary conditions do not affect SMR anymore for the US models. Unless otherwise stated, α is set to zero for all studies as though whole tissue volume participates in reaction.

The first factor studied was the capillary oxygen concentration levels. Capillary pO_2 levels were varied from 10 mmHg to 100 mmHg while keeping all other inputs the same as the base study and the resulting SMR was found to linearly increase with increasing pO2. Figure 49 shows the SMR results for η_{eff} same as the O2 models and figure 50 shows SMR results for η_{eff} =1 for the US models.

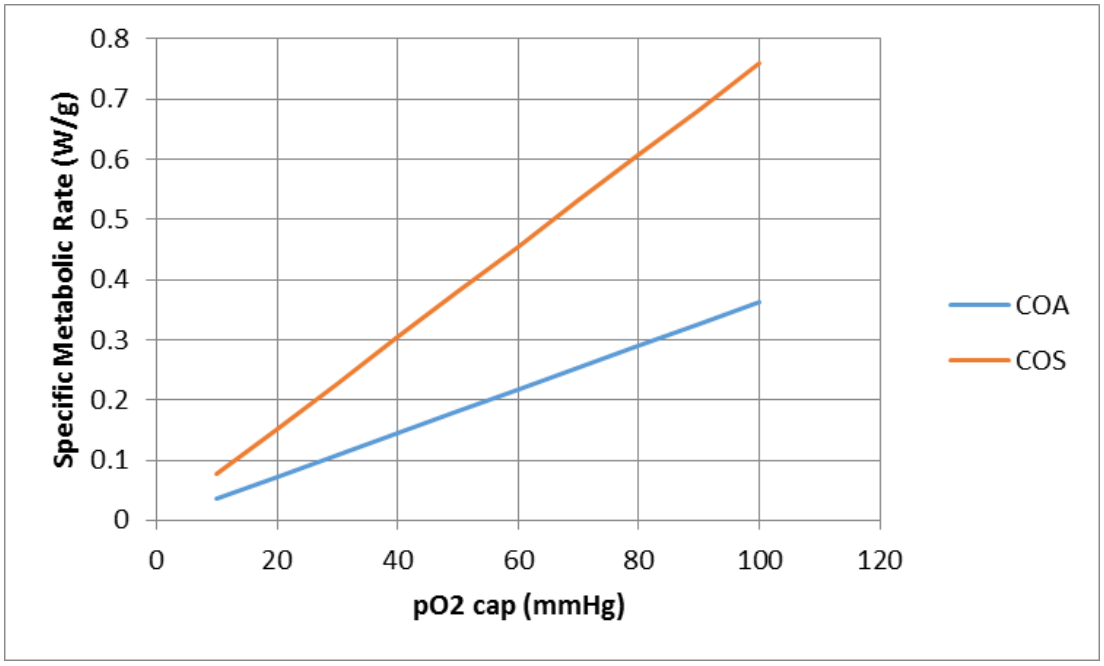

Figure 49. Specific metabolic rate is plotted vs the partial pressure in the capillary, pO_2 (mmHg), for the four models. The uniform source is calculated using η_{eff} from the O2 models. COA models overlap as do the COS models. FCOS=0.1447.

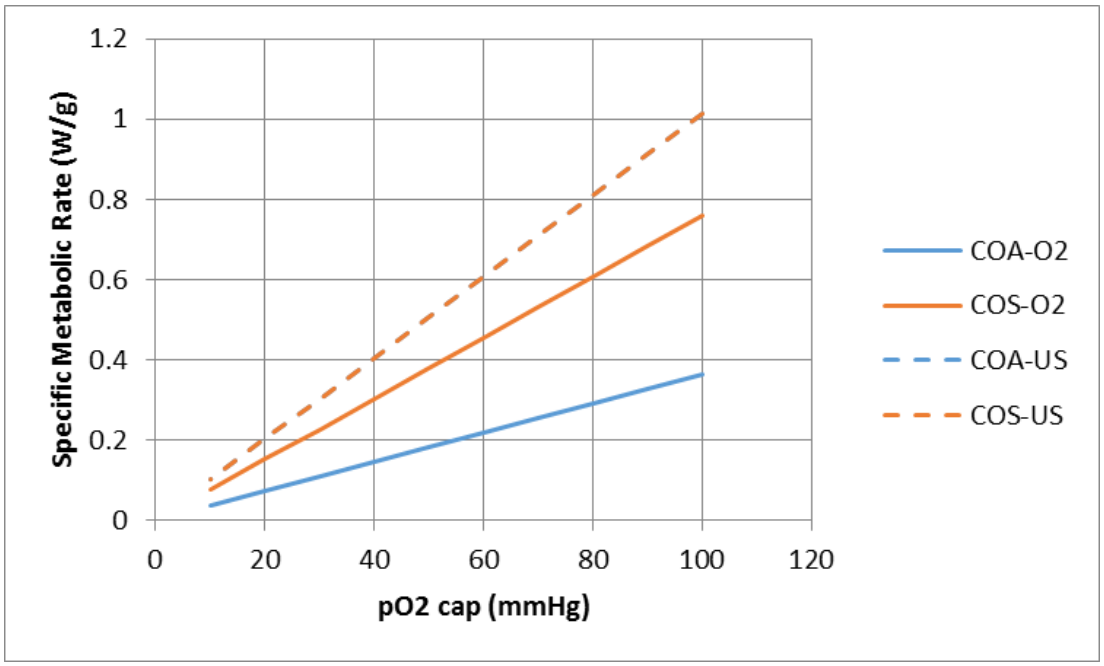

Figure 50. Specific metabolic rate is plotted vs the partial pressure in the capillary, pO_2 (mmHg), for the four models. The effectiveness factor is set equal to one for the US models. US models overlap. FCOS=0.1447.

Up until this point, FCOS was set such that the tissue radius and specific capillary surface area between the COA and COS models were equal. Figure 51 shows the plot of SMR versus capillary pO_2 where FCOS is set equal to one as though the surface is completely covered by capillaries (solid model). Additionally, η_{eff} for the US model was set equal to one. In order to keep the specific capillary surface area the same between all the models, RCOS had to be made much larger so as to account for the increased capillary surface area. This results in a lower SMR for the COS-O2 model.

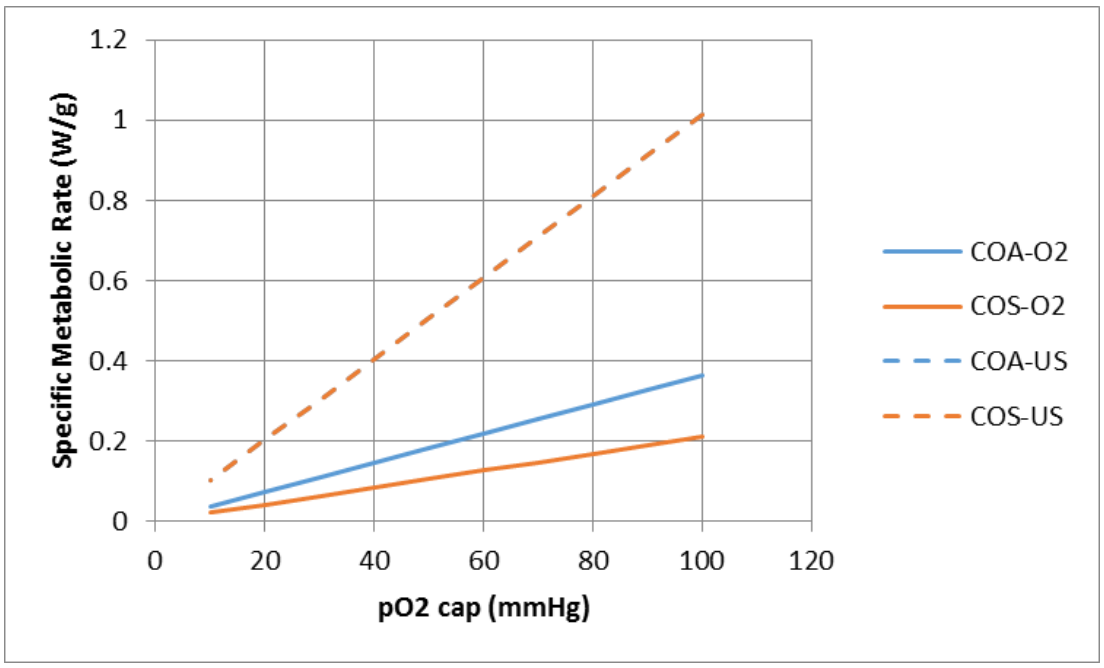

Figure 51. Specific metabolic rate is plotted vs the partial pressure in the capillary, pO_2 (mmHg), for the four models. The effectiveness factor is set equal to one for the US models. US models overlap. FCOS=1.

Another factor studied was the capillary permeability coefficient, K' (cm/s). Once again, all other inputs were kept the same as the base study while K' was varied

from 0.005 cm/s to 10 cm/s and the resulting SMR was plotted for each model. As K' increases, SMR increased rapidly before leveling off since the rate is now controlled by transport from capillaries across the interface with $Y_{O2,cap\text{-}IF}$ approaching almost zero. Figure 52 shows the SMR results for η_{eff} same as the O2 models and figure 53 shows SMR results for η_{eff} =1 for the US models.

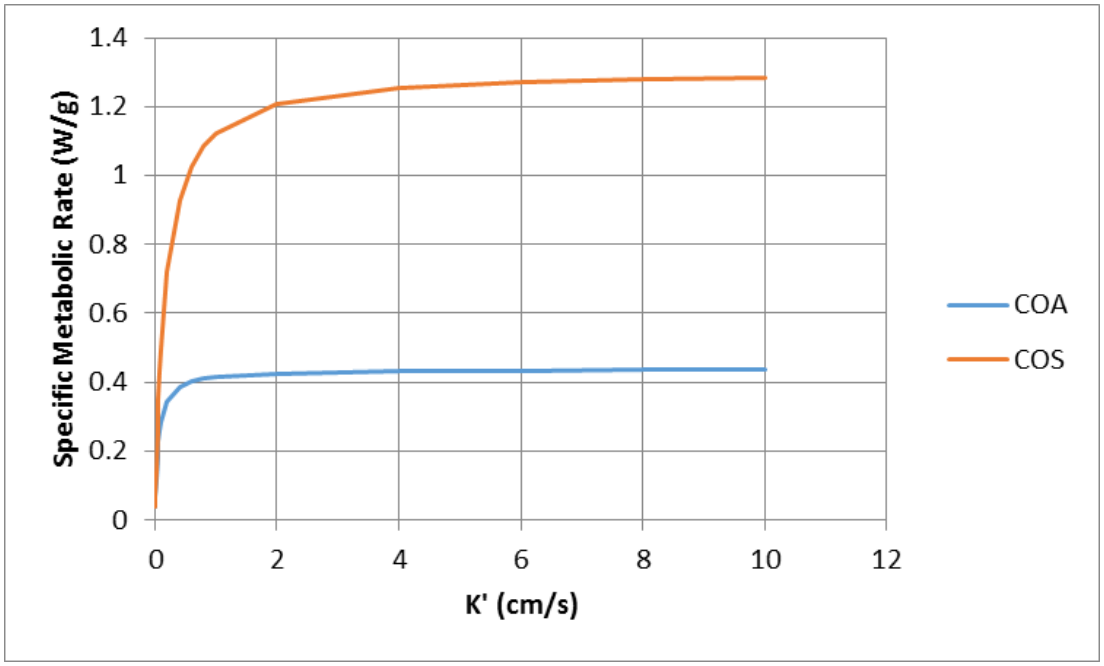

Figure 52. Specific metabolic rate is plotted vs the permeability coefficient, K' (cm/s), for the four models. The uniform source is calculated using η_{eff} from the O2 models. COA models overlap as do the COS models.

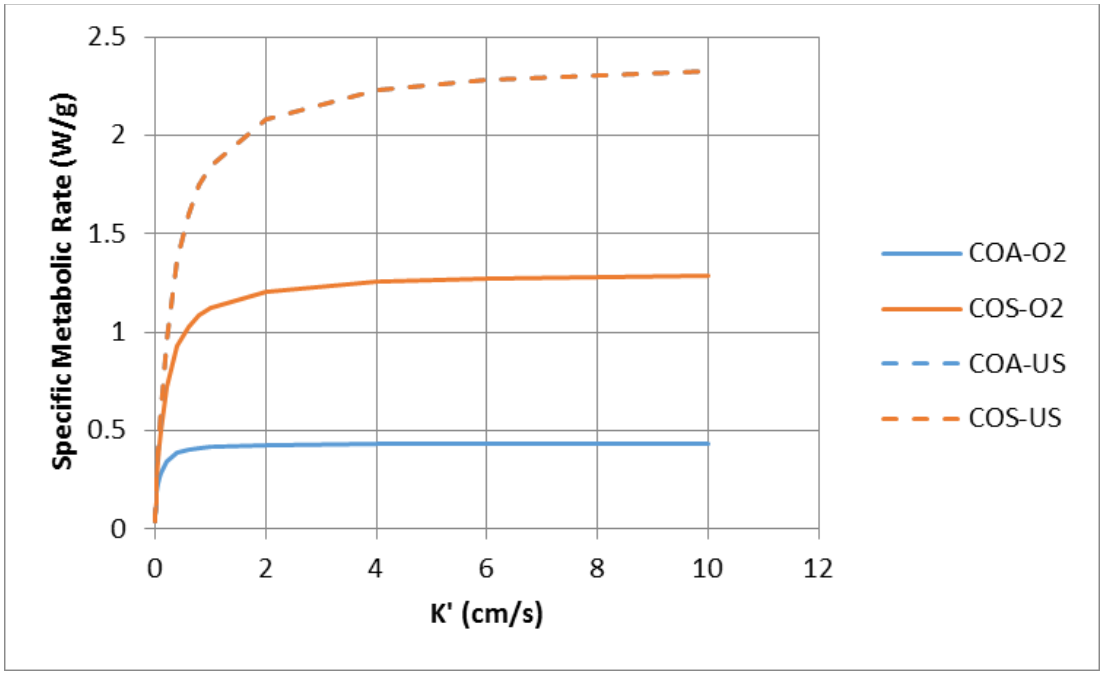

Figure 53. Specific metabolic rate is plotted vs the permeability coefficient, K' (cm/s), for the four models. The effectiveness factor is set equal to one for the US models. US models overlap.

Additionally, the parameter α was changed to one to ensure metabolic rate was only calculated in the reacting tissue (i.e. α=1). The study on K' was then repeated and the results have been plotted in figure 54 with the SMR calculated for η_{eff} same as the O2 models for the US models. Furthermore, a zoomed in plot is shown in figure 55 so the effects closer to zero can be seen. Both O2 models were unaffected by the change in α while both US models showed a decrease in SMR compared to the case with α=0. COA-US showed a larger percentage decrease than COS-US because of the larger LVF as described previously.

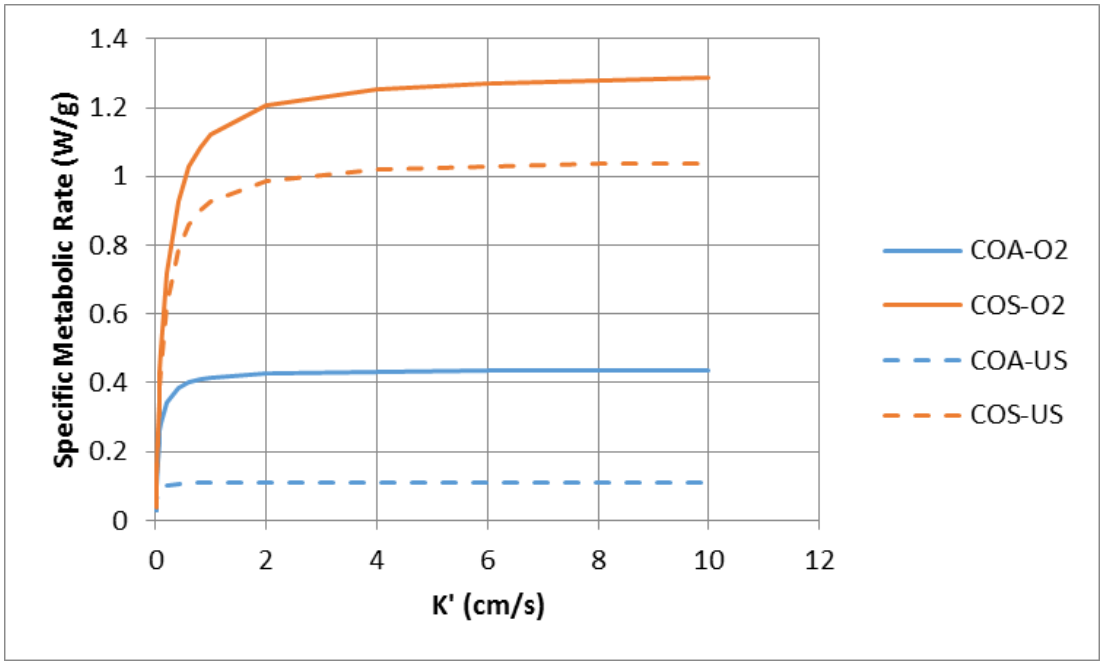

Figure 54. Specific metabolic rate is plotted vs the permeability coefficient, K' (cm/s), for the four models with α = 1. The uniform source is calculated using η_{eff} from the O2 models.

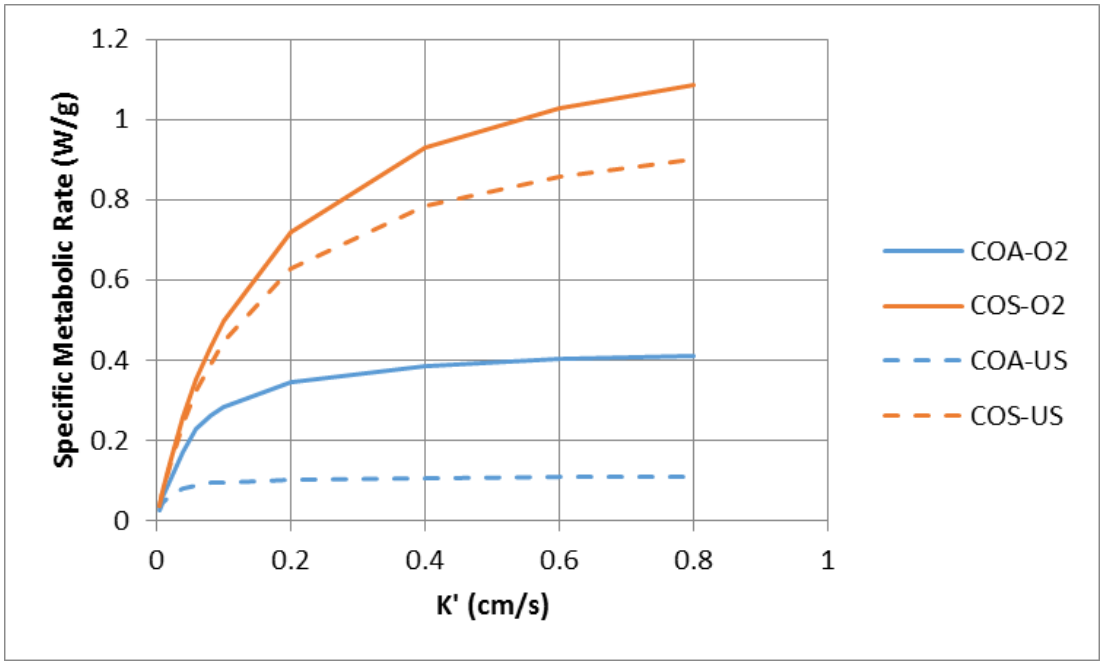

Figure 55. A zoomed in plot of specific metabolic rate plotted vs the permeability coefficient, K' (cm/s), for the four models with α = 1. The uniform source is calculated using η_{eff} from the O2 models.

In addition, the intercellular spacing was examined. The distance from one cell center to an adjacent cell center, ℓ, needs to be greater than the given cell diameter, d, otherwise the cells would overlap. Since number density $n=1 / \ell^3$, the corresponding cell number density was also plotted in figure 56 on the right axis; decrease in ℓ is equivalent to increasing "n" and hence increasing G. Therefore, the parameter ℓ / d was varied from 1 (high G) to 10 (low G) and the resulting SMR was plotted in figure 47. All other parameters were kept consistent with the base study and η_{eff} for US was adopted from the O2 model.

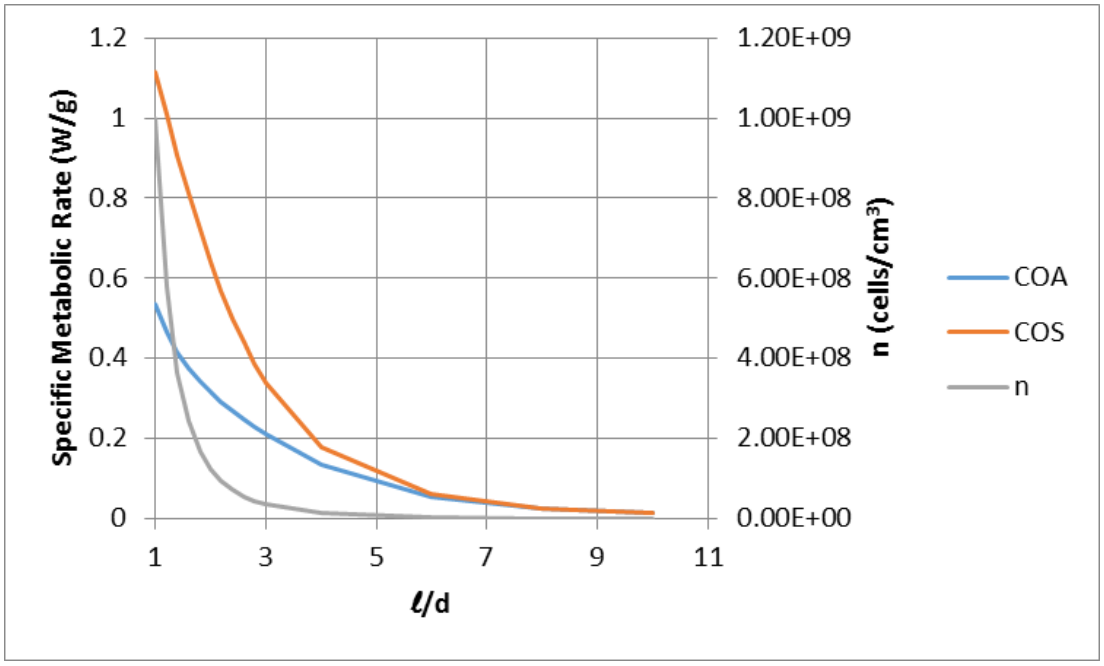

Figure 56. Specific metabolic rate is plotted vs ℓ/d, a measure of the intercell spacing, for COA and COS and corresponds to the left axis. The uniform source is calculated using η_{eff} from the O2 models causing the COA models to overlap as well as the COS models. Cell number density, n, is plotted on the right axis.

As the cells become further apart, there will be less total cells in the tissue and they will approach the isolated case of SMR. In the isolated case, each cell is treated on its own, independent from the effects of the other cells. Thus, the oxygen concentration near the cell is close to that at the capillary – interstitial fluid interface. A plot of SMR for both the isolated and actual rates as a function of ℓ / d can be seen in figure 57.

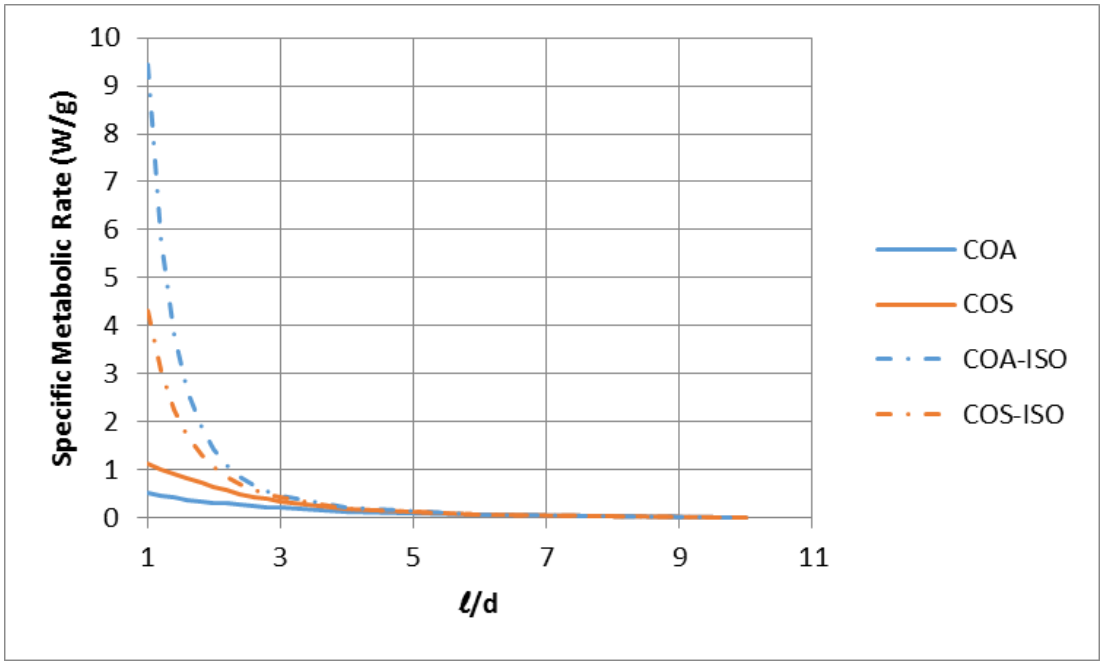

Figure 57. Specific metabolic rate is plotted vs ℓ/d, a measure of the intercell spacing, for COA and COS as well the isolated case, where each cell consumes oxygen as though it is isolated, independent of the crowding effect. The uniform source is calculated using η_{eff} from the O2 models causing the COA models to overlap as well as the COS models.

Finally, the parameter of specific capillary surface area, $S_{cap,m}$ (cm^2/g), was varied from 5 (large organ radius) to 500 (small organ or smaller radius) and two effects were studied while all other inputs remained the same as the base study. First, the tissue radius was analyzed for changing $S_{cap,m}$ when FCOS was kept constant (figure 58). Secondly, SMR was calculated for two cases, when α equals zero and one (figure 59 and 60 respectively). For these studies, η_{eff} for the US model was maintained the same as that of the O2 model.

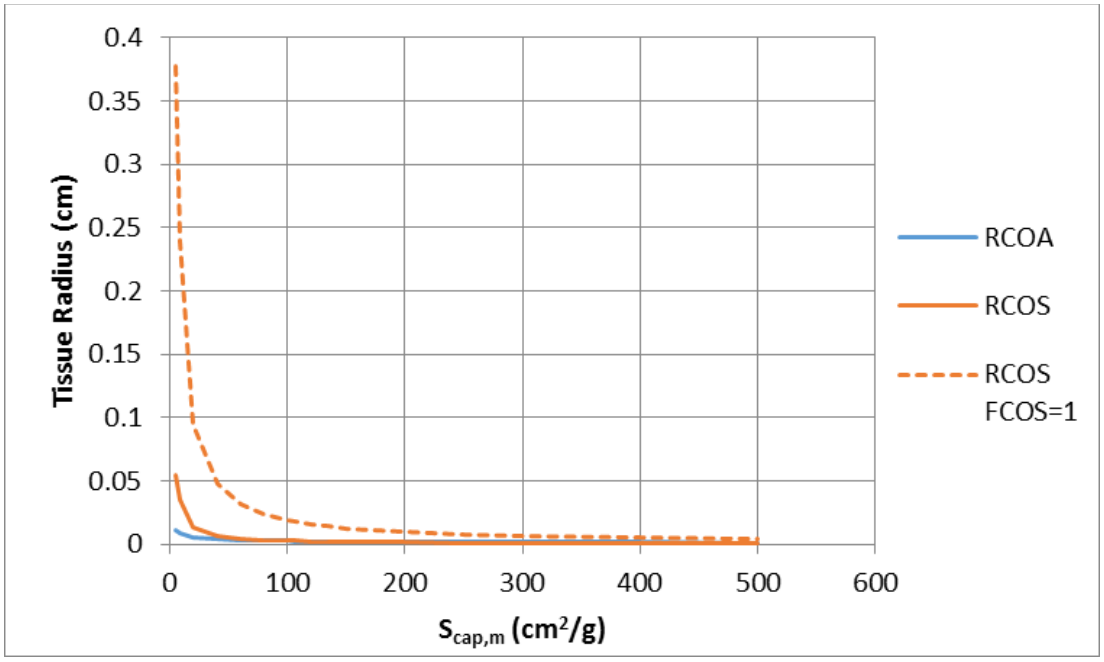

Figure 58. Tissue radius is plotted vs the specific capillary surface area, $S_{cap,m}$ (cm^2/g), for the COA and COS models. The COS model is plotted for both FCOS = 0.1447 and FCOS = 1.

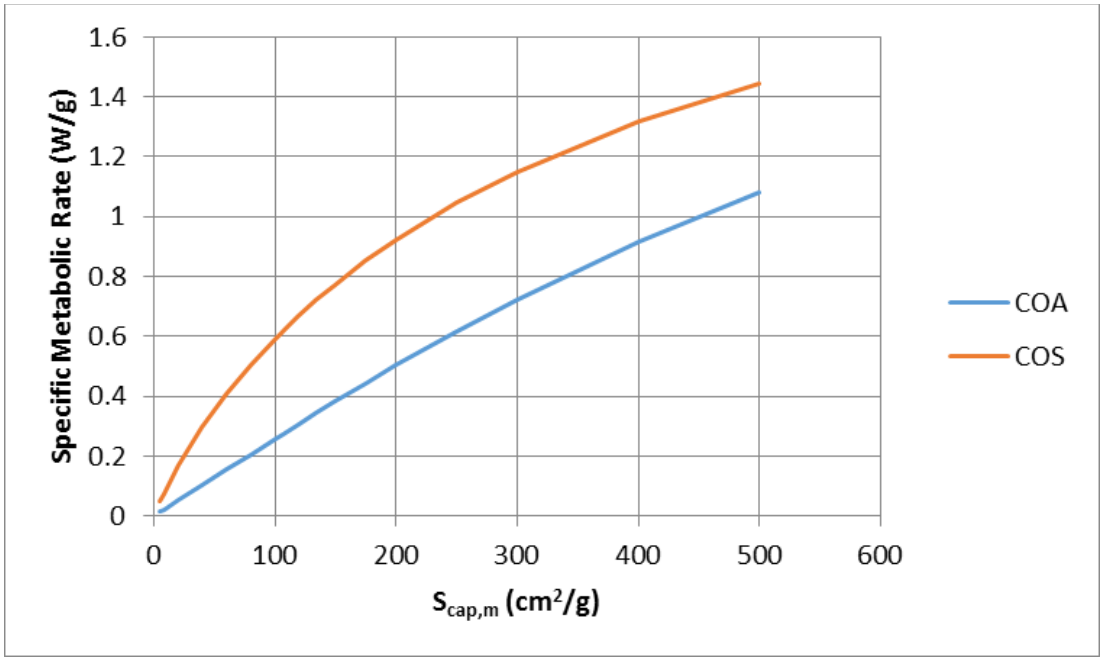

Figure 59. Specific metabolic rate is plotted vs the specific capillary surface area, $S_{cap,m}$ (cm^2/g), for the four models. The uniform source is calculated using η_{eff} from the O2 models. COA models overlap as do the COS models. α=0, FCOS=0.1447.

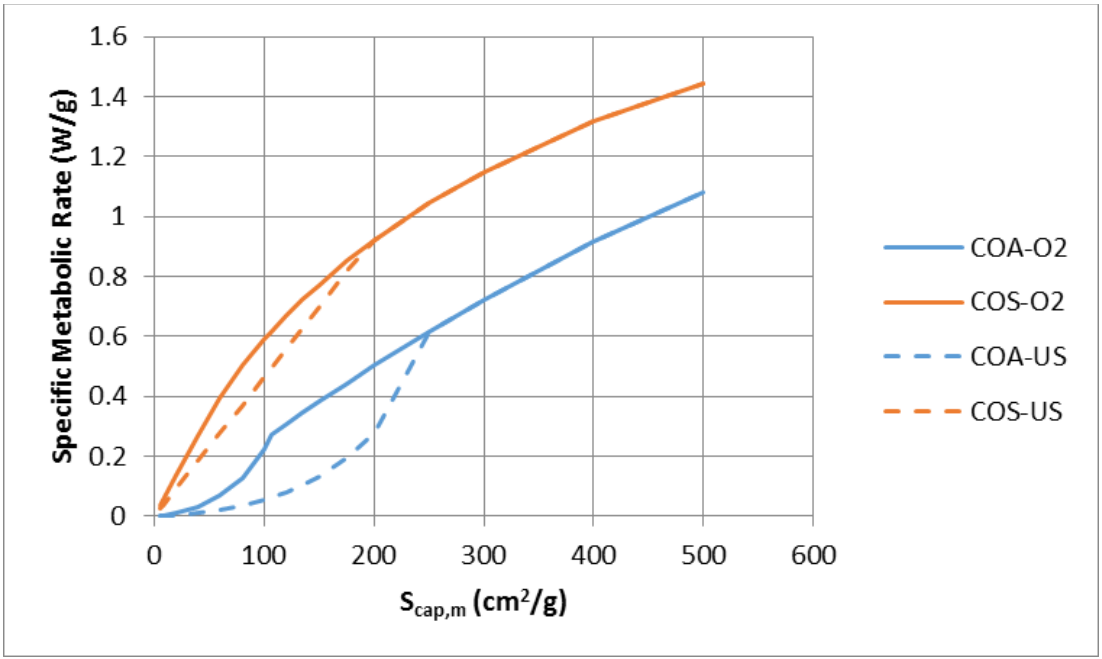

Figure 60. Specific metabolic rate is plotted vs the specific capillary surface area, $S_{cap,m}$ (cm^2/g), for the four models. The uniform source is calculated using η_{eff} from the O2 models. α=1, FCOS=0.1447.

From figure 60, one sees that by using α equal to one, the entire shape of the curve changes until $S_{cap,m}$ is large enough such that LVF is zero. At this point the SMR follows the same behavior as figure 59, when α equals zero.

V. 10 Experimental Data

Experimental data from various biological literature sources has been collected for comparison to the models and results previously shown. First, the computed pO2cap-IF were compared with experimental data; then O_2 profiles were compared between our models and those of Tsai et. al. who used phosphorescence quenching microscopy on the rat mesentery system to experimentally measure O_2 profiles *in vivo*

[53]. In order to compare our models, the inputs needed to be changed to match Tsai's inputs as much as possible. The inputs changed are presented in table 5. $S_{cap,m}$ was calculated from the tissue radius, R, given by Tsai et. al. and FCOS was calculated such that R_{COS} would equal R_{COA}.

Table 5. Values changed so that our models may be compared with the experimental data from Tsai et. al. The new values used here were taken from inputs used by Tsai et. al. [53].

Variable	Meaning	Original Value	New Value	Units
pO2,cap	Dissolved oxygen concentration in capillary	95	55.6	mmHg
R	Tissue radius	–	0.00936	g/cm^3
r_{cap}	Capillary radius	0.0003	0.00116	cm
t_{cap}	Capillary wall thickness	0.0001	.00023	cm
D	Oxygen tissue diffusivity	2 E-05	1.7 E-05	cm^2/s
K'_{cap}	Oxygen permeability across capillary	0.2	0.074	cm/s
$S_{cap,m,L}$	Specific capillary surface area of liver	135	25.4	cm^2/g
FCOS	Surface area fraction covered by capillaries	0.1447	0.126	

V.10.1 Interface Oxygen Pressure and Oxygen Profiles

With the new inputs along with remaining inputs being kept the same as the base study, the O_2 profiles were recalculated and plotted. The resultant plot alongside the experimental measurements from Tsai et. al. can be seen in figure 61. η_{eff} for the US model was calculated as the same as the O2 model and alpha was set to zero.

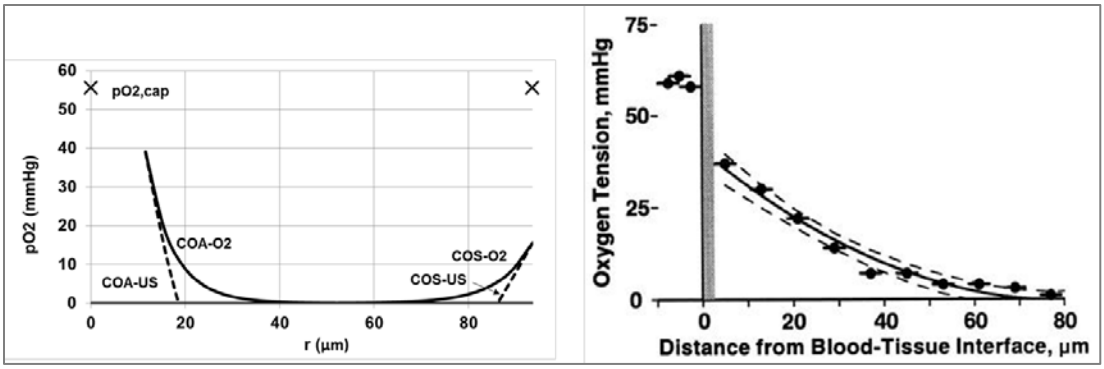

Figure 61. Comparison between our models (left; model predictions with α=0; $pO_{2,cap-IF}$ = 39.0 mm of Hg for COA and 15.6 mm of Hg for COS models) and the experimentally measure O2 profiles by Tsai et. al. (right; $pO_{2,cap-IF}$ ≈ 38 mm of Hg) [53]. The uniform source is calculated using η_{eff} from the O2 models. Right figure adopted from [53].

With α=0, the model predictions yield pO2cap-IF = 39.0 mm of Hg for COA and 15.6 mm of Hg for COS models while experimental data suggests about 38 mm of Hg. From figure 61, one can see the COA models' O_2 concentration at the capillary – interstitial fluid interface is much closer to the experimentally determined concentrations from Tsai et. al. Conversely, the shape of the both COA profiles is much steeper than experimentally measured, while the COS-O2 profile comes closest in slope to Tsai's data.

With α=1, the model predictions yield pO2cap-IF = 54.5 mm of Hg for COA-O2, 38.1 mm of Hg for COS-O2, 55.3 for COA-US, 46.2 for COS-US while experimental data still suggests about 38 mm of Hg. Newly formed O_2 profiles were plotted and can be seen in figure 62 alongside the experimental data from Tsai et. al. for comparison. None of the models have a similar curve to the experimental data.

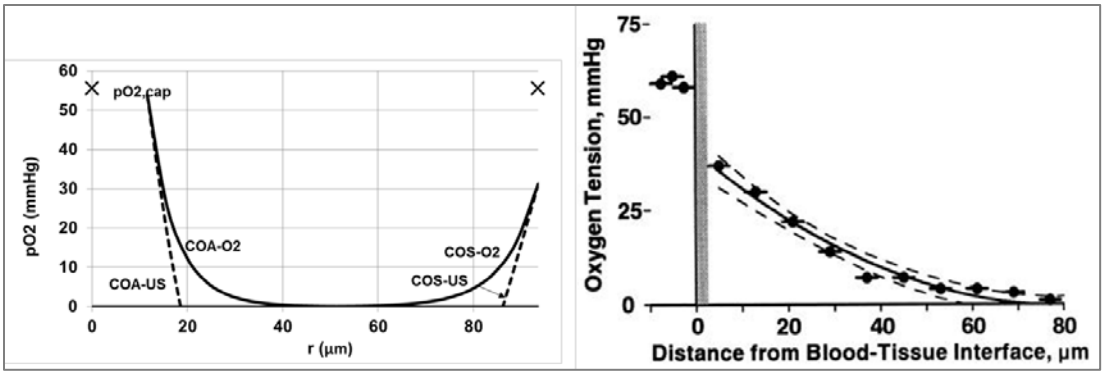

Figure 62. Comparison between our models (left; model predictions with α=1; $pO_{2,cap-IF}$ = 50.4 mm of Hg for COA-O2, 28.8 mm of Hg for COS-O2, 53.4 for COA-US, 36.8 for COS-US) and the experimentally measure O2 profiles by Tsai et. al. (right; $pO_{2,cap-IF}$ ≈ 38 mm of Hg) [53]. The uniform source is calculated using η_{eff} from the O2 models and alpha was set to one. Right figure adopted from [53].

From figure 62, one can see the COA models' O_2 concentration at the capillary – interstitial fluid interface is now much higher than the experimentally determined concentrations from Tsai et. al. On the other hand, the COS oxygen concentration at the capillary – interstitial fluid interface is now much closer to the experimental values of Tsai et. al.

Figure 63 shows the plots of YO2 / YO2,cap-IF versus the distance from the capillary (x*) for the four models. This modified distance allows for easier comparison of the profile shapes versus each other as well as versus the experimental data. For COA

$$x^* = \frac{r - r_{cap}}{R - r_{cap}}, \quad \text{COA} \tag{145}$$

and for COS

$$x^* = \frac{R - r}{R}, \quad COS \tag{146}$$

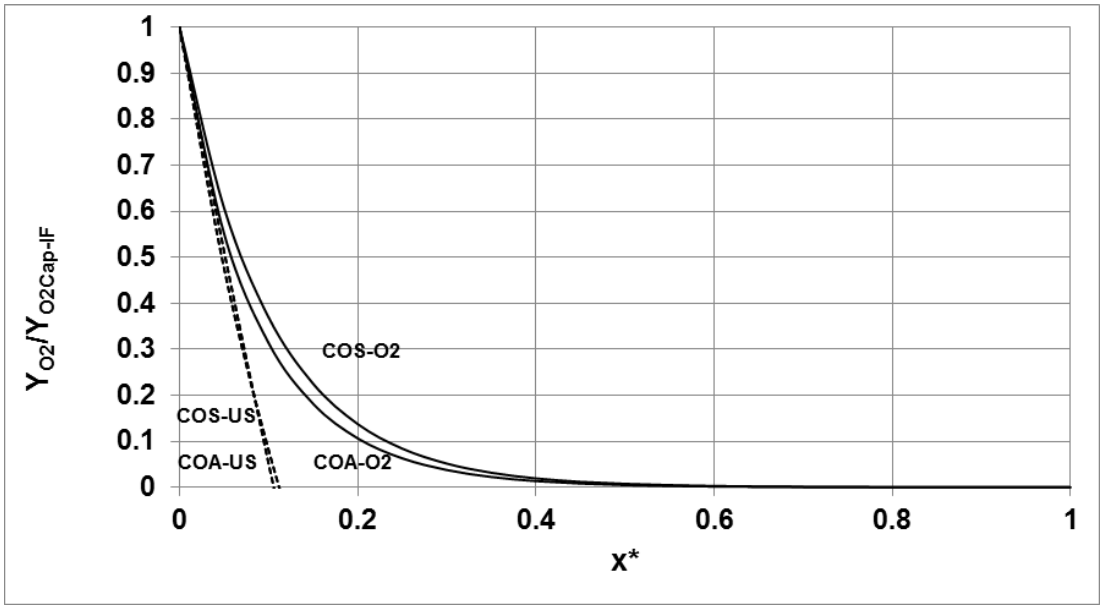

Figure 63. Oxygen profiles versus the dimensionless distance from the capillary, x*. Using x* allows for easier comparison of profiles between models and experimental data.

It is now clear from figure 63 that while all profiles exhibit a much steeper slope close to the capillary compared to the experimental data of Tsai et. al, the O2 models are closer in shape than the US models. All of models have a much steeper slope, going to zero much faster, than the experimental results of Tsai et. al.

V.10.2 Specific Metabolic Rate

Tsai et. al. found the average oxygen consumption rate to be $2.4x10^{-04}$ mL of O2 per second per cm^3 of tissue or an SMR of $4.59x10^{-03}$ W/g [53]. With α=0, the SMR was found to be $13.5x10^{-3}$ W/g and $32.6x10^{-3}$ W/g for the COA and COS models respectively. Both values are an order of magnitude higher than the experimental results from Tsai et. al. Thus, an adjustment was made and alpha was set to one. With α=1, the SMRs calculated from our models were $1.35x10^{-3}$ for W/g COA-O2, $19.9x10^{-3}$ W/g for COS-O2, $0.4x10^{-3}$ W/g for COA-US, and $11.9x10^{-3}$ W/g for COS-US. The COA-O2 model oxygen consumption comes closest to that of Tsai et. al.

The second experimental data used for comparison is the SMR of a typical human liver as given by Wang et. al. (2010) [54]. The calculated SMR of the tissue cylinder models is the same as the SMR for the entire organ, assuming many identical tissue cylinders are used as building blocks for said organ. Therefore, a typical liver may be made up of a large amount of the tissue cylinders modeled here, but both the liver and model will still have the same SMR. Wang et. al. (2010) found for a typical human liver, the SMR is $9.68x10^{-03}$ W/g [54] or approximately 0.01 W/g. When the SMR for the four models was initially calculated, with alpha set to zero and all other inputs the same as the base study, the results were all two orders of magnitude higher than reported by Wang et. al. (2010). If alpha is then changed to one, the resulting SMRs are 0.006 W/g for COA-O2, 0.032 W/g for COS-O2, 0.003 W/g for COA-US, and 0.022 W/g for COS-US. These values are all reasonable with the COS models having the same order of magnitude as the experimental data.

Thirdly, the average oxygen concentration of the models was compared to the average concentration, as reported by Vaupel et. al., of 24 mmHg [55]. Using the inputs of the base study and setting alpha equal to one, the resulting average pO_2 values, with α=0, are 13.7 mmHg for COA and 28.7 mmHg for COS. When α=1, the average pO2 values become 13.7 mmHg for COA-O2, 28.7 mmHg for COS-O2, 16.3 mmHg for COA-US, and 31.7 mmHg for COS-US By comparison, one sees the COS-O2 model comes closest to predicting the correct average O_2 concentration.

V.10.3 Allometric Exponents

The final experimental validation comes from the allometric comparisons. If organ k is considered, then the allometric law for the SMR of organ k is given as

$$\dot{q}_{m,k}\left(\frac{W}{\text{kg of k}}\right)=\frac{\dot{q}_k}{m_k}=a_k\, m_k(kg)^{b_k} \tag{147}$$

where $\dot{q}_{m,k}$ is the SMR of organ k, $\dot{q}_k$ is the metabolic rate of organ k, m_k is the mass of organ k, a_k is the allometric constant of organ k, and b_k is the allometric exponent of organ k. The limits of the allometric exponent have been evaluated before by Annamalai [56]. The derivations for COS-O2 along with COA-O2 are briefly given in Appendix C.

To summarize the derivations, all models follow the isometric law when organ k is small and thus, $b_k = 0$. If organ k is large then $b_k = -1/3$ for COS models and $b_k = -2/3$ for COA models. A plot of the allometric exponents for various organs versus their

mass is shown in figure 64. The data was taken from Wang et. al. (2001) [57]. All of the organs fall between the limits set by the COS model while none approach the limit of the COA model. Also note how smaller organs approach the isometric law while larger organs approach the -1/3 limit as predicted by the COS models.

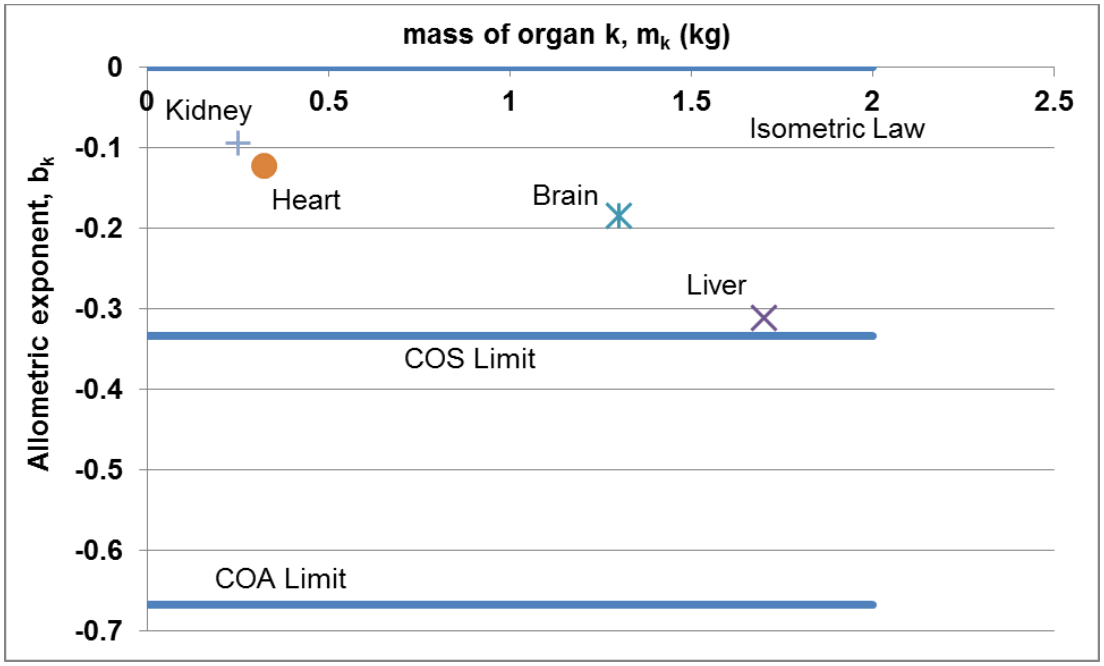

Figure 64. Allometric exponents versus organ mass for liver, brain, heart, and kidney plotted along with the derived limits from the COA and COS model (see paper for explanation).

CHAPTER VI

CONCLUSION

First, the concentrations of the different modes of Hb were found for varying partial pressures of O_2 with $HB(O_2)_4$ dominating at higher levels of pO_2. Next, Hb and Mb O_2 saturation curves were modeled from thermodynamics of the reactions. Even at relatively low values of pO_2, such as 40 mm of Hg, Mb maintained a high level of O_2 saturation while Hb fell to about 60%.

Second, Four models have been discussed and evaluated for the one dimensional, steady state, diffusion controlled oxygen diffusion problem through tissue: COS-O2, COS-US, COA-O2, COA-US. The oxygen profiles generated show a decrease in concentration radially with the uniform source models falling below zero. When only aerobic part of the tissue participates in metabolism, (α=1), the SMRs were found to be 0.006 W/g, 0.032 W/g, 0.003 W/g, and 0.022 W/g for COA-O2, COS-O2, COA-US, and COS-US models respectively. SMR values for the COS models were of the same magnitude as the experimental SMR value for a typical human liver (~0.01 W/g) from Wang et. al. (2010) [54]. Additionally, with parameters set to match the experimental factors, interface $pO_{2,cap\text{-}IF}$ (capillary wall – interstitial fluid interface partial pressure of O2) for the COS model (38.1 mm of Hg) was closest to that experimentally measured by Tsai et al (~35 mm of Hg) [53]. Finally, the COS-O2 model was the most accurate in predicting the average pO_2 level ($\eta_{eff}=pO_{2,avg}/pO_{2,cap\text{-}IF}$) in the tissue (28.7 mm of Hg) when compared to the experimental data from Vaupel et. al. (24 mm of Hg) [55].

Limits on the allometric exponent for each model were also derived. At small organ sizes, each model goes to isometric law (b_k=0) while for large organs, the COS model has a limit of -1/3 and the COA model has a limit of -2/3. When compared to various experimentally determined allometric exponents for different organs, the COS model better predicts the limiting level as seen in figure 51.

Lastly, a modified lethal corner was established for when pO2 drops below 3.6 mm of Hg in the tissue. The LVF was calculated and hypothesized to be proportional to the cancer cell fraction based on Warburg's efforts that showed damage to cellular respiration leads to cancerous cell development [26]. LVF was 0 for both O2 models, 0.78 (78%) for COA-US and 0.25 (25%) for COS-US. The large difference in LVF between COA and COS models was determined to be due to the geometric factors of each model.

According to Warburg's hypothesis, oxygen deficiency may lead to growth of cancer cells and hence, lethal volume fractions (LVF) were also predicted for the various models and which kind of capillary arrangement (COA vs COS) leads to more LVF under identical capillary surface area per unit mass ($S_{cap,m}$ cm^2/g). In order to validate the current approach from extension of combustion science models to oxygen deficient metabolism within organs, the model results are verified with the following different types of experimental data: A) If SMRs ($\dot{q}_m$ W/g) are given by the allometric law, $\dot{q}_m = a_k \; m_k^{\;b_k}$ for organ k, then the COS models under limiting conditions suggest -1/3<b_k<0 where b_k=0 for small organs following isometric law and -1/3 for large organs while COA models suggest -2/3<b_k<0 under similar conditions. Most experimental data

for vital organs yield -0.27<bk<0 which seems to suggest better correlation with COS models. B) The measured capillary-IF interface pressure of O_2 ($pO_{2,cap\text{-}IF}$) for the rat mesentery system as given by Tsai et. al. is about 38 mmHg while the predicted $pO_{2,cap\text{-}IF}$ is 54.5 mmHg for COA-O2, 38.1 mmHg for COS-O2, 55.3 mmHg for COA-US, 46.2 mmHg for COS-US. C) Further, the reported SMR for the average human liver is about 0.01 W/g as given by Wang et. al. (2010) while the COA-O2 and COS-O2 models yield 0.006 W/g and 0.032 W/g respectively, while COA-US and COS-US yields 0.003 W/g and 0.022 W/g. The COS models are of the same order magnitude as the experimental value while the COS-US model seems to be the closest D) Finally, the comparison of measured O_2 profiles with predicted O_2 profiles shows fair agreement for the O2 models. It is noted the dissolved oxygen concentration shows more errors due to its low concentration of the order of ppm (g of O_2 per g of IF).

In conclusion, the COS-O2 has been determined to be the most accurate of the models presented here when compared to the experimental data. Thus, group combustion concepts have been shown to be transferable to the field of biology, specifically, the microvascular transport of oxygen through tissue. COA models were simultaneously developed for combustion processes in which the particular geometry may apply.

CHAPTER VII

FUTURE WORK

The differential equation used for each of the models is a linear equation and thus, the solutions can be added together. This would represent one capillary in the center surrounded by several other capillaries each contributing the oxygen concentration of the tissue in between. Further expanding on this, one could set up an array of capillaries, including the capability of turning them on or off, to possibly better simulate larger tissue sizes and whole organs.

Also, more data should be gathered on ℓ, n, R, and d_{cell}. While every effort was made here to obtain accurate and appropriate values from biology literature, there are deviations and new methods often result in more accurate values. Moreover, one should investigate whether these values change between organs as well as species to gather a more complete picture.

An assumption made throughout this study was the diffusion coefficients were all approximately equal. By removing this assumption, one would increase the difficulty of the problem but also be able to now see the effects of changing the diffusion coefficient. The relationship between density and the diffusion coefficient should be examined as well because they are often linked parameters, appearing simultaneously throughout the equations.

In order to obtain simplified results, the cells within lethal volume region, or anaerobic region, are assumed to be at same YO2,avg as cells in aerobic region leading

to under prediction of SMR for tissues for COS-O2 and OCA-O2 models; however it is unaffected for COS-US and COA-US models.

Additionally, while this study assumed a diffusion controlled process, one could take the approach of assuming a kinetic controlled process similar to the work by West et al. This would also include the use of Michaelis-Menten kinetics in addition to the zero order and first order kinetics at cellular level.

Finally, one could model the other geometries (slab and sphere) as well as increase the number of dimensions and consider the transient case. While a slab and sphere model may seem impractical at a single capillary level, they may prove useful when analyzing a larger chunk of tissue or whole organ. By considering the longitudinal effects as well as angular distribution of O_2 profiles, one will gather a much more detailed picture of O_2 transport at the microvascular level. While increasing the difficulty, removing the angular equilibrium assumption may be especially important when considering the COS model in the future. Finally, since the circulatory is not a steady process (e.g. the beating of the heart), a transient case should be considered and modeled.

REFERENCES

[1] E. Britannica. (2006). *Pulmonary Alveolus: Alveoli and Capillaries in the Lungs*. Available: http://www.britannica.com/EBchecked/media/107200/The-alveoli-and-capillaries-in-the-lungs-exchange-oxygen-for

[2] TutorVista.com. (September 18, 2014). *Gaseous Exchange*. Available: http://www.tutorvista.com/content/biology/biology-iv/respiration-animals/gaseous-exchange.php

[3] B. Santiago. (2010, September 2, 2014). *Hemoglobin Molecule*. Available: http://billysantiago.files.wordpress.com/2010/10/hemoglobin.jpg

[4] TutorVista.com. *Circulation of Blood Through the Mammalian Heart*. Available: http://www.tutorvista.com/content/biology/biology-iv/circulation-animals/blood-circulation-mammalian-heart.php#

[5] E. Britannica. (2006, September 2, 2014). *Heart: Blood Flow*. Available: http://kids.britannica.com/elementary/art-88593/Blood-flows-from-the-heart-through-arteries-and-into-capillaries

[6] TheOpenUniversity. (September 2, 2014). *Unit 23: Physiology*. Available: http://labspace.open.ac.uk/file.php/5461/S102_1_Unit23.pdf

[7] H. H. Chiu and T. M. Chiu, "Group Combustion of Liquid Droplets," *Combustion Science and Technology,* vol. 17, pp. 127-142, 1977.

[8] K. Annamalai and S. C. Ramalingam, "Group Combustion of Char/Carbon Particles," *Combustion and Flame,* vol. 70, pp. 307-332, 12// 1987.

[9] W. Ryan and K. Annamalai, "Group Ignition of a Cloud of Coal Particles," *Journal of Heat Transfer,* vol. 113, pp. 677-687, 1991.

[10] K. Annamalai, "Evaporation of Multicomponent Drop Arrays," *Journal of Heat Transfer,* vol. 115, 1993.

[11] K. Annamalai and I. K. Puri, *Combustion Science and Engineering*. Boca Raton: CRC Press/Taylor & Francis, 2007.

[12] D. Singer, "Size Relationship of Metabolic Rate: Oxygen Availability as the "Missing Link" Between Structure and Function?," *Thermochimica Acta,* vol. 446, pp. 20-28, 7/1/ 2006.

[13] D. Singer, O. Schunck, F. Bach, and H. J. Kuhn, "Size Effects on Metabolic Rate in Cell, Tissue, and Body Calorimetry," *Thermochimica Acta,* vol. 251, pp. 227-240, 3/1/ 1995.

[14] K. N. Prestwich, "The Efficiency of Energy Conservation in Aerobic and Anaerobic Metabolism - and - The Creatine-Phosphate System," ed. Worcester, MA: College of the Holy Cross, 2003.

[15] CliffsNotes. (2013, September 2, 2014). *Hemoglobin and Myoglobin*. Available: http://www.cliffsnotes.com/sciences/biology/biochemistry-i/oxygen-binding-by-myoglobin-and-hemoglobin/hemoglobin-and-myoglobin

[16] O. College. (2013). *Transport of Gases in Human Bodily Fluids*. Available: http://cnx.org/content/m44799/latest/?collection=col11541/latest

[17] M. J. Shea. (2013, September 14, 2014). *Blood Vessels*. Available: http://www.merckmanuals.com/home/heart_and_blood_vessel_disorders/biology_of_the_heart_and_blood_vessels/blood_vessels.html

[18] IvyRose. (2014, October 14, 2014). *Blood Vessels*. Available: http://www.ivy-rose.co.uk/HumanBody/Blood/Blood_Vessels.php

[19] H. R. Horton, *Principles of Biochemistry*. Englewood Cliffs, NJ: N. Patterson Publishers, 1993.

[20] OpenStax. (2014, September 2, 2014). *Energy Conversion in Humans*. Available: http://cnx.org/content/m42153/latest/?collection=col11406/latest

[21] M. E. Daly, C. Vale, M. Walker, A. Littlefield, K. G. Alberti, and J. C. Mathers, "Acute Effects on Insulin Sensitivity and Diurnal Metabolic Profiles of a High-Sucrose Compared with a High-Starch Diet," *American Journal of Clinical Nutrition,* vol. 67, pp. 1186-96, Jun 1998.

[22] B. Griggs. (2014, April 4, 2014). The Next Frontier in 3-D Printing: Human Organs. Available: http://www.cnn.com/2014/04/03/tech/innovation/3-d-printing-human-organs/index.html?hpt=hp_t2

[23] R. Lawson. (2008). *Blood Circulation Labeled*. Available: http://wikieducator.org/File:Blood_circulation_labeled.JPG

[24] NIH. (Apr 18). *Tissue Engineering and Regenerative Medicine*. Available: http://www.nibib.nih.gov/science-education/science-topics/tissue-engineering-and-regenerative-medicine

[25] G. Grist, "Oxygen Pressure Field Theory: A Detailed Description of Vital Gas Exchange, at the Capillary Level for Perfusionists," *Progress in Pediatric Cardiology,* vol. 24, pp. 89-99, 2008.

[26] O. Warburg, "On the Origin of Cancer Cells," *Science,* vol. 123, pp. 309-14, Feb 24 1956.

[27] A. Krogh, "The Number and Distribution of Capillaries in Muscles with Calculations of the Oxygen Pressure Head Necessary for Supplying the Tissue," *Journal of Physiology,* vol. 52, pp. 409-15, May 20 1919.

[28] I. S. Longmuir and A. Bourke, "The Measurement of the Diffusion of Oxygen Through Respiring Tissue," *Biochemical Journal,* vol. 76, pp. 225-9, Aug 1960.

[29] J. E. Fletcher, "On Facilitated Oxygen Diffusion in Muscle Tissues," *Biophysics Journal,* vol. 29, pp. 437-58, Mar 1980.

[30] G. A. Truskey, F. Yuan, and D. F. Katz, *Transport Phenomena in Biological Systems*. Upper Saddle River, N.J.: Pearson Prentice Hall, 2004.

[31] F. Kreuzer, "Oxygen Supply to Tissues: The Krogh Model and its Assumptions," *Experientia,* vol. 38, pp. 1415-26, Dec 15 1982.

[32] G. Zubieta-Calleja and P.-E. Paulev. (2004). *New Human Physiology (2nd ed.).* Available: http://www.zuniv.net/physiology/book/index.htm

[33] A. V. Hill, "The Diffusion of Oxygen and Lactic Acid through Tissues," *Proceedings - Royal Society. Biological sciences,* vol. 104, pp. 39-96, 1928.

[34] H. Mercker, B. Mercker, and W. Ochwadt, "Der EinfluB der Erregungsfre quenz und der Belastung auf Durchblutung und Sauerstoffaufnahme des Skeletmuskels," *PfluÌˆgers Archiv : European journal of physiology,* vol. 251, pp. 73-82, 1949.

[35] J. Piiper and P. Scheid, "Cross-Sectional PO2 Distributions in Krogh Cylinder and Solid Cylinder Models," *Respiration Physiology,* vol. 64, pp. 241-51, Jun 1986.

[36] K. Annamalai, I. K. Puri, and M. A. Jog, *Advanced Thermodynamics Engineering*, 2nd ed. Boca Raton, Fla.: CRC Press, 2011.

[37] TheOpenUniversity, "Unit 23 Physiology," *The Open University: A Science Foundation Course,* p. 6.

[38] M. Kleiber, *The Fire of Life; An Introduction to Animal Energetics*. New York,: Wiley, 1961.

[39] K. Schmidt-Nielsen, *Scaling, Why is Animal Size so Important?* Cambridge ; New York: Cambridge University Press, 1984.

[40] J. K. L. da Silva, G. J. M. Garcia, and L. A. Barbosa, "Allometric Scaling Laws of Metabolism," *Physics of Life Reviews,* vol. 3, pp. 229-261, 12// 2006.

[41] R. R. Seeley, T. D. Stephens, and P. Tate. (2006, February 23). *Anatomy and Physiology (7 ed.)*. Available: http://highered.mcgraw-hill.com/sites/0072507470/student_view0/chapter23/animation__changes_in_the_partial_pressures_of_oxygen_and_carbon_dioxide.html

[42] P. W. Atkins and J. De Paula, *Physical chemistry*, 7th ed. New York: W.H. Freeman, 2002.

[43] teutonic13. (2012). *Perfused Capillary Density: Oxygen Pressure Field Theory III*. Available: http://circuitsurfers.com/2012/07/22/perfused-capillary-density-oxygen-pressure-field-theory-iii/

[44] D. F. Wilson, M. Erecinska, C. Drown, and I. A. Silver, "The Oxygen Dependence of Cellular Energy Metabolism," *Archives of Biochemistry and Biophysics,* vol. 195, pp. 485-93, Jul 1979.

[45] M.-S. Lih, *Transport Phenomena in Medicing and Biology*. New York, NY: John Wiley & Sons, 1975.

[46] N. L. Edwin and A. D. Karen, "The Roles of Mass Transfer in Tissue Function," in *The Biomedical Engineering Handbook, Second Edition. 2 Volume Set*, ed: CRC Press, 1999.

[47] J. D. Cutnell and K. W. Johnson, *Physics*, 5th ed. New York: John Wiley, 2001.

[48] C. Y. Liu, S. G. Eskin, and J. D. Hellums, "The Oxygen Permeability of Cultured Endothelial Cell Monolayers," *Advances in Experimental Medicine and Biology,* vol. 345, pp. 723-30, 1994.

[49] J. G. O'Leary, A. J. Demetris, L. S. Friedman, H. M. Gebel, P. F. Halloran, A. D. Kirk, *et al.*, "The Role of Donor-Specific HLA Alloantibodies in Liver Transplantation," *American Journal of Transplantation,* vol. 14, pp. 779-87, Apr 2014.

[50] S. R. Ward and R. L. Lieber, "Density and Hydration of Fresh and Fixed Human Skeletal Muscle," *Journal of Biomechanics,* vol. 38, pp. 2317-20, Nov 2005.

[51] C. J. Epstein, "Cell Size, Nuclear Content, and the Development of Polyploidy in the Mammalian Liver," *Proceedings of the National Academy of Sciences USA,* vol. 57, pp. 327-34, Feb 1967.

[52] E. R. Weibel, W. Staubli, H. R. Gnagi, and F. A. Hess, "Correlated Morphometric and Biochemical Studies on the Liver Cell. I. Morphometric Model, Stereologic Methods, and Normal Morphometric Data for Rat Liver," *Journal of Cell Biology,* vol. 42, pp. 68-91, Jul 1969.

[53] A. G. Tsai, B. Friesenecker, M. C. Mazzoni, H. Kerger, D. G. Buerk, P. C. Johnson*, et al.*, "Microvascular and Tissue Oxygen Gradients in the Rat Mesentery," *Proceedings of the National Academy of Sciences USA,* vol. 95, pp. 6590-5, Jun 9 1998.

[54] Z. Wang, Z. Ying, A. Bosy-Westphal, J. Zhang, B. Schautz, W. Later*, et al.*, "Specific Metabolic Rates of Major Organs and Tissues Across Adulthood: Evaluation by Mechanistic Model of Resting Energy Expenditure," *American Journal of Clinical Nutrition,* vol. 92, pp. 1369-77, Dec 2010.

[55] P. Vaupel, F. Kallinowski, and P. Okunieff, "Blood Flow, Oxygen and Nutrient Supply, and Metabolic Microenvironment of Human Tumors: a Review," *Cancer Research,* vol. 49, pp. 6449-65, Dec 1 1989.

[56] K. Annamalai, "Invited Speech II: Group Combustion of Char/Carbon Particles: A Bridge to Metabolism of Biological System and Sudden Infant Death Syndrome (SIDS) Victims?," in *The 1st International Conference on Group Combustino of Droplets and Sprays*, Institute of Aeronautics and Astronautics, National Cheng Kung University (IAA/NCKU), 2011, pp. 98-102.

[57] Z. Wang, T. P. O'Connor, S. Heshka, and S. B. Heymsfield, "The Reconstruction of Kleiber's Law at the Organ-Tissue Level," *Journal of Nutrition,* vol. 131, pp. 2967-70, Nov 2001.

APPENDIX A

KROGH MODEL ASSUMPTIONS

The following is a list of the assumptions made by August Krogh in his original model [27]. This list is taken from Kreuzer [31].

1. "There is only radial but no longitudinal or axial diffusion.
2. The intracapillary chemical reactions in the blood are neglected, i.e., the oxygen concentration is the same over the capillary cross section, and chemical equilibrium is assumed between oxygen and hemoglobin.
3. The oxygen consumption in the tissue does not depend on the local oxygen pressure (zero-order reaction).
4. The cells may be represented as an homogeneous volume distribution of minute sinks of oxygen independent of time and position.
5. The capillaries are straight, run parallel, have a unidirectional blood flow, and are homogeneously distributed.
6. Capillary radius and length are constant, implying, with constant blood flow, a constant transit time.
7. The capillary wall does not present any resistance to oxygen diffusion.
8. The capillary blood flow is constant. With unchanging oxygen consumption this implies the same venous oxygen concentration in all capillaries (Fick principle).
9. The flow of oxygen from the capillary is cylindrically symmetric.

10. The oxygen exchange occurs only in the capillary, not in arterioles and venules.
11. The oxygen does not diffuse out of the tissue cylinder.
12. The diffusion coefficient is the same throughout the tissue.
13. There is no facilitated diffusion of oxygen, e.g., by myoglobin in muscle.
14. The whole configuration is independent of time (steady state).
15. The transfer is by diffusion only (no stirring). [31]"

APPENDIX B

OXYGEN SATURATION

The partial pressure of oxygen in the blood (p_{O2}) corresponds to the percent saturation of oxygen. The following is a derivation of this relationship [42]. First, the oxygen dissolves into the blood by Henry's law:

$$O_2(aq) = \alpha p_{O_2} \tag{B1}$$

where α is Henry's constant, pO2 is the partial pressure of oxygen, and O2(aq) is amount of aqueous oxygen in mL per L of blood. The aqueous oxygen is then picked up by the hemoglobin of the red blood cells. As the oxygen is picked up, more is dissolved into the blood from the alveoli until equilibrium is reached.

The reaction equations for the pickup of oxygen by hemoglobin can be given in two ways.

$$\begin{aligned} Hb + O_2 &\rightleftharpoons HbO_2 \\ Hb + 2O_2 &\rightleftharpoons Hb(O_2)_2 \\ Hb + 3O_2 &\rightleftharpoons Hb(O_2)_3 \\ Hb + 4O_2 &\rightleftharpoons Hb(O_2)_4 \end{aligned} \tag{B2}$$

$$\begin{aligned} Hb + O_2 &\rightleftharpoons HbO_2 \\ HbO_2 + O_2 &\rightleftharpoons Hb(O_2)_2 \\ Hb(O_2)_2 + O_2 &\rightleftharpoons Hb(O_2)_3 \\ Hb(O_2)_3 + O_2 &\rightleftharpoons Hb(O_2)_4 \end{aligned} \tag{B3}$$

Equation set (B2) represents a situation where the oxygen all bind at once to the given hemoglobin while equation set (B3) represents a situation where the oxygen bind one at a time.

At chemical equilibrium

$$K^0 = \frac{\left(\frac{f_{Hb\text{-}nO2}(T,P)}{f_{Hb\text{-}nO2}(T,P^0)}\right)\hat{\alpha}_{Hb\text{-}nO2}}{\left(\frac{f_{Hb}(T,P)}{f_{Hb}(T,P^0)}\right)\hat{\alpha}_{Hb}\ \left(\frac{f_{O2}(T,P)}{f_{O2}(T,P^0)}\right)^n \hat{\alpha}_{O2}{}^n} \tag{B4}$$

For an ideal mixture, $\hat{\alpha}_{Hb\text{-}nO2} = X_{Hb\text{-}nO2}$ and equation (B4) becomes

$$K^0 = \frac{\left(\frac{f_{Hb\text{-}nO2}(T,P)}{f_{Hb\text{-}nO2}(T,P^0)}\right)X_{Hb\text{-}nO2}}{\left(\frac{f_{Hb}(T,P)}{f_{Hb}(T,P^0)}\right)X_{Hb}\ \left(\frac{f_{O2}(T,P)}{f_{O2}(T,P^0)}\right)^n X_{O2(aq)}{}^n} \tag{B5}$$

where X is the mole fraction, f is the fugacity, and K^0 is the equilibrium constant. The mole fraction of dissolved oxygen is given by

$$X_{O2(aq)} = \left(\frac{P_{O2}}{P_{O2}^{sat}} \right) \tag{B6}$$

With $P_{O2}^{sat} = H_{O2}$ and $H_{O2}' = H_{O2} / N$ where H_{O2}' is Henry's constant and N is the number of moles per volume of the blood. Equation (B6) then becomes

$$\frac{N_{O2(aq)}}{N} = X_{O2(aq)} = \left(\frac{P_{O2}}{H_{O2}'} \right) \left(\frac{1}{N} \right) \tag{B7}$$

The fugacity ratios can be approximated as follows

$$\left(\frac{f_{Hb\text{-}nO2}(T,P)}{f_{Hb\text{-}nO2}(T,P^0)} \right) \approx 1, \quad \frac{f_{Hb}(T,P)}{f_{Hb}(T,P^0)} \approx 1, \left(\frac{f_{O2}(T,P)}{f_{O2}(T,P^0)} \right) \approx 1 \tag{B8}$$

simplifying equation (B4) to

$$K_n^{\,0} = \frac{X_{Hb\text{-}nO2} \left(H_{O2}' \right)^n N^n}{X_{Hb} \; p_{O2}^{\,n}} \tag{B9}$$

The oxygen saturation percent is defined as the amount of oxygen actually bound to the oxidized hemoglobin over the maximum that could be bound to all hemoglobin or

$$S_{O2} = \frac{\text{O2 actually bound to oxidixed Hb}}{\text{Maximum that can be bound with all Hb}} \tag{B10}$$

where S_{O2} is the oxygen saturation percent. For example, if 50% of Hb exists as HbO2, 40% of Hb exists as $Hb(O2)_2$, and 10 % exists as Hb, then

$$S_{O2} = \frac{\{0.5*1 + 0.4*2\}}{\{(0.5 + 0.4 + 0.1)*4\}} = \frac{0.9}{4} = 0.225 \tag{B11}$$

or 22.5 % saturation.

Now suppose that hemoglobin only exists as $Hb(O2)_n$ and pure Hb. Then,

$$S_{O2} = \frac{n * X_{HbnO2}}{4} \tag{B12}$$

$$X_{Hb\text{-}nO2} = \frac{N_{Hb\text{-}nO2}}{N} \tag{B13}$$

$$S_{O2} = \frac{N_{HbnO2} * n}{4\ N} \tag{B14}$$

Using equation (B12) in equation (B9) results in

$$K_n^{\,0} = \frac{\left(\frac{4 * S_{O2}}{n}\right)\left(H_{O2}'\right)^n N^n}{X_{Hb}\ \ p_{O2}{}^n} = \left(\frac{4}{n}\right)\frac{S_{O2}\left(H_{O2}'\right)^n N^n}{X_{Hb}\ p_{O2}{}^n} \tag{B15}$$

or

$$p_{O2}{}^n = \left(\frac{4}{n}\right)\frac{S_{O2}\left(H_{O2}'\right)^n N^n}{X_{Hb}\ K_n^{\,0}} \tag{B16}$$

Atkins and De Paula used the following method to find the saturation percent and will be referred to as the Atkins method [42]. First we look at the following chemical equation

$$Hb + a * O2 + inerts(I) = b * HbO2 + c * Hb(O2)_2 + d * Hb(O2)_3 + e * Hb(O2)_4 + f * Hb + g * O2 + I$$

with a, b, c, d, e, f, and g as seven unknowns. The term g is known from Henry's Law. Next, atom balances can be applied to oxygen and hemoglobin as follows. For oxygen

$$2a = 2b + 4c + 6d + 8e + 2g \tag{B17}$$

or

$$a = b + 2c + 3d + 4e + g \tag{B18}$$

$$a = X_{HbO2} * N + 2X_{Hb(O2)_2} * N + 3X_{Hb(O2)_3} * N + 4X_{Hb(O2)_4} * N + g \quad \text{(B19)}$$

For hemoglobin

$$1 = b + c + d + e + f = X_{HbO2} * N + X_{Hb(O2)_2} * N + X_{Hb(O2)_3} * N + X_{Hb(O2)_4} * N \quad \text{(B20)}$$

Recalling equation (B9),

$$K_n{}^0 = \frac{X_{Hb\text{-}nO2} \left(H_{O2}'\right)^n N^n}{X_{Hb} \quad p_{O2}{}^n} \quad \text{(B21)}$$

where $X_{Hb\text{-}nO2}$= [Hb-nO2] / N= (mols of Hb-nO2 per m^3 / Mixture mols per m^3) and N= [c] = mixture mols/m^3.

$$K_n{}^0 = \frac{X_{Hb\text{-}nO2}}{X_{Hb} \quad X_{O2(aq)}{}^n} \quad \text{(B22)}$$

$$X_{O2(aq)} = \frac{[O2(aq)]}{[c]} = \frac{1}{[c]}\left(\frac{P_{O2}}{H_{O2}'}\right) \quad \text{(B23)}$$

$$X_{Hb\text{-}nO2} = \frac{[Hb - nO2]}{N}, \; X_{Hb} = \frac{[Hb]}{N}, \; N = [c] \quad \text{(B24)}$$

$$K_n^{\,0} = \frac{[c][Hb - nO2][c]^n}{[c][Hb]\ \ [O2(aq)]^n} = \frac{[Hb - nO2][c]^n}{[Hb]\ \ [O2(aq)]^n} \tag{B25}$$

$$K_n^{\,0} = \frac{[Hb - nO2][c]^n}{[Hb]\ \ [O2(aq)]^n} = \frac{[Hb - nO2][c * H_{O2}']^n}{[Hb]\ \ [p_{O2}]^n} \tag{B26}$$

$$\frac{K_n^{\,0}}{[c * H_{O2}']^n} = K'^{\,0}_{n,mod} = \frac{[Hb - nO2]}{[Hb]\ \ [p_{O2}]^n}, \quad K'^{\,0}_{n,mod} = \frac{K_n^{\,0}}{[c * H_{O2}']^n} \tag{B27}$$

With n=1, $Hb + O_2 \rightleftharpoons HbO_2$,

$$K'^{\,0}_{1,mod} = \frac{[Hb - O2]}{[Hb]\ \ p_{O2}}, \tag{B28}$$

and Atkins defines the following

$$K_1'^{\,0} = \frac{[Hb - O2]}{[Hb]\ \ p_{O2}} \tag{B29}$$

Thus,

$$K_1'^{\,0} = K'^{\,0}_{1.mod} \tag{B30}$$

For n=2 and $Hb + 2O_2 \rightleftharpoons Hb(O_2)_2$, then

$$K'_{2,mod}{}^{0} = \frac{[Hb\text{-}O2]}{[Hb]\ p_{O2}{}^{2}}, \qquad K'_{2,mod}{}^{0} = \frac{K_2{}^{0}}{[c^{*}H_{O2}']^{2}} \tag{B31}$$

Using $HbO_2 + O_2 \rightleftharpoons Hb(O_2)_2$, one gets

$$K'_2{}^{0} = \frac{[Hb(O2)_2]}{[HbO2]p_{O2}} = \frac{[Hb(O2)_2]}{K_1'[Hb]p_{O2}{}^{2}} = \frac{K'_{2,mod}{}^{0}}{K'_1{}^{0}} \tag{B32}$$

Similarly, for n=3 and $Hb + 3O_2 \rightleftharpoons Hb(O_2)_3$

$$K'_{3,mod}{}^{0} = \frac{[Hb\text{-}3O2]}{[Hb]\ p_{O2}{}^{3}}, \qquad K'_{3,mod}{}^{0} = \frac{K'_{3,mod}{}^{0}}{[c^{*}H_{O2}']^{3}} \tag{B33}$$

And with $Hb(O_2)_2 + O_2 \rightleftharpoons Hb(O_2)_3$, Atkins finds

$$K'_3{}^{0} = \frac{[Hb(O2)_3]}{[Hb(O2)_2]p_{O2}} = \frac{[Hb(O2)_3]}{K'_2{}^{0}K'_1{}^{0}[Hb]p_{O2}{}^{3}} = \frac{K'_{3,mod}{}^{0}}{K'_2{}^{0}K'_1{}^{0}} \tag{B34}$$

Finally, for n=4 and $Hb + 4O_2 \rightleftharpoons Hb(O_2)_4$

$$K'_{4,mod}{}^{0} = \frac{[Hb - 4O2]}{[Hb]\ p_{O2}{}^{4}}, \qquad K'_{4,mod}{}^{0} = \frac{K_4{}^{0}}{[c * H_{O2}']^4} \tag{B35}$$

With $Hb(O_2)_3 + O_2 \rightleftharpoons Hb(O_2)_4$

$$K'_4{}^{0} = \frac{[Hb(O2)_4]}{[Hb(O2)_3]p_{O2}} = \frac{[Hb(O2)_4]}{K'_3{}^{0}K'_2{}^{0}K'_1{}^{0}[Hb]p_{O2}{}^{4}} = \frac{K'_{4,mod}{}^{0}}{K'_1{}^{0}K'_2{}^{0}K'_3{}^{0}} \tag{B36}$$

Atkins gives the following as constants when the pressure is expressed in units of torr or mmHg

$$\begin{aligned} K'_1{}^{0} &= K'_{1,mod}{}^{0} = 0.01 \\ K'_2{}^{0} &= \frac{K'_{2,mod}{}^{0}}{K'_1{}^{0}} = 0.02 \\ K'_3{}^{0} &= \frac{K'_{3,mod}{}^{0}}{K'_2{}^{0}K'_1{}^{0}} = 0.04 \\ K'_4{}^{0} &= \frac{K'_{4,mod}{}^{0}}{K'_1{}^{0}K'_2{}^{0}K'_3{}^{0}} = 0.08 \end{aligned} \tag{B37}$$

Therefore, $K'_{2,mod}{}^{0}=0.0002$, $K'_{3,mod}{}^{0}= 8\times10^{-6}$, $K'_{4,mod}{}^{0}=6.4\times10^{-7}$.

Recall from equation (B27)

$$K'_{n,mod}{}^{0} = \frac{K_n{}^{0}}{[c * H_{O2}']^n} \tag{B38}$$

where $1/H_{O2}$' =0.031 mL of O2 per mm of Hg per unit L of blood is Henry's constant.

$$K'_{n,mod}{}^{0} = \frac{K_n{}^{0}}{[c * H_{O2}']^n} = \frac{K_n{}^{0}}{[c / 0.031]^n} = \frac{K_n{}^{0} * 0.031^n}{[c]^n} \tag{B39}$$

Thus, for n=1, 2, 3, and 4

$$K'_{1,mod}{}^{0} = \frac{K_1{}^{0} * 0.031}{[c]},\ K'_{2,mod}{}^{0} = \frac{K_2{}^{0} * 0.031^2}{[c]^2}, K'_{3,mod}{}^{0} = \frac{K_3{}^{0} * 0.031^3}{[c]^3}, K'_{4,mod}{}^{0} = \frac{K_4{}^{0} * 0.031^4}{[c]^4} \tag{B40}$$

Now if [c] is known, then $K_1{}^{0}$, $K_2{}^{0}$, $K_3{}^{0}$, and $K_4{}^{0}$ can be evaluated.

Recalling equation (B14)

$$S_{O2} = \frac{N_{HbnO2} * n}{4\ N} \tag{B41}$$

$$S_{O2} = \frac{\sum_{1}^{4} n * N_{Hb\text{-}nO2}}{4 * N_{Hb\,total}} \tag{B42}$$

$$S_{O2} = \frac{\frac{K_1{}^{0}\ \ p_{O2}}{(H_{O2}')N} + \frac{2\ K_2{}^{0}\ \ p_{O2}{}^{2}}{(H_{O2}')^2 N^2} + \frac{3\ K_3{}^{0}\ \ p_{O2}{}^{3}}{(H_{O2}')^3 N^3} + \frac{4\ K_4{}^{0}\ \ p_{O2}{}^{4}}{(H_{O2}')^4 N^4}}{4\left\{1 + \frac{K_1{}^{0}\ \ p_{O2}}{(H_{O2}')N} + \frac{K_2{}^{0}\ \ p_{O2}{}^{2}}{(H_{O2}')^2 N^2} + \frac{K_3{}^{0}\ \ p_{O2}{}^{3}}{(H_{O2}')^3 N^3} + \frac{K_4{}^{0}\ \ p_{O2}{}^{4}}{(H_{O2}')^4 N^4}\right\}} \tag{B43}$$

$$S_{O2} = \frac{K_{1m}'^{0}\ p_{O2} + 2\ K_{2m}'^{0}\ p_{O2}^{\ 2} + 2\ K_{3m}'^{0}\ p_{O2}^{\ 3} + 4\ K_{4m}'^{0}\ p_{O2}^{\ 4}}{4\left\{11 + K_{1m}'^{0}\ p_{O2} + K_{2m}'^{0}\ p_{O2}^{\ 2} + K_{3m}'^{0}\ p_{O2}^{\ 3} + K_{4m}'^{0}\ p_{O2}^{\ 4}\right\}} \quad \text{(B44)}$$

$$S_{O2} = \frac{K^{0}_{1}'(p_{O2}) + 2K^{0}_{1}'K^{0}_{2}'(p_{O2})^{2} + 3K^{0}_{1}'K^{0}_{2}'K^{0}_{3}'(p_{O2})^{3} + 4K^{0}_{1}'K^{0}_{2}'K^{0}_{3}'K^{0}_{4}'(p_{O2})^{4}}{4\left\{1 + K^{0}_{1}'(p_{O2}) + K^{0}_{1}'K^{0}_{2}'(p_{O2})^{2} + K^{0}_{1}'K^{0}_{2}'K^{0}_{3}'(p_{O2})^{3} + K^{0}_{1}'K^{0}_{2}'K^{0}_{3}'K^{0}_{4}'(p_{O2})^{4}\right\}} \quad \text{(B45)}$$

From equation (B45) we can now solve the oxygen saturation percent of hemoglobin for a given partial pressure of oxygen [42].

APPENDIX C

ALLOMETRIC LAWS

The allometric law for the SMR of organ k is given as

$$\dot{q}_{m,k}\left(\frac{W}{kg\ of\ k}\right)=\frac{\dot{q}_k}{m_k}\ =\ a_k\ m_k(kg)^{\ b_k} \tag{C1}$$

where $\dot{q}_{m,k}$ is the SMR of organ k, $\dot{q}_k$ is the metabolic rate of organ k, m_k is the mass of organ k, a_k is the allometric constant of organ k, and b_k is the allometric exponent of organ k. The limits of the allometric exponent for COS- O2 model have been evaluated before by Annamalai [2012, 201; Taiwan and Comb Institute meeting paper; include this ref] and are briefly given below.

First, the oxygen consumption rate for the COS-O2 model is given by

$$\left|\dot{m}_{O2}\right|=\eta\left(2\pi\ n\ d_{cell}\left(\rho D\right)_{IF\text{-}cell}\ Y_{O2,cap}\right)\left(n\ \pi\ R_{COS}{}^{2}\ L\right)=\eta G\left(\rho D\right)_{IF\text{-}cell}\ Y_{O2,cap}\left(\pi L\right) \tag{C2}$$

When organ k is small, the consumption rate is very low and $Y_{O2cap,IF} \approx Y_{O2cap}$. Oxygen concentration is almost uniform and is available to all cells with uniform strength. Thus,

each cell consumes oxygen as though it is isolated without the crowding effect and η goes to one. Under these conditions, equation (C2) becomes

$$\left|\dot{m}_{O2}\right| = \left(2\pi\ n\ d_{cell}\left(\rho D\right)_{IF\text{-}cell} Y_{O2,cap}\right)\left(n\ \pi\ R_{COS}{}^{2}\ L\right) \tag{C3}$$

where the terms in the first parentheses represent the individual cell consumption rate and the terms in the second parentheses represents the number of cells in the tissue cylinder of radius R_{COS}. Dividing equation (C3) by the mass of the tissue cylinder yields

$$\left|\dot{m}_{O2,m}\right| = \frac{\dot{m}_{O2}}{m} = \frac{\left(2\pi\ n\ d_{cell}\left(\rho D\right)_{IF\text{-}cell} Y_{O2,cap}\right)\left(n\ \pi\ R_{COS}{}^{2} L\right)}{\rho\pi R_{COS}{}^{2}\ L} \tag{C4}$$

$$\left|\dot{m}_{O2,m}\right| = \frac{\dot{m}_{O2}}{m} = \frac{\left(2\pi\ n\ d_{cell}\left(\rho D\right)_{IF\text{-}cell} Y_{O2,cap}\right)}{\rho} \tag{C5}$$

By multiplying equation (C5) by HHV_{O2}, the SMR is obtained and given as

$$\left|\dot{q}_{O2,m}\right| = \frac{\left(2\pi\ n\ d_{cell}\left(\rho D\right)_{IF\text{-}cell} Y_{O2,cap}\right) HHV_{O2}}{\rho} \tag{C6}$$

Comparing with the allometric law (equation (C1)), one can identify

$$a_k = \frac{\left(2\pi\ n\ d_{cell} \left(\rho D\right)_{IF\text{-}cell} Y_{O2,cap} \right) HHV_{O2}}{\rho}, \quad b_k = 0 \tag{C7}$$

Therefore, the small organ k follows isometric law for the COS-O2 model. Now consider organ k is a large organ. Then G becomes so large that $Y_{O2,cap\text{-}IF}$ becomes extremely small compared to $Y_{O2,cap}$. Thus only cells near the capillary surface will consume O_2 and the metabolic rate is controlled by the mass transfer across the capillaries. Now, oxygen consumption rate is given as

$$\left|\dot{m}_{O2}\right| = K'\rho Y_{O2,cap} \left(2\pi\ R_{COS} L\right) \tag{C8}$$

Where $K'\rho Y_{O2,cap}$ represents the mass transfer across capillaries per unit area and $\left(2\pi R_{COS} L\right)$ represents surface area. Then, SMR is given as

$$\dot{q}_{O2,m} = \frac{K'\rho Y_{O2,cap} \left(2\pi\ F_{cos} R_{COS}\ L\right) HHV_{O2}}{\rho\pi R_{COS}{}^2 L} = \frac{2\ K' Y_{O2,cap}\ F_{cos} HHV_{O2}}{R_{COS}} \tag{C9}$$

Knowing R_{COS} is proportional to $m_k^{(1/3)}$ and comparing equation (C9) to the allometric law (equation (C1)), it is seen $b_k = -1/3$ for a large organ using the COS-O2 model.

Next, the COA-O2 model is analyzed. For a small organ, one can simply change RCOS to RCOA in equations (C3) to (C6) and come to the same conclusion as for the COS-O2 model: for small organs, the COA-O2 model follows the isometric law. Now

considering a large organ, G once again becomes very large so that only cells near the capillary will consume oxygen. Therefore, R_{COS} can be replaced with r_{cap} in equation (C8) yielding

$$\left|\dot{m}_{O2}\right| = K'\rho Y_{O2,cap}\left(2\pi \quad r_{cap} L\right) \tag{C10}$$

The SMR is then given as

$$\dot{q}_{O2,m} = \frac{K'\,\rho Y_{O2,cap}\left(2\pi r_{cap} L\right) HHV_{O2}}{\rho\pi R_{COA}{}^2 L} = 2\,Y_{O2,cap}\,HHV_{O2}\,\frac{K'\,r_{cap}}{R_{COA}{}^2} \tag{C11}$$

and when compared to the allometric law (equation (C1)), with R_{COA} proportional to $m_k^{(1/3)}$, it is seen that $b_k = -2/3$.

The third model to be examined is COS-US and the oxygen consumption rate is given by

$$\left|\dot{m}_{O2}\right| = \dot{m}_{O2}''' \,\pi\left\{R_{COS}{}^2 - \left(R_{COS}-\delta\right)^2\right\} L = \dot{m}_{O2}''' \,\pi R_{COS}{}^2 L\left\{1-\left(1-\frac{\delta}{R_{COS}}\right)^2\right\} \tag{C12}$$

As mentioned previously, δ is the aerobic shell thickness which surrounds an anaerobic core and here is assumed to be constant. The uniform source is not limited by the diffusion across the capillary wall or the diffusion between the interstitial fluid and the

cell. When organ k is small, the O_2 consumption is slow and the organ is fully aerobic and δ equals R_{COS}. Using this, equation (C12) becomes

$$\left|\dot{m}_{O2}\right| = \dot{m}_{O2}''' \, \pi R_{COS}^{\,2} L \tag{C13}$$

and

$$\dot{q}_{O2,m} = \frac{\dot{m}_{O2}''' \, HHV_{O2}}{\rho} = 2\pi n \, d_{cell} \, D_{IF\text{-}cell} \, Y_{O2,US} \, HHV_{O2} \tag{C14}$$

Comparing equation (C14) with the allometric law (equation (C1)), one sees the isometric law still applies for small organs using the COS-US model and $b_k = 0$. For a large organ using the COS-US model, the term δ divided by R_{COS} is extremely small and equation (C12) becomes

$$\left|\dot{m}_{O2}\right| = \dot{m}_{O2}''' \, \pi R_{COS}^{\,2} L \left(\frac{2\delta}{R_{COS}} \right) = \dot{m}_{O2}''' \, 2\pi R_{COS} \delta L \tag{C15}$$

and the resulting SMR is given as

$$\dot{q}_{O2,m} = \frac{\dot{m}_{O2}''' \, 2 \, \delta}{\rho \, R_{COS}} \tag{C16}$$

If equation (C16) is compared with the allometric law (equation (C1)) and with R_{COS} proportional to $m_k^{(1/3)}$, it is seen $b_k = -1/3$ for a large organ using the COS-US model.

Finally, the COA-US model is considered. The oxygen consumption rate is given as

$$\left|\dot{m}_{O2}\right| = \dot{m}_{O2}''' \, \pi \left\{ \left(\delta + r_{cap}\right)^2 - r_{cap}^{\,2} \right\} L = \dot{m}_{O2}''' \, \pi R_{COA}^{\,2} L \left\{ \left(\frac{\delta}{R_{COA}} + \frac{r_{cap}}{R_{COA}} \right)^2 - \left(\frac{r_{cap}}{R_{COA}} \right)^2 \right\} \tag{C17}$$

When organ k is small, the O_2 consumption is slow and the organ is fully aerobic and δ equals R_{COA}. Using this, equation (C17) becomes

$$\left|\dot{m}_{O2}\right| = \dot{m}_{O2}''' \, \pi \left\{ \left(R_{COA} + r_{cap}\right)^2 - r_{cap}^{\,2} \right\} L = \dot{m}_{O2}''' \, \pi R_{COA}^{\,2} L \left\{ \left(1 + \frac{r_{cap}}{R_{COA}} \right)^2 - \left(\frac{r_{cap}}{R_{COA}} \right)^2 \right\} \tag{C18}$$

$$\left|\dot{m}_{O2,m}\right| = \frac{\dot{m}_{O2}}{m} = \frac{\dot{m}_{O2}''' \, \pi R_{COA}^{\,2} L \left\{ \left(1 + \frac{r_{cap}}{R_{COA}} \right)^2 - \left(\frac{r_{cap}}{R_{COA}} \right)^2 \right\}}{\rho \pi R_{COA}^{\,2} \left\{ 1 - \left(\frac{r_{cap}}{R_{COA}} \right)^2 \right\} L} \approx \frac{\dot{m}_{O2}'''}{\rho} \tag{C19}$$

and

$$\dot{q}_{O2,m} = \frac{\dot{m}_{O2}''' \, HHV_{O2}}{\rho} = 2\pi n \; d_{cell} \, D_{IF\text{-}cell} Y_{O2,US} \, HHV_{O2} \tag{C20}$$

Comparing equation (C20) with the allometric law (equation (C1)), one sees the isometric law still applies for small organs using the COA-US model and $b_k = 0$. For a large organ using the COA-US model, the term δ divided by R_{COA} is extremely small but δ divided by r_{cap} is extremely large and equation (C17) becomes

$$\left|\dot{m}_{O2}\right| = \dot{m}_{O2}''' \, \pi \left\{ \left(\delta + r_{cap} \right)^2 - r_{cap}^{\,2} \right\} L = \dot{m}_{O2}''' \, \pi \delta^2 L \left\{ \left(1 + \frac{r_{cap}}{\delta} \right)^2 - \left(\frac{r_{cap}}{\delta} \right)^2 \right\} \tag{C21}$$

$$\left|\dot{m}_{O2}\right| = \dot{m}_{O2}''' \, \pi \delta^2 L \left(\frac{2 r_{cap}}{\delta} \right) = \dot{m}_{O2}''' \, 2\pi \delta r_{cap} L \tag{C22}$$

and

$$\dot{q}_{O2,m} = \frac{\dot{m}_{O2}''' \, 2 \delta r_{cap} HHV_{O2}}{\rho \, R_{COA}^{\,2}} \tag{C23}$$

If equation (C23) is compared with the allometric law (equation (C1)) and with R_{COA} proportional to $m_k^{(1/3)}$, it is seen $b_k = -2/3$ for a large organ using the COA-US model.